University of Alberta

AN EXPERIMENTAL INVESTIGATION OF THE HYDRAULICS OF STREET INLETS

ZAHIRANIZA MUSTAFFA

A thesis submitted to the Faculty of Graduate Studies and Research in partial fulfillment of the requirements for the degree of Master of Science

in

WATER RESOURCES ENGINEERING
DEPARTMENT OF CIVIL AND ENVIRONMENTAL ENGINEERING

Edmonton, Alberta
Fall 2003

National Library of Canada
Acquisitions and Bibliographic Services
395 Wellington Street
Ottawa ON K1A 0N4
Canada

Bibliothèque nationale du Canada
Acquisisitons et services bibliographiques
395, rue Wellington
Ottawa ON K1A 0N4
Canada

Your file Votre référence
ISBN: 0-612-87844-9
Our file Notre référence
ISBN: 0-612-87844-9

The author has granted a non-exclusive licence allowing the National Library of Canada to reproduce, loan, distribute or sell copies of this thesis in microform, paper or electronic formats.

The author retains ownership of the copyright in this thesis. Neither the thesis nor substantial extracts from it may be printed or otherwise reproduced without the author's permission.

L'auteur a accordé une licence non exclusive permettant à la Bibliothèque nationale du Canada de reproduire, prêter, distribuer ou vendre des copies de cette thèse sous la forme de microfiche/film, de reproduction sur papier ou sur format électronique.

L'auteur conserve la propriété du droit d'auteur qui protège cette thèse. Ni la thèse ni des extraits substantiels de celle-ci ne doivent être imprimés ou aturement reproduits sans son autorisation.

Canada

University of Alberta

Library Release Form

Name of Author: **Zahiraniza Mustaffa**

Title of Thesis: **An Experimental Investigation of the Hydraulics of Street Inlets**

Degree: **Master of Science**

Year this Degree Granted: **2003**

Permission is hereby granted by the University of Alberta Library to reproduce single copies of this thesis and to lend or sell such copies for private, scholarly or scientific research purposes only.

The author reserves all other publication and other rights in association with the copyright in the thesis, and except as herein before provided, neither the thesis nor any substantial portion thereof may be printed or otherwise reproduced in any material form whatever without the author's prior written permission.

Date: August 25, 2003

University of Alberta

Faculty of Graduate Studies and Research

The undersigned certify that they have read, and recommend to the Faculty of Graduate Studies and Research for acceptance, a thesis entitled **An Experimental Investigation of the Hydraulics of Street Inlets** submitted by **Zahiraniza Mustaffa** in partial fulfillment of the requirements for the degree of **Master of Science** in **Water Resources Engineering.**

Dr. D.Z. Zhu

Dr. N. Rajaratnam

Dr. T.Y. Gan

Dr. S. Liu

Date: 18th Aug 03

ABSTRACT

The purpose of this study was to obtain insight into the hydraulics of street inlets, through the variation of the discharge coefficient *(C_d)* with the Reynolds number *(R)* and Froude number *(F)*. It focuses on grate inlets with different configurations that were placed in reservoirs and channels, which correspond to ponding and gutter flow conditions, respectively. In addition, an orifice-oriented inlet was tested for single orifice, multiple orifices and orifices with roughness on the surrounding bed. The results summarize a complete variation of C_d that are applicable to the computations of the actual flows entering the inlet for different flow conditions. Depth computations near the inlets for flows in the channel were also a major concern. Therefore, three approaches were proposed in determining the head for the C_d computations. Interesting results were obtained on the pattern of flow in the vicinity of the inlets.

To my family and friends

who graciously offered me their support, advice and encouragement.

ACKNOWLEDGEMENT

The author would like to express her sincere gratitude to Dr. N. Rajaratnam and Dr. D.Z. Zhu for their sustained encouragement and guidance throughout the course of this study.

The technical assistance provided by Mr. Sheldon Lovell and Mr. Perry Fedun is gratefully acknowledged. Financial support of the author was provided by the Universiti Teknologi PETRONAS, Malaysia and supplemented by Dr. N. Rajaratnam and Dr. D.Z. Zhu. These are gratefully acknowledged.

Special appreciation to my parents, Mr. Mustaffa and Mrs. Zaharah, my brother Ahmed Muzairee, sister Maria Hani and cousin Alina Shamsuddin, for their unlimited support and spiritual encouragement throughout the years of academic. In addition, the author is immeasurably indebted to her best friend, Bilkiss Issack, for her friendship, advice, encouragement as well as understanding throughout the study.

TABLE OF CONTENTS

1.	**INTRODUCTION**	**1**
	1.1 Historical Background of Study	1
	1.2 Thesis Organization and Objectives	4
2.	**CHARACTERISTICS OF STREET INLETS**	**5**
	2.1 Introduction	5
	2.2 Road Drainage	6
	2.2.1 Road Slopes	6
	2.2.2 Road Surfaces	7
	2.2.3 Curbs and Gutters	7
	2.2.4 Street Flows	7
	2.3 Design Criteria	10
	2.3.1 Design Discharge	10
	2.3.2 Allowable Water Spread and Depth at Curb	12
	2.4 Types of Inlets	12
	2.5 Literature Review	15
	2.5.1 Grate Inlet Performances	15
	2.5.2 Current Design Practices for Grate Inlets	17
	2.5.3 Grate Inlet Characteristics on the Gutter	20
	2.5.4 Grate Inlet Characteristics in the Sump	22
	2.5.5 Critical Review	26
3.	**EXPERIMENTAL INVESTIGATION**	**27**
	3.1 Introduction	27
	3.2 Dimensional Analysis	27
	3.3 Model Laws	29
	3.3.1 Similarity	29

3.3.2 Scaling 29
3.4 Models 31
3.4.1 Orifices in Reservoirs 31
3.4.2 Orifices in Channels 34
3.4.3 Street Inlets 38
3.5 Experiments 44
3.5.1 Orifices in Reservoirs 44
3.5.2 Orifices in Channels 44
3.5.3 Street Inlets 45
3.6 Estimate of Uncertainty 46

4. EXPERIMENTAL RESULTS, ANALYSIS AND DISCUSSION **48**

4.1 Introduction 48
4.2 Discharge Coefficient *(C_d)* with Reynolds Number *(R)* 49
4.3 Discharge Coefficient *(C_d)* with Froude Number *(F)* 52
4.3.1 Depth Above Inlet, y as the Head 53
4.3.2 Average Depth Above Inlet, $\bar{y}$ as the Head 56
4.3.3 Approach Depth, y_a as the Head 65
4.3.4 Approach Specific Energy, E_a as the Head 69
4.3.5 Comparison Between C_d', C_d'' and C_d''' 72
4.3.6 Efficiency 75
4.4 Observations 82
4.4.1 Turbulences 82
4.4.2 Ridge Characteristics 84
4.4.3 Flows Transformation 92
4.4.4 Flow Circulation 96

5. CONCLUSIONS **99**

REFERENCES 102

APPENDIX I 105

Other Types of Street Inlets or Similar Structures

APPENDIX II 108

Model Experimental Data for Orifices in Reservoir

APPENDIX III 113

Model Experimental Data for Orifices in Channel

APPENDIX IV 124

Model Experimental Data for Street Inlets

LIST OF TABLES

Table	Title	Page
3.1	Properties of the street inlet models	44
4.1	Comparison between $\bar{y}$ and $\bar{y}'$	65
4.2	Statistical analyses on the discharge coefficients	73
4.3	Full catch capacity for street inlets	95
II.1	Model experimental data for orifice 1 *(O1)*	109
II.2	Model experimental data for orifice 2 *(O2)*	110
II.3	Model experimental data for orifice 2 *(O2)* in the wall study	112
II.4	Model experimental data for orifice 2 *(O2)* with roughness on surrounding bed	112
III.1	Model experimental data for orifice 1 *(O1)* in the single orifice study	114
III.2	Model experimental data for orifice 2 *(O2)* in the single orifice study	116
III.3	Model experimental data for orifice 2 *(O2)* in the multiple orifices study	119
III.4	Model experimental data for orifice 3 *(O3)* in the multiple orifices study	120
III.5	Model experimental data for orifice 4 *(O4)* in the multiple orifices study	121
III.6	Model experimental data for orifices with roughness on surrounding bed study	123
IV.1	Model experimental data for street inlet type F-51	125
IV.2	Model experimental data for street inlet type NF80-Slotted Lid	126

IV.3 Model experimental data for street inlet type #6B(F-39) normal to the flow 127

IV.4 Model experimental data for street inlet type #6B(F-39) parallel to the flow 128

LIST OF FIGURES

Figure	Title	Page
1.1	Ponding in a sag location	3
1.2	Gutter flow in the street	3
1.3	Debris blocking the gutter flow	3
2.1	Street cross section	6
2.2(a)	Gutter with straight cross slope	9
2.2(b)	Gutter with changing cross slope	9
2.3	Types of street inlets [Adapted from Mays, 2001]	14
2.4	Channel with a bottom inlet	16
2.5	Angle setting for grating opening [Adapted from Bouchard and Townsend, 1984]	19
2.6	Comparison of grating performance at different flow rates [Adapted from Bouchard and Townsend, 1984]	20
2.7	Side view of experimental set up for ponding study [Adapted from Adam and Brandson, 1974]	24
2.8	Plan view of experimental set up for ponding study [Adapted from Moss and Townsend, 1980]	24
3.1	Prototype street inlets provided by the City of Edmonton	32
3.2(a)	Plan view of orifices in the reservoir (not to scale)	33
3.2(b)	Side view of orifices in the reservoir (not to scale)	33
3.3	Diagrammatic layout of orifices in channel	35
3.4	Single orifice in the reservoir and channel	36
3.5	Multiple orifices in the channel	36
3.6	Orifices with roughness on surrounding bed	36
3.7(a)	Plan view of orifices in the channels (not to scale)	37

3.7(b)	Side view of orifices in the channels (not to scale)	37
3.8(a)	Plan view of street inlet models in the channels (not to scale)	39
3.8(b)	Side view of street inlet models in the channels (not to scale)	39
3.9	V-notch weir used in the inlet study	40
3.10	Street inlet model type NF80-Slotted Lid	41
3.11	Street inlet model type #6B(F-39)	42
3.12	Street inlet model type F-51	43
4.1	C_d versus R [Adapted from Brater *et al.*, 1963]	50
4.2	Discharge coefficient, C_d versus Reynolds number, R for orifices studies	51
4.3	C_d/C_{do} versus Froude number, F for orifices in the channel	55
4.4	Photograph of flow above street inlet type F-51 at low discharge (Q = 2.72 L/s and S_o = 0%)	57
4.5	Sample profile above street inlet type F-51 at low discharge (Q = 2.72 L/s and S_o = 0%)	58
4.6	Cross sections of water surface profile for street inlet type F-51 at low discharge (Q = 2.72 L/s and S_o = 0%)	59
4.7	Discharge coefficient, C_d' versus the Froude number, F for street inlet type F-51	61
4.8	Discharge coefficient, C_d' versus the Froude number, F for street inlet type NF80-Slotted Lid	61
4.9	Discharge coefficient, C_d' versus the Froude number, F for street inlet type #6B(F-39) normal to the flow	62
4.10	Discharge coefficient, C_d' versus the Froude number, F for street inlet type #6B(F-39) parallel to the flow	62
4.11	Comparison between C_d' for flow with and without complete flow-cover for inlet F-51	63

4.12	$\bar{y}$ and $\bar{y}'$ as the average depth above the inlet	64
4.13	Discharge coefficient, C_d'' versus the Froude number, F for street inlet type F-51	67
4.14	Discharge coefficient, C_d'' versus the Froude number, F for street inlet type NF80-Slotted Lid	67
4.15	Discharge coefficient, C_d'' versus the Froude number, F for street inlet type #6B(F-39) normal to the flow	68
4.16	Discharge coefficient, C_d'' versus the Froude number, F for street inlet type #6B(F-39) parallel to the flow	68
4.17	Discharge coefficient, C_d''' versus the Froude number, F for street inlet type F-51	70
4.18	Discharge coefficient, C_d''' versus the Froude number, F for street inlet type NF80-Slotted Lid	70
4.19	Discharge coefficient, C_d''' versus the Froude number, F for street inlet type #6B(F-39) normal to the flow	71
4.20	Discharge coefficient, C_d''' versus the Froude number, F for street inlet type #6B(F-39) parallel to the flow	71
4.21	Plan view of gutter flow on the street	78
4.22	Efficiency, η (%) versus model total flow, Q_o (m^3/s) for multiple inlet studies	79
4.23	Intercepted flow, Q_i (m^3/s) versus model total flow, Q_o (m^3/s) for multiple inlet studies	80
4.24	Efficiency, η' (%) versus model total flow, Q_o (m^3/s) for multiple inlet studies	81
4.25	C_d/C_{do} versus Froude number, F for single orifice in the channel study	83
4.26(a)	Plan view of subcritical flow for street inlet type F-51 at Q =5.32 L/s and S_o = 0.2%	85
4.26(b)	Side view of subcritical flow for street inlet type F-51 at Q =5.32 L/s and S_o = 0.2%	85

4.26(c)	Sketch of subcritical flow for street inlet type F-51 at Q =5.32 L/s and S_o = 0.2%	85
4.27(a)	Cross section 1-1 of subcritical flow for street inlet type F-51 at Q =5.32 L/s and S_o = 0.2%	86
4.27(b)	Cross section 2-2 of subcritical flow for street inlet type F-51 at Q =5.32 L/s and S_o = 0.2%	86
4.28(a)	Plan view of supercritical flow for street inlet type F-51 at Q =21.08 L/s and S_o = 0.5%	87
4.28(b)	Side view of supercritical flow for street inlet type F-51 at Q =21.08 L/s and S_o = 0.5%	87
4.28(c)	Sketch of supercritical flow for street inlet type F-51 at Q =21.08 L/s and S_o = 0.5%	87
4.29(a)	Cross section 1-1 of supercritical flow for street inlet type F-51 at Q =21.08 L/s and S_o = 0.5%	88
4.29(b)	Cross section 2-2 of supercritical flow for street inlet type F-51 at Q =21.08 L/s and S_o = 0.5%	88
4.30(a)	Undular ridge: Inlet NF80-Slotted Lid (Q_o = 8.28 L/s and S_o = 0.1%)	90
4.30(b)	Undular ridge: Inlet #6B(F-39): Parallel to flow (Q_o = 6.1 L/s and S_o = 0.2%)	90
4.30(c)	Undular ridge: Inlet F-51 (Q_o = 4.28 L/s and S_o = 0.2%)	90
4.30(d)	Undular ridge: Inlet #6B(F-39): Normal to flow (Q_o = 8.78 L/s and S_o = 0.1%)	90
4.31(a)	Wedge ridge: Inlet NF80-Slotted Lid (Q_o = 17.76 L/s and S_o = 1%)	91
4.31(b)	Wedge ridge: Inlet #6B(F-39): Parallel to flow (Q_o = 6.16 L/s and S_o =0.5%)	91
4.31(c)	Wedge ridge: Inlet F-51 (Q_o = 21.2 L/s and S_o = 0.5%)	91
4.31(d)	Wedge ridge: Inlet F-51 (Q_o = 13.2 L/s and S_o = 0.5%)	91
4.32	Flow transformation in the inlet studies	92
4.33	Sketch of water circulation above the inlet	97

4.34(a)	Flow circulation: Inlet #6B(F-39): Parallel to flow (Q_o = 2 L/s and S_o =0%)	98
4.34(b)	Flow circulation: Inlet NF80-Slotted Lid (Q_o = 2.08 L/s and S_o =0.1%)	98
4.34(c)	Flow circulation: Inlet #6B(F-39): Normal to flow. (Q_o = 1.76 L/s and S_o =0%)	98
4.34(d)	Flow circulation: Inlet NF80-Slotted Lid (Q_o = 2.32 L/s and S_o =0.05%)	98
I.1	Other types of street inlets	106
I.2	Inlets in the Butchard Garden, Victoria	107

LIST OF SYMBOLS

a	Area of orifice or area of opening
a'	Ratio of the opening area to the total area
A_b	Area of basin drainage
B	Width of channel
C	Runoff coefficient
C_d	Coefficient of discharge
C_d'	Discharge coefficient based on $\bar{y}$ computation
C_d''	Discharge coefficient based on y_a computation
C_d'''	Discharge coefficient based on E_a computation
C_w	Coefficient of weir
$\overline{C_d}$	Mean discharge coefficient
d	Diameter of orifice or inlet model
E	Specific energy
E_a	Approach specific energy
F	Froude number
g	Acceleration due to gravity
h	Depth of water above inlet/orifice
i	Average rainfall intensity
K	Coefficient for basin
l	Length of opening in the inlet model
L_b	Length of the overland flow
n	Manning coefficient
Q_b	Basin peak discharge
Q_c	Carryover flow
Q_i	Intercepted flow
Q_o	Approach/Total/ Theoretical flow
Q_w	Frontal flow
Q_x	Side flow

r	Radius of circular inlet model
R	Reynolds number
R_h	Hydraulic radius
s	Separation between bars in the inlet model
S_o	Longitudinal slope
S_w	Gutter slope
S_x	Transverse slope
S_{Cd}	Standard deviation for the discharge coefficient
T	Total spread of water on the road
t_c	Time of concentration
v	Velocity of flow through the opening
v_o	Velocity of approach
W	Width of the grate inlet
y_a	Approach depth
$\bar{y}$	Average depth above the inlet
$\bar{y}'$	Average depth in the area with complete flow-cover
η	Efficiency of an inlet
η'	Modified efficiency of an inlet

CHAPTER 1
INTRODUCTION

1.1 HISTORICAL BACKGROUND OF STUDY

Urbanization is a gradual advancement of technology that is spreading out all over the globe since the last few decades in order to create a better civilization. The continuous development of urbanization has resulted in major disadvantages to the society. Drainage system, for instance, is a component that is significantly being affected by problems associated with urbanization. If in early times engineers designed the drainage system by entirely depending on their personal experiences, the approach has been refined recently from the knowledge of hydraulics, fluid mechanics, hydrology and statistical techniques. The system is now requires sophisticated engineering skills for planning, building, operating and maintaining its components. The system constitutes physical facilities that collect, store, convey and treat both stormwater and wastewater.

In the city like Edmonton, source of stormwater comes from rainfall, snowmelt or excess water from lawn. It can be captured by either the storm sewer or combination sewer via the catch basins. Catch basins are sometimes addressed as stormwater inlets or street inlets. During dry weather, the inlets are able to intercept water normally. In the wet weather, however, if the amount of water exceeds certain limit, the inlet might not be able to fully capture the water, resulting ponding to occur. Ponding as shown in Figure 1.1 is a situation in which free water accumulates on the street and covers the surfaces that are normally located in the sump. Ponded water on the street that is not cleared by normal inlets will be removed naturally by percolation, evaporation or transpiration process. However, these processes consume a very long time.

Not only the occurrence of ponding interferes the roadway users, but also its components are harmful to the environment. The stormwater is sometimes consists of chemicals, lubricants and animal wastes. It is true that the water collected by the storm sewers will be treated once it enters the wastewater treatment plant. However, when the water is collected during severe wet weather by the combination sewers, only part of the water is delivered to the treatment plant. The rest is discharged directly into creeks or rivers without being treated. This condition is considered to be not environmentally friendly.

This situation captures many interests and concerns. Engineers and environmentalists are gathering together to find the best solutions to solve the problems. As the drainage system itself is complicated, any modifications for improvements will involve a lot of effort and money. In some cases, there is a need in developing numerous research groups and mathematical models for simulating the stormwater processes. It is not only the structural components (*e.g.* diversion, storage, channel improvements) that need to be looked into but also the policy aspects (*e.g.* insurance, flood-warning systems, legislations).

A question arises whether the problem can be solved at a very early stage before the water enters the whole system. Therefore, there is no need to modify the whole drainage systems. As described earlier, the street inlets are the initial structures in which water starts to enter the system. The knowledge of locating and designing the inlets is the main key to prevent excess stormwater. Improving the existing inlets may be costly mainly because of the resultant interruptions of traffic, but this modification is considered to be minor compared to the whole drainage system components. It is hoped that later, excess stormwater will be flowing freely without ponding (Figure 1.2). With this in mind, this study was developed, aiming to obtain a method that is simple, practical and applicable at the initial design stage of the street inlets.

Figure 1.1: Ponding in a sag location

Figure 1.2: Gutter flow in the street

Figure 1.3: Debris blocking the gutter flow

1.2 THESIS ORGANIZATION AND OBJECTIVES

The purpose of this study is to devise a simple approach that can best describe the hydraulics of grate inlets. The study covers aspects of flows in the gutters as well as ponding in the sumps. An ideal consideration is to look into the basic equation used to compute the flow. It was also necessary to critically study the flow behavior observed during the experiments, as earlier studies did not seriously emphasize this matter.

A simplified and general experiment involving orifice-oriented inlets was first conducted. Actual inlets with different patterns and configurations were studied at a later stage. These inlets were selected from the existing city of Edmonton street inlets. Chapter 2 is devoted to the review of grate inlets. The experiments are later described in Chapter 3 while Chapter 4 presents results and observations obtained from these studies. Finally, Chapter 5 provides conclusions and recommendations for future studies.

CHAPTER 2
CHARACTERISTICS OF STREET INLETS

2.1 INTRODUCTION

Street inlets are structures that intercept excess storm water on the street and convey them to another drainage system such as the underground sewer. No single type of inlet can be considered the best (John Hopkins University, 1956). Proper design of street inlets will lead to good performance by means of the capability in intercepting water as well as producing a nuisance-free environment for the traffic. Brune *et al.* (1975) suggested several factors that need to be taken into consideration when designing an inlet. These factors include:

a. The assumed capacity of an inlet based on past experience
b. The structural strength of the inlet grating
c. The effect of the inlet on traffic
d. The effect of the grating on pedestrians
e. The costs of installation and maintenance

This chapter presents overviews of the principles applied in the study. The principles of the road drainage are presented at the beginning of the chapter followed by descriptions on the inlet design criteria. Later, the chapter introduces types of inlets that can be found on the street while the literature review concluded the section.

2.2 ROAD DRAINAGE

2.2.1 Road Slopes

Slope is a simple mechanism that conveys water surface runoff on the road from one place to another with the effect of gravity. There are three main components in the road slope classifications, namely the longitudinal slope *(S_o)*, cross slope *(S_x)* and gutter slope *(S_w)*. Different areas and provinces have different road slope classification. The longitudinal slope, S_o covers slope along the road and varies depending on the ground surface elevation. The cross slope, S_x covers half of the road cross section, starting from the street crown to the curb, as sketched in Figure 2.1. Cross slope is designed by considering the necessity between the need for reasonably steep cross slopes for drainage and relatively flat cross slopes for driver comfort.

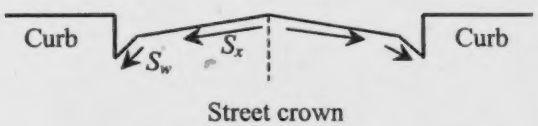

Figure 2.1: Street cross section

The gutter slope, S_w is another component that can be found near the curb when a depressed gutter is required. Depressed gutter is designed when an inlet fails to intercept most of the flow. Its existence will concentrate the flow into the inlet. The gutter slope is designed continuously from the cross slope itself.

2.2.2 Road Surfaces

Road surfacing affects the performance of a road in many ways. Grooving the pavements is useful for removing small amounts of water as in a light drizzle (Bohac, 1992). Pavement with rough surface enables inlets to intercept water easily but at the same time it causes wider spread of water on the road or gutter. However, a rough pavement has the capability to dry quickly. A permeable road enables the water to seep through the upper layer. The manning n is the parameter describes the texture of the road. Researchers normally choose n in the range of 0.010 to 0.016 for the street inlet studies; depend upon the criteria of the roadways.

2.2.3 Curbs and Gutters

Curbs and gutters are structures used to provide a barrier by which runoff is guided, concentrated and transferred to the storm water collection system. They can be attached or detached to the roadway sidewalk. Curbs and gutters are classified by referring to their functions. For example, a spill curb-gutter only delineates the roadway and not as a drainage. Catch curb-gutter on the other hand, drains the water from the pavement. A curb height of 6 inches has greater street flow capacity compared to a 4 inches curb. Some curbs are designed without the gutters. In this case, normally the road will function as the drainage.

2.2.4 Street Flows

In a normal design storm event, the curbs and gutters collect flows along the street and convey them in the form of a triangular channel as sketched in Figure 2.2(a). This condition is best described as flows in an open channel mode. Stormwater flow on the street can be classified into two categories; the frontal and

side flow. Frontal flow is governed by the amount of flow carried within the gutter width. Side flow is flow around the grate when the water spread, T is larger than the grate width, W. Splash over flow is a portion of flow that splashes over the grate. Normally the inlet does not intercept this flow.

The velocity is governed principally by the shape of the channel cross-section, the slope along the channel and the roughness of the wetter perimeter. This relationship is commonly expressed in term of the Manning equation as,

$$v = \frac{\phi}{n} R_h^{2/3} S_o^{1/2} \tag{2.1}$$

where v is the mean velocity, ϕ is 1 (SI units) or 1.49 (U.S. Customary units), R_h is the hydraulic radius, S_o is the longitudinal slope and n is the coefficient of roughness. However, equation 2.1 is for channels of arbitrary shape.

The modified Manning equation for flows in the gutter is given by the equation,

$$Q_o = \frac{\phi}{n} S_o^{1/2} S_x^{5/3} T^{8/3} \tag{2.2}$$

where Q_o is the total flow, ϕ is 0.375 (SI units) or 0.56 (U.S. Customary units), S_x is the cross slope and T is the top width of flow. This equation is valid for undepressed gutter but some modifications needed for depressed gutter (Figure 2.2 (b)). The total flow, Q_o in the depressed gutter is defined as,

$$Q_o = Q_w + Q_x \tag{2.3}$$

where Q_w is the frontal flow carried by the gutter width and Q_x is the side flow carried by street width.

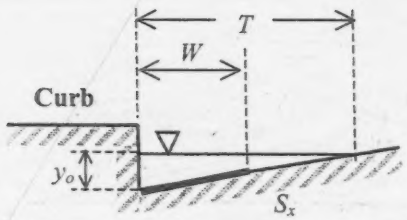

(a) Gutter with straight cross slope

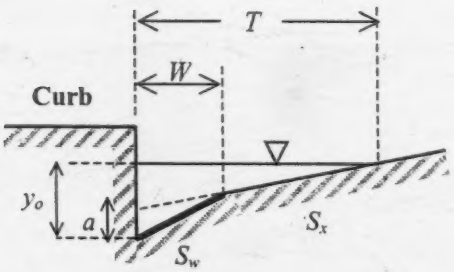

(b) Gutter with changing cross slope

Figure 2.2: Gutter cross sections

The discharge for the side flow is given by,

$$Q_x = \frac{0.56}{n} \frac{S_o^{1/2}[(T - W)S_x]^{8/3}}{S_x} \tag{2.4}$$

The discharge for the frontal flow is written as,

$$Q_w = \frac{0.56}{n} \frac{S_o^{1/2}}{S_w} \left[(T S_x + a)^{8/3} - [(T - W)S_x]^{8/3}\right] \tag{2.5}$$

where W is the gutter width for depression and a is the gutter depression depth. These equations can directly be applied during a normal storm event. However, when the storm water capacity gets higher, careful consideration needs to be given to the amount of spread water above the street because the water tends to cover not only the gutter width, but also any parking lanes or shoulders and certain portions of the traveled surface.

Another flow component that is also important is the carryover flow (Q_c), which refers as flow that is not intercepted by the inlet and flows to the downstream inlet. Q_c can easily be computed as follows,

$$Q_c = Q_o - Q_i \tag{2.6}$$

where Q_o is the total flow and Qi is the intercepted flow through the inlets.

2.3 DESIGN CRITERIA

Pavement drainage structures are designed to accommodate certain limits of water and failure in designing this limit will cause flooding on the road. This section presents three main factors that affect the design limits of pavement drainage, which include the magnitude and frequency of the design discharge, the allowable water spread and surface water depth.

2.3.1 Design Discharge

The magnitude of floods and their intervals can be determined by conducting the flood frequency analysis, in which two systems, the minor and major systems are involved. The minor system is designed to minimize the inconveniences caused by the more frequent storm event such as the 2, 5 and 10-

year storms (Guo, 1997). Some of its components are the street curb and gutter, storm sewers and the roadside ditches. On the other hand, the major system carries the excess storm water that cannot be accommodated by the minor system and is normally designed for 100-year storm. There are many factors that affect the design flood frequency such as street classification, traffic volume, design speed and pedestrian traffic.

The Rational Method is used to compute the discharges of the pavement drainage as is written as,

$$Q_b = KCiA_b \tag{2.7}$$

where Q_b is the basin peak discharge, K is 1.0 (U.S. customary units) and 0.00275 (SI units), C is the runoff coefficient, i is the average rainfall intensity and A_b is the drainage area.

It is necessary to measure the design rainfall duration for above method as well. Design rainfall duration is referred as the flow time required for storm water to travel from the most remote point in the basin to the design point. This period of time is also called the time of concentration (t_c) and consists of three elements; flow times of overland flow, swale flow and gutter flow. It can be written as,

$$t_c = \frac{KL_b^{0.6} n^{0.6}}{i^{0.4} S_o^{0.3}} \tag{2.8}$$

where t_c is the time of concentration, K is 56 (U.S. customary units) and 26.285 (SI units), L_b is the overland flow length, n is the Manning's roughness coefficient, S_o is the average slope of the overland flow area and i is the average rainfall intensity.

2.3.2 Allowable Water Spread and Depth at Curb

Water spread is defined as the amount of water that is allowed to accommodate in the area between the curb and gutter section, and the adjacent roadway. Beyond this limit, the water will cause nuisance to the pedestrians and vehicles. The permissible depth of water in most cities is limited to 6 inches, 18 inches in a residential whereas a major street requires at least one traffic lane remain free from the water spread. The limitations should be addressed by considering factors such as the traffic characteristic, number of roadway lanes, absence of gutters, area of roadway given up to design storm water spread and safety. When the roadway is wet, the friction factor is lower than a dry surface, in which this will produce inconvenient environment for the vehicles steering and acceleration.

2.4 TYPES OF INLETS

The John Hopkins University reported that there are four major groups of inlets, which include the grate inlets, curb inlets, combination inlets and multiple inlets. In addition, Guo (1997) and Mays (2001) introduced another inlet, known as the slotted drain. These inlets are defined as follows (John Hopkins University (1956) and Mays (2001)):

i. **Grate Inlets**: A gutter inlet is an opening in the gutter covered by one or more grates that are parallel with the flow.

ii. **Curb Inlets**: A curb is a vertical opening in the curb through, covered by a top slab.

iii. **Combination Inlets**: A combination inlet is composed of a curb and grate inlet acting as a unit. Usually the grate inlet is placed directly in

front of the curb opening and this arrangement is called a *contiguous combination inlet* or a *combination inlet*. Sometimes, the grate inlets are placed at the end of either upstream or downstream of the curb inlets. These arrangements can be either called an *overlapping*, *offset* or *special combination inlet*. The intercepted flow in a combination inlet can be approximated by the sum of the amount of flow intercepted by the grates and curb openings.

iv. **Multiple Inlets**: A multiple inlet is two closely spaced inlets acting as a unit. Two identical inlets end-to-end are called *double inlets*.

v. **Slotted Drain Inlet**: Slotted drain inlet comprises a pipe cut along the longitudinal axis with a grate of spacer bars to form slot openings.

Figure 2.3 illustrates the types of inlets described above while Appendix I are examples of other similar structures. Depending on the inlet operations and performances, some of them are designed with or without a gutter depression, as sketched in Figure 2.2. Inlets are normally installed either on a continuous gutter or in the sump. A gutter inlet refers to an inlet located on a continuous slope while a sump describes a low point in a depressed roadway section. Surface runoff flows continuously over the grate inlet that is located on the gutter whereas the water normally accumulates at the inlet in the sump.

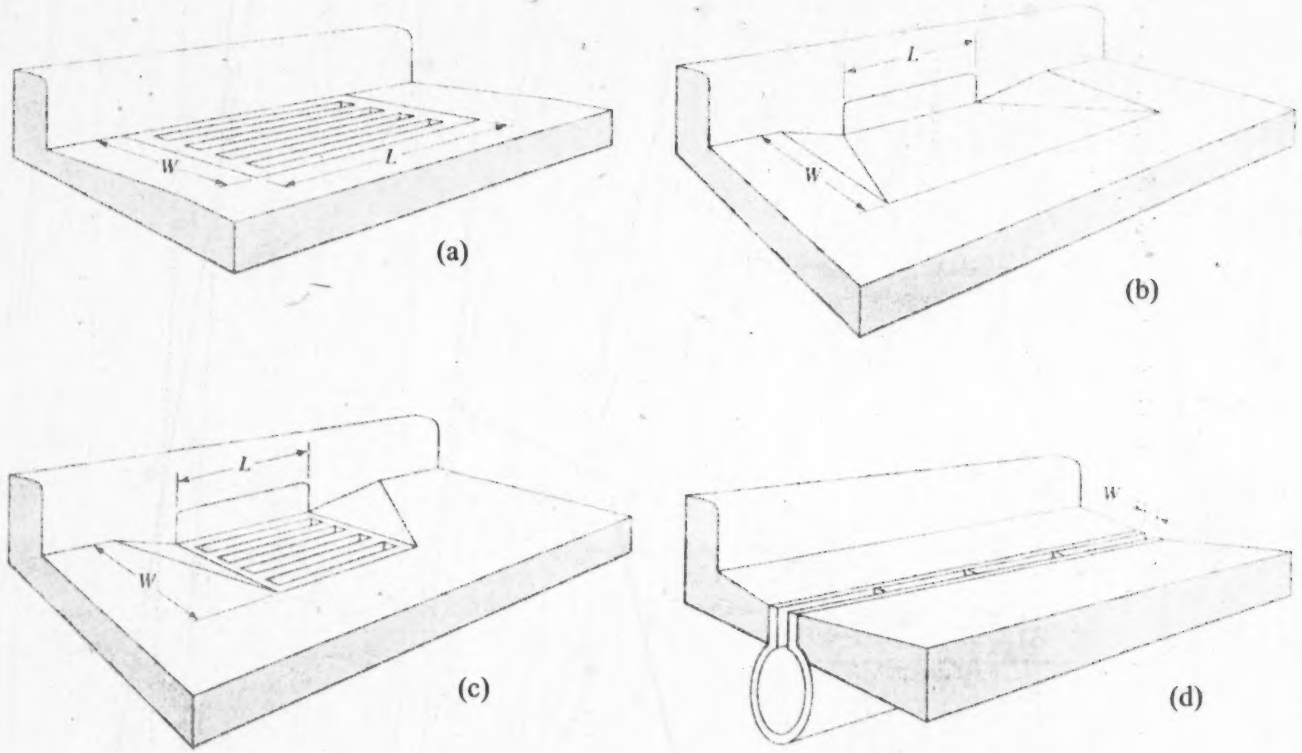

(a) Grate inlet (b) Curb inlet (c) Combination inlet (d) Slotted drain inlet

Figure 2.3: Types of street inlets [Adapted from Mays, 2001]

2.5 LITERATURE REVIEW

The studies on grate inlets covered multiple interesting fields. Most researchers were keen in investigating the effectiveness of the grate inlets and comparisons were made for various designs and patterns. Quite often researchers proposed several potential modifications on the existing grate inlet designs. This section does not attempt to review all of the researches and literatures related to the street inlets but the emphasize is placed on grate inlets without depression that are located on the gutters and sumps.

2.5.1 Grate Inlet Performances

Grate inlets capacity can be distinguished by looking at the way the inlets operate in a particular stormwater event. Generally, a grate inlet can either operate as an orifice or a weir, depending on the condition of water above the inlet (Guo, 1997 and Mays, 2001). The inlet functions like a weir when it operates under shallow condition while an orifice-operated inlet takes place when the inlet operates under the submergence condition. For a grate inlet that operates as a weir, the capacity is given by the equation,

$$Q_i = C_w L h^{1.5} \tag{2.9}$$

where Q_i is the discharge intercepted by the inlet, C_w is the weir coefficient, which is equal to 3.0 (U.S customary units) and 1.66 (SI units), L is the length of inlet and h is the depth of water over the inlet. On the other hand, the capacity of a grate inlet that operates as an orifice is written as,

$$Q_i = C_d a \sqrt{2gh} \tag{2.10}$$

where C_d is orifice discharge coefficient and is equal to 0.6, a is the grate clear opening area and g is the acceleration due to gravity. For grate inlets that function like an orifice, the total opening area is more important factor than the arrangement of bars (John Hopkins University, 1956).

Besides the methods explained above, grate inlets could also be analyzed from the principles of bottom inlets. The function of bottom inlets is similar to that of grate inlet, i.e. to divert flow from one stream to another. In hydraulics, the bottom inlet is described as spatially varied flow with decreasing discharge. Chow (1959) reported that this type of flow does not affect the energy head, therefore, the specific energy remain constant along the channel.

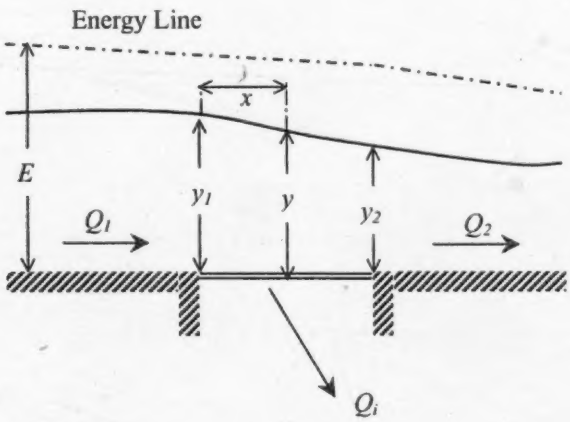

Figure 2.4: Channel with a bottom inlet

By referring to Figure 2.4, the dynamic equations for bottom inlet can be computed. When the intercepted flow through the bottom inlet is vertical, the equation is given by Chow (1959) as,

$$\frac{dy}{dx} = \frac{2EC_d\sqrt{E(E-y)}}{3y-2E} \tag{2.11}$$

The equation for inclined flow through the bottom inlet becomes,

$$\frac{dy}{dx} = \frac{2EC_d\sqrt{y(E-y)}}{3y-2E} \tag{2.12}$$

where dy and dx are respectively a section depth and length of a prismatic channel with constant slope in a gradually varied flow, E is the specific energy, C_d is the coefficient of discharge through the openings and y is the depth above the inlet. If the conditions at the upstream section of the inlet are known, these equations can theoretically compute the flow profiles and the optimum inlet length.

2.5.2 Current Design Practices for Grate Inlets

A grate inlet which is located horizontally on the street is more attractive compared to a curb inlet on the curb. It is normally designed with bars or perforated screens to avoid traffic falling into the holes. These bars, however, reduce the inlet capability to intercept water (Stephenson, 1981). Wilson (1983) noted that the allowable bar widths for grate inlets are in the range of 10 mm to 38 mm. It is necessary to design proper bar arrangement that does not cause splashing and carryover flow, but provide a sufficient area of opening to accommodate the design flow.

Unlike curb inlets, grate inlets are less sensitive to street slopes. Disadvantages of grated inlets include their interference with motorized vehicles and bicycles and their tendency for debris blockage, with resultant loss of capacity (American Society of Civil Engineers, 1992). This type of inlet is liable to damage by heavy vehicles, especially the long and thin bars; therefore, the inlet requires one or two transverse bars to provide additional strength.

There are many factors contribute to the performance of a grate inlet. The level of control achieved is a function of several physical and hydraulic parameters that include (i) the type, size and shape of the grating, (ii) the hydraulic area and the pattern of openings (iii) the width and depth of the approach flow and (iv) the cross and longitudinal street slopes (Bouchard and Townsend, 1984 and John Hopkins University, 1956). In addition, Mays (2001) reported that the amount of water over the inlet and the velocity of flows in the gutter significantly affect the capacity of the inlet.

The inlet bar orientations and configurations significantly influence the inlet behavior. Grate inlets with longitudinal bars are more preferable than inlets with transverse bars. The occurrence of the latter reduces the grating effective length and increases the component of flow outside the grate. Short-wide grates are better than long-narrow grates for usual street conditions (John Hopkins University, 1956). If transverse bars must be included in the grate inlet, they should be as few as possible. The performance of inlets with transverse bars can be improved by inclining the tops of the upstream bars (louvers) and rounding the top of bars at the downstream section (John Hopkins University, 1956 and Bouchard and Townsend, 1984). Another reason for having grates with longitudinal bars is to eliminate splashing across the inlet, in which this can be done by providing sufficient inlet length.

A crucial study on grate inlet bar orientations was conducted by Bouchard and Townsend (1984). Their studies involved a full-scale model of multiple grate inlet patterns, in which the openings (θ) were ranged from 0° to 180° at 15° intervals. These openings were measured with respect to the curb line as sketched in Figure 2.5. Openings with 0° and 180° resembled the longitudinal bars whereas 90° corresponded to transverse bars. The experiments were conducted for different discharges, Q_o. Figure 2.6 presents results obtained for multiple inlet openings in three different discharges. From this figure it can be seen that inlets with 0°/180° openings intercepted more flows than the others. The transverse

bars oriented (90°) were found to be the least effective. Inlets with 135° openings showed good correlation with the longitudinal bars for low discharges but slightly inefficient for high discharge. Owing to the longitudinal bar arrangement that was considered to be unsafe for bicyclist, the authors believed that it was more preferable to design inlet with 135° opening. Stephenson (1981) proposed that bar widths narrowed to 25 mm are safer for bicyclists.

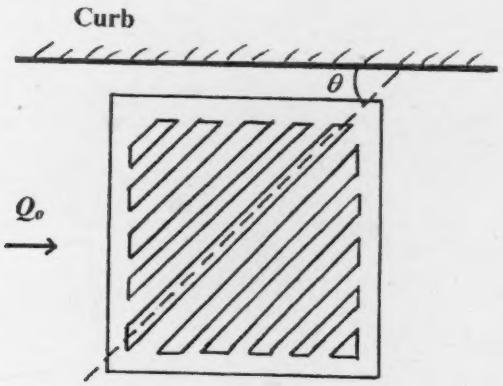

Figure 2.5: Angle setting for grating opening
[Adapted from Bouchard and Townsend, 1984]

Besides bar orientation, researchers also studied the performance of inlets when they were place in different locations. One of the common approaches made is to locate two inlets next to each other. For instance, the city of Edmonton requested Rajaratnam (1992) to study the performance of grate inlet referred as to *K-7 Grating* in a single and double frames. The author found that the efficiency of a double frame grating was higher than the single frame. The reason for this is that more gutter flow would be intercepted because of the enhancement in the inlet length. Similar results were obtained by Hotchkiss (1994) when he found that the efficiency of inlets in series increased by almost 20% more compared to the single inlet.

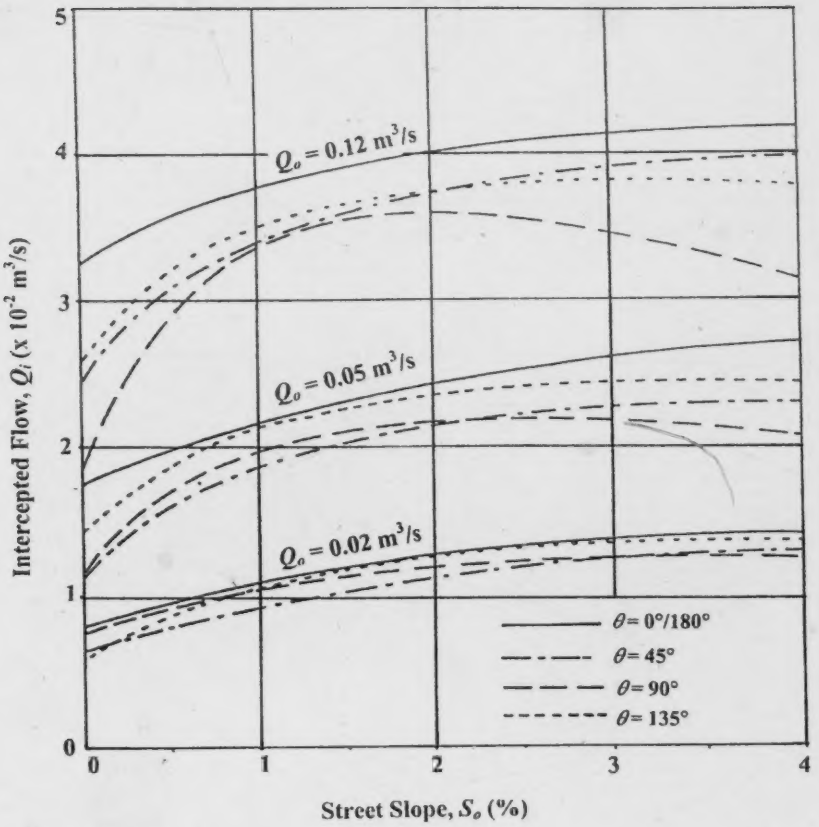

Figure 2.6: Comparison of grating performance at different flow rates
[Adapted from Bouchard and Townsend, 1984]

2.5.3 Grate Inlet Characteristics on the Gutter

Water flowing laterally off the road surface may either discharge into the countryside or into a lateral ditch, or be collected in shoulder drains (Stephenson, 1981). Stormwater on the street normally flows in a triangular cross section channel formed by the road chamber and the curb as described in section 2.2.4. The water will flow longitudinally along the street until intercept by an inlet which directs the flow into the subsurface drainage system.

Grate inlet on the gutter or a continuous grade has greater capacity than other inlets. Most of the flow passing through the inlet is likely to be captured except for low velocity and shallow flows. In this case, it is better to provide a depressed grate inlet or a combination inlet instead of the grate inlet alone. A grate inlet could intercept most of the flows that pass over it and some 20% or 100% more (McNown and Tai, 1972). Even though the inlet has the potential to intercept most flows passing through it, studies have proved that this criterion is limited to certain amount of flow. For example, Bouchard and Townsend (1984) and Rajaratnam (1992) found that the grate inlet efficiency diminishes when the total flow increases. In addition, Brune *et al.* (1975) reported that efficiency also decreases when the longitudinal slope (S_o) increases. These behaviors are explained by the higher amount of carryover flow on the gutter. Water can be inaccessible because of its inertia, in which the high velocity and steep slopes make it difficult to divert the flow. On the other hand, Bouchard and Townsend (1984) revealed that steeper cross slopes (S_x) produced higher capture of water through the grate inlets. This leads to a reduction in the amount of spread of water near the gutter and street surface. Stephenson (1981) addressed that the cross slopes should be as steep as practical accompanied by depressions near the inlet in order to improve the inlet efficiency. He concluded that a small amount of carryover flow is acceptable.

Another concern arises when dealing with grate inlets on the gutter, i.e. the flow patterns observed near the inlet area. In some cases when the flow is not fully intercepted, it tends to move towards the inlet, resulting in the formation of small family waves above the inlet. Rajaratnam (1992) referred to this type of flow as the *oblique waves*, in which these waves were observed near the downstream end of the inlet. Guo (1997) in his book, quoted the waves as *splash*, and he also came out with an equation describing the splash velocity. Mays (2001) on the other hand, described the flow that skips over the grate without being captured as the *threshold*. No matter what the title is, when these waves become larger in size, they will definitely interfere the roadway users. By increasing the street

slopes, Rajaratnam (1992) found that the waves slowly disappeared. However, as mentioned earlier, the increment in street slopes would also result in the increment of the carryover flows. Careful attention should be given when designing grate inlets on certain street slopes. Moss and Townsend (1980) who also observed unstable water surface profiles near the inlet proposed that it was not practical to measure the head within this area. As a result, depth measurement was made just upstream of the grate inlet where the flow is almost uniform.

2.5.4 Grate Inlet Characteristics in the Sump

A sump is described as the lowest point in an area in which water normally accumulates, resulting in a condition that is referred to as *ponding*. Sumps are normally located at the street junctions. A grate inlet that is located in the sump can either operate as an orifice or a weir; depend upon depths of flow above the inlet. Most likely all flows will be intercepted by the inlet except when it is blocked by trash or debris. In this situation, the capacity of the inlet will be reduced. As mentioned earlier in section 2.5.1, for inlets located in the sumps, the bar orientation is of little importance compared to the area of the opening. It is important to know the capacity of inlets in the sumps in order to estimate the width and depth of ponding.

Ponding is considered to be unfavorable if its occurrence produced nuisance to the roadway users. The impact is even worse during heavy stormwater event. Splashing of water affects visibility and comfort for passengers, and the noise can impair driving (Stephenson, 1981).

Studies on ponding have captured researchers' interests since 1970's. Different researchers, however, conducted ponding studies in different ways. For instance, Adam and Brandson (1974) conducted a full-scale laboratory model for four inlets located in the sumps for the city of Winnipeg. In the model, the flume was

hinged at the center with flow sources coming from either end (Figure 2.7). Both ends together with sides opposite the inlet could be set for desired gutter and crown slopes. On the other hand, Moss and Townsend (1980) experimented a simpler model to study ponding for the city of Edmonton street inlets. The model was designed in a way it could only be experimented under a fix cross slope (2%) while the longitudinal slopes varied from 0% to 5%. The gutter flow was released from the upstream section of the flume and the intercepted flow was collected by using a weir. To create ponding in the model, a vertical wall or *dam* was installed at the downstream half of the inlet along its centerline, as sketched in Figure 2.8. With this special feature in place, the larger street flows ponded along the upstream side of the dam and entered the inlet via the upstream half of the grating only (Moss and Townsend, 1980). The results were later doubled to give an equivalent of a whole grate inlet. It is believed that there are many possible uncertainties took place from this method. In 1992, Rajaratnam studied a preliminary ponding condition for the city of Edmonton street inlets as well. The main idea of the experimental set up resembled the Moss and Townsend's model. The ponding condition, however, was created by using a different approach, in which the outlet of the flume was closed and water was then allowed to enter the flume. Measurements were only made when the flow was stable.

As the nature of water flowing into the inlet is sometimes inconsistent and unpredictable, the measurement of depths in the ponding study is one of a major concern. Adam and Brandson (1974) found that data measured at the upstream section of the inlet were not applicable in describing the inlet performance as the velocity of approach decreases when it reaches the ponding area. Instead, depths near the inlet were believed to significantly affect the inlets. Therefore, only the average depth near the inlet opening as sketched in Figure 2.7 was taken into consideration.

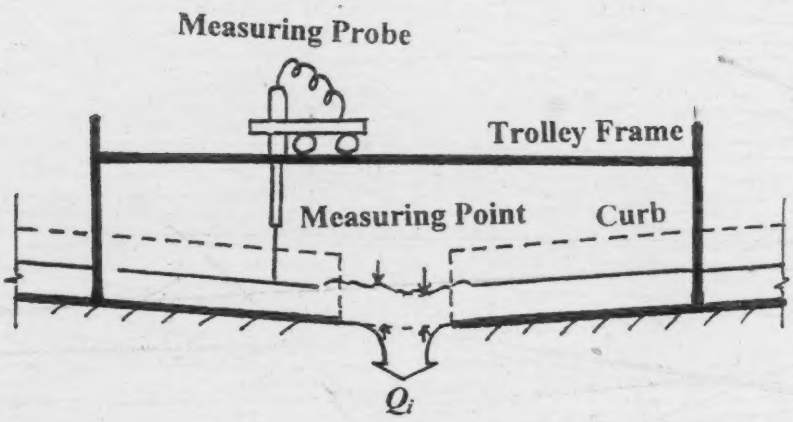

Figure 2.7: Side view of experimental set up for ponding study
[Adapted from Adam and Brandson, 1974]

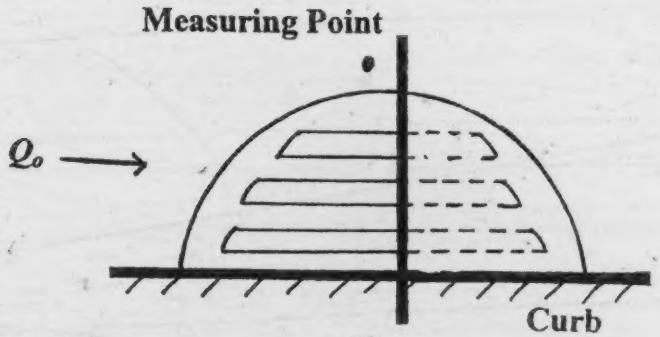

Figure 2.8: Plan view of experimental set up for ponding study
[Adapted from Moss and Townsend, 1980]

Similar idea was found in the Moss and Townsend's (1980) studies, in which depth measurements were taken close to the inlet and wall (Figure 2.8), where the flow was reasonably stable and tranquil. However, Wilson (1983) who applied Moss and Townsend's methodology to measure ponding depths for similar inlets encountered some discrepancies in his results. The author compared the laboratory results to the theoretical results obtained from equation 2.10. The laboratory results produced lower values than the theoretical results. This discrepancy was likely due to the location of depth measurement, in which it was believed that the curvilinear flow near the inlet reduced the effective head acting upon the inlet. Therefore, the theoretical head and the observed head would never be consistent. Rajaratnam (1992) also noticed the values provided by the city of Edmonton were higher than results obtained from his laboratory study. Since the theoretical values were also calculated by using the orifice equation (Equation 2.10), it was believed that this equation could not be applied freely for any ponding conditions. Flows entering an inlet can be classified as flows in an open channel mode; therefore the orifice equation cannot be applied directly. Not only that, since the inlet is not located horizontally, the head acting upon it would not be constant. Thus, a single head measurement at one particular place will not be able to describe the actual inlet performance.

By now we could see that there are many possible ways to conduct ponding study. However, it is hard to decide the best approach that would provide reliable results in describing the inlet performances. Some of the studies conducted were restricted to certain limit of parameters, i.e. the gutter slope, cross slope and longitudinal slope. Consequently, these limitations made it difficult to produce general results that are applicable to other types of inlets.

2.5.5 Critical Review

In view of the fact that almost all researchers conducted their tests on the existing residential street inlets, their results are not directly applicable to others unless similar conditions and inlets are applied. Even modification or interpolation of the existing results is believed to be impossible. Owing to the complexity of an inlet and its environment, it is not always easy to develop general analyses that describe the whole performance of any inlets.

Waves formation near the inlet area was addressed as part of the problems encountered by the grate inlets on the gutter. Even though many researchers have experienced this phenomenon in the laboratory, there are no specific descriptions being made on its characteristics. Crucial investigation should also be carried out in order to firmly understand disturbances that occur near the inlet. It is also hoped that later the phenomenon can be solved hydraulically with the knowledge gained from its characteristics.

Ponding condition is still hydraulically unsolved. Assumptions and recommendations were given by previous researchers without really looking into the matter experimentally. Strong arguments followed by its solutions should be addressed as general as possible because ponding is a common problem that occurs in most parts of the world. The first attempt in solving the ponding problems is to revise the orifice equation that describes the inlet operation. Among all parameters that govern the equation, the discharge coefficient is believed to significantly influence the inlet behavior. It is true that researchers always assume a constant value for the discharge coefficient in all cases, regardless of the vicinity of the flow. The coefficient that is defined as 0.6 is doubt to be invariant at all time. With this regard, this study is conducted in order to investigate the characteristics of the discharge coefficient of the street inlets.

CHAPTER 3
EXPERIMENTAL INVESTIGATION

3.1 INTRODUCTION

This chapter introduces the types of experiments conducted, involving two flow conditions, namely the reservoirs and channels. Explanation will first be given on dimensional considerations, followed by the scaling procedures. The procedures on accomplishing these experiments are later presented, accompanied by some diagrams and pictures describing the experimental work. The section is concluded by some discussions related to error measurements.

3.2 DIMENSIONAL ANALYSIS

Dimensional analysis is one of the important methods used to solve a physical problem in the field of hydraulics. All physical variables involved in the study can be classified into several dimensionless parameters. These terms are later applied for further experimental and theoretical analyses.

The main idea for the whole study was to define the best dimensionless parameters that describe the street inlet flow behavior. Alternatively, the dimensional analysis was conducted for an orifice, as its function is similar to the operation of an inlet. Based on the Buckingham π-Theorem technique, seven properties from an orifice study were taken into consideration, which include the discharge through the orifice (Q_i), depth of water above the orifice (h), diameter of the orifice (d), acceleration due to gravity (g), mass density of water (ρ), dynamic viscosity (μ), and surface tension (σ). This relationship can be written as,

$$Q_i = f_1 (g, d, h, \mu, \rho, \sigma) \tag{3.1}$$

The dimensions of the variables are,

$$[Q_i] = \frac{L^3}{T}, \quad [g] = \frac{L}{T^2}, \quad [d] = L, \quad [h] = L$$

$$[\mu] = \frac{M}{LT}, \quad [\rho] = \frac{M}{L^3}, \quad [\sigma] = \frac{M}{T^2}$$

The variables, *n*, is equal to 7 and the repeating variables, *m*, is 3. Therefore, *(n-m)* gives values of 4 π-parameters. By following the dimensional analysis procedures, the final π-parameters are given by,

$$\pi_1 = \frac{h}{d}, \qquad \pi_2 = \frac{v}{\sqrt{gh}}, \qquad \pi_3 = \frac{vd}{\nu}, \qquad \pi_4 = \frac{\sigma}{dv^2\rho}$$

The surface tension term in π_4 can comfortably be neglected, assuming that the experiments would avoid any influences of surface tension. The general expression for the discharge coefficient of an orifice can be written as,

$$\frac{Q}{a\sqrt{2gh}} = C_d = f_2\left(\frac{v}{\sqrt{gh}}, \frac{vd}{\nu}, \frac{h}{d}\right) \tag{3.2}$$

where C_d is the orifice discharge coefficient, a is the cross section of the orifice, $v/\sqrt{gh}$ is the Froude number *(F)* and vd/ν is the Reynolds number *(R)*, in which kinematic viscosity, ν is equal to the dynamic viscosity, μ divided by the density, ρ. However, since h and d are already included in the orifice equation i.e. h in the velocity term $(\sqrt{2gh})$ and d in the area term $(\pi d^2/4)$, the h/d term is negligible. Above expression can be simplified as,

$$\frac{Q}{a\sqrt{2gh}} = C_d = f_3(F, R) \tag{3.3}$$

Chapter 4 described the hydraulics of C_d with these dimensionless parameters.

3.3 MODEL LAWS

3.3.1 Similarity

Since the models used in the studies were modified from the existing street inlets, a good correlation is needed between the model and the prototype so that measurements in the model can be translated into different quantities in the prototype. It is necessary to consider the kinematic, geometric and dynamic similarities between the model and prototype.

3.3.2 Scaling

Flows in the gutter can be categorized as free surface flows. The forces that affect this type of flow are inertia, gravity, viscosity, surface tension, roughness and elasticity. Among all these, both gravitational and inertial are the most important forces that driving the flows. Therefore, Froude number *(F)* similarity is definitely the best correlation required to analyze the flow. This relationship can be stated as,

$$F_p = F_m \tag{3.4}$$

$$\left(\frac{V_p}{\sqrt{g_p L_p}}\right) = \left(\frac{V_m}{\sqrt{g_m L_m}}\right) \tag{3.5}$$

in which V is the velocity scale, L is the length scale and g is the gravitational force. Subscripts, m and p are for model and prototype respectively.

If the same gravitational force is expected to operate in the model and prototype, the equation is simplified to,

$$\frac{V_p}{V_m} = \sqrt{\frac{L_p}{L_m}} = \sqrt{L_r} \tag{3.6}$$

where L_r is a length scale for the study. If Q_i in equation 2.10 is the discharge through the grate inlet with $\sqrt{2gh}$ as the velocity term, the equations in the model and prototype can be written as,

$$Q_{im} = C_{dm} A_m V_m \tag{3.7}$$

$$Q_{ip} = C_{dp} A_p V_p \tag{3.8}$$

Thus, the ratio of Q_i prototype to model is defined as,

$$\frac{Q_{ip}}{Q_{i,m}} = \frac{C_{dp}}{C_{dm}} \frac{A_p}{A_m} \frac{V_p}{V_m} \tag{3.9}$$

By simplifying equation 3.9,

$$\frac{Q_{ip}}{Q_{im}} = L_r^{5/2} \tag{3.10}$$

Since the ratio of model to prototype lengths is 1:4, the above expression yields,

$$\frac{Q_{ip}}{Q_{im}} = 32 \tag{3.11}$$

3.4 MODELS

The experiment involves four types of the City of Edmonton street inlets, namely type #6(F-39), F-51, NF80-Slotted Lid and #6B(F-39). These inlets are presented in Figure 3.1. Unlike inlet F-51, NF80-Slotted Lid and #6B(F-39), inlet #6(F-39) was an orifice-oriented inlet, therefore its discussion is made separately.

Inlet #6(F-39) was investigated under the reservoir and channel conditions, in which the former corresponds to ponding while the latter is in the gutter flow conditions. Brief discussion on these conditions is presented separately in section 3.4.1 and 3.4.2.

On the other hand, inlet F-51, NF80-Slotted Lid and #6B(F-39) were only experimented under the channel conditions due to some limitations on the experimental set up.

3.4.1 Orifices in Reservoirs

In the study, the ratio of model to prototype was approximately equal to 1:2. The prototype comprises four holes of 1 inch in diameter each with surface roughness surrounding the surface. In the model, the manhole cover holes were substituted with circular orifices with 13 mm in diameter each. The experiments were performed in a reservoir with 0.40 m width, 0.30 m height and 4.84 m length. Two orifices were located at the bottom of the reservoir, namely orifice 1 *(O1)* and orifice 2 *(O2)*. *O1* was located at a distance of 0.805 m from *A* while *O2* was 0.60 m from *B* (Figure 3.2). *A* was an invisible border of an inactive pump while *B* was a wall with 0.5 cm thickness. The inactive pump covered 0.682 m length of the other side of the flume.

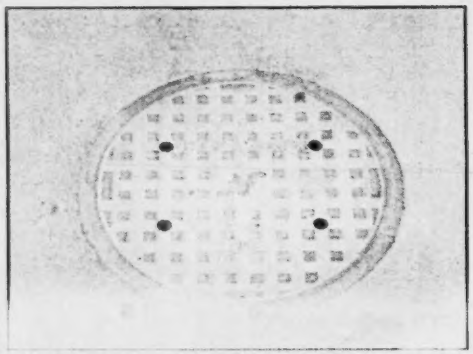

Type #6(F-39)

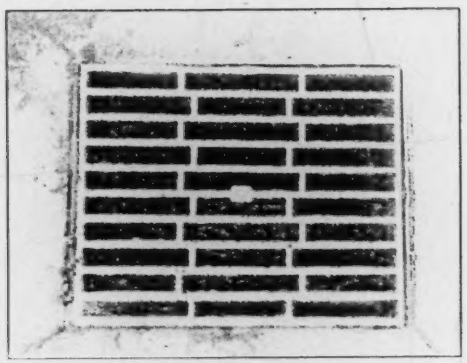

Type F-51

Type NF80-Slotted Lid

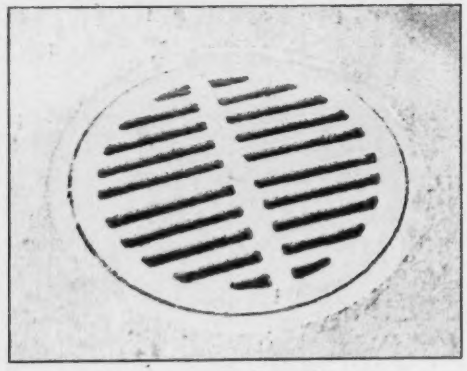

Type #6B(F-39)

Figure 3.1: Prototype street inlets provided by the City of Edmonton

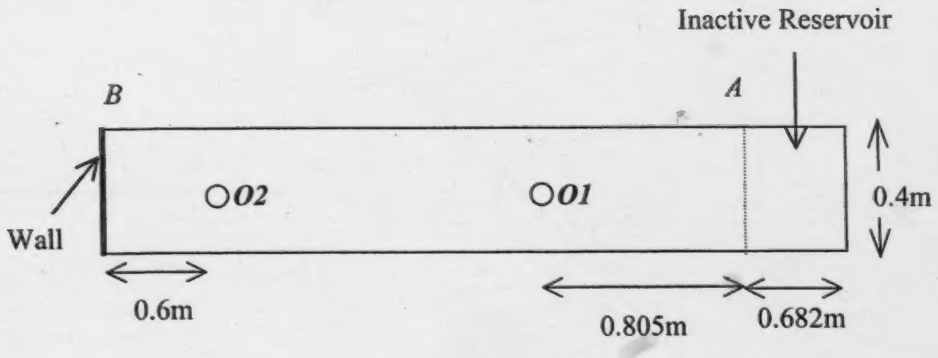

(a)

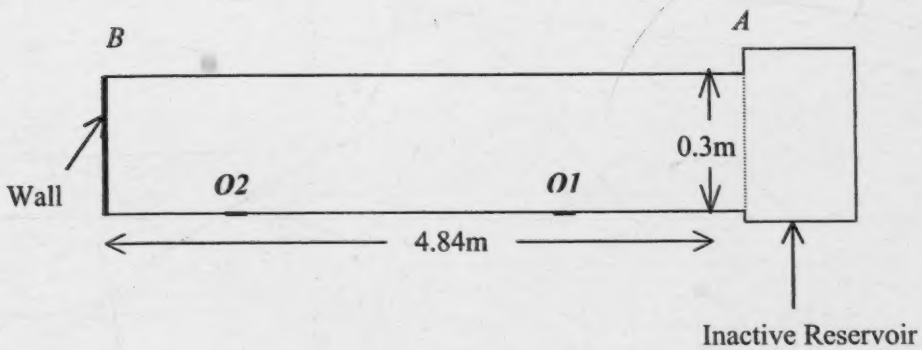

(b)

Figure 3.2: (a) Plan view (b) Side view of orifices in the reservoir (not to scale)

3.4.2 Orifices in Channels

For the orifices in the channel, three studies were conducted, which involved a single orifice, multiple orifices and orifices with roughness on surrounding bed. The major experiments were performed in a flume with 0.40 m width, 0.30 m height and 9.78 m length with Manning *n* roughness of 0.009. Source of water came from a turbine pump located at the basement and a constant head tank located at the upper level of the laboratory. A magnetic flow meter was used to supply the water and a control valve was used to regulate the flow. The water from the flume flows back to the sump tank. Figure 3.3 shows a diagrammatic layout of orifices in the channel study.

In the single orifice study, two orifices were used, namely orifice 1 *(O1)* and orifice 2 *(O2)*. The former was located at 0.805 m while 4.240 m for the latter; both distances were measured with respect to the upstream channel. Figure 3.4 shows the type of single orifice used in this study.

The multiple orifice study was conducted in order to determine the effect of the discharge coefficient *(C_d)* on multiple orifices and the results were then compared to the single orifice. An additional two other orifices, namely orifice 3 *(O3)* and orifice 4 *(O4)* were included in the flume. *O3* was located next to *O2* with 0.039 m separation (measurement from center to center), while *O4* was 4.305 m measured with respect to the upstream channel. The arrangement of these orifices was partly similar to the orifices orientation in the prototype. This arrangement is shown in Figure 3.5. *O1* was no longer in the interest of study due to the turbulences above the orifice. Detail discussion on the effect of turbulences is presented in 4.4.1.

The study on orifices with roughness on surrounding bed was conducted to observe the effect of surface roughness on C_d and the results were then compared to the single orifice. Only *O2* was taken into consideration. The experimental set

up was modified by gluing a 11mm x 11mm x 2mm-thick tape surrounding *O2* in order to produce surface roughness effect as the one in the prototype. Only thirty-six tapes were used, in which this quantity was equal to a quarter of the manhole cover area. Figure 3.6 is the model of orifices with roughness on surrounding bed and Figure 3.7 is a complete sketch of the orifices in the channel configuration.

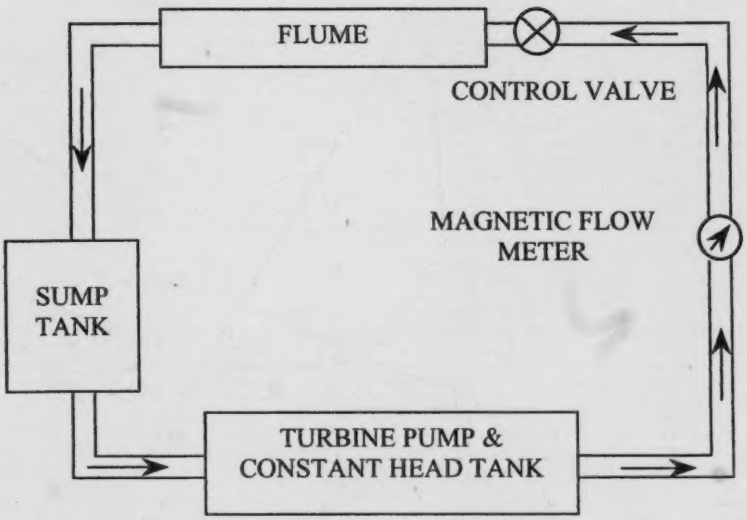

Figure 3.3: Diagrammatic layout of orifices in channel study

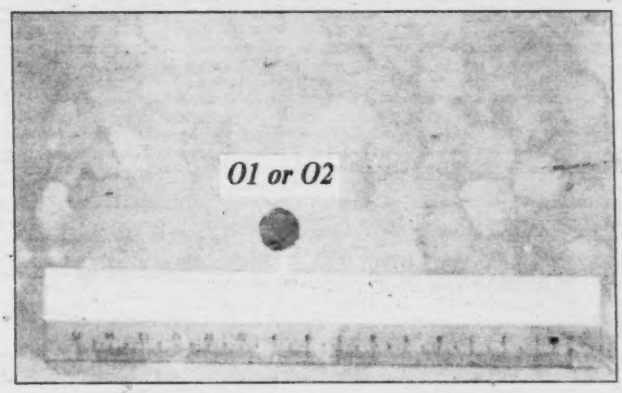

Figure 3.4: Single orifice in the reservoir and channel

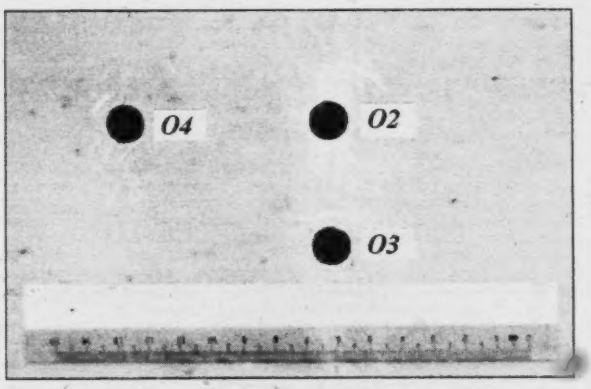

Figure 3.5: Multiple orifices in the channel

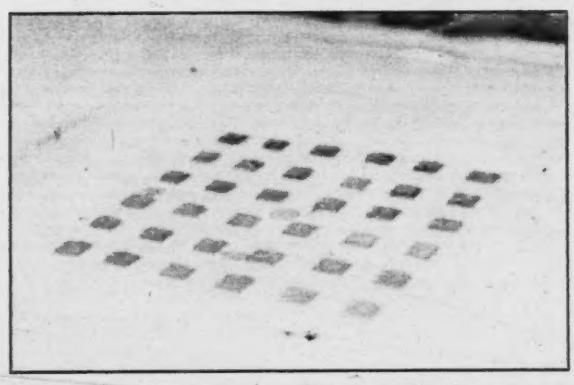

Figure 3.6: Orifices with roughness on surrounding bed

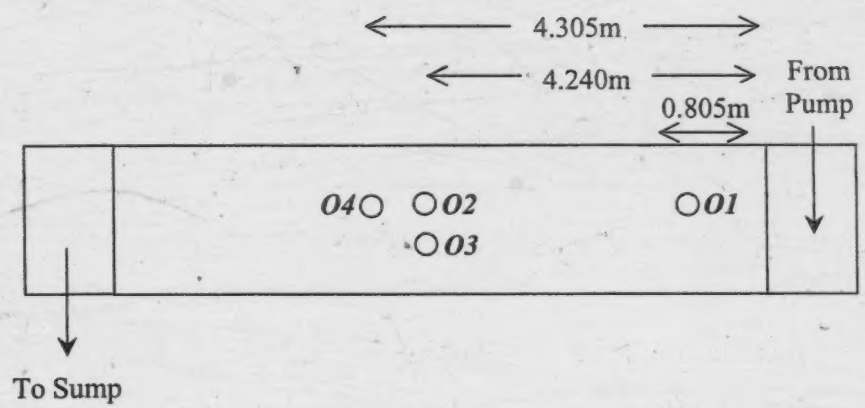

(a)

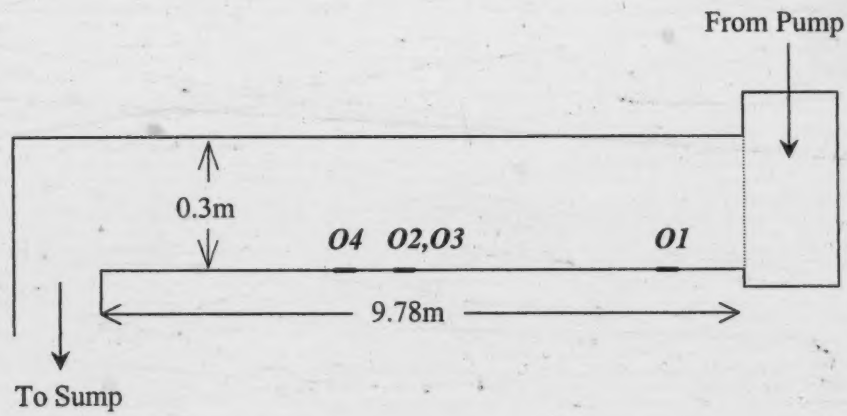

(b)

Figure 3.7: (a) Plan view (b) Side view of orifices in the channels (not to scale)

3.4.3 Street Inlets

Unlike inlet type #6(F-39), other inlets were performed under channel condition only. Similar channel as described in section 3.4.2 was used with minor modification on the inlet location. Each street inlet was located exactly in the middle at a distance of 4.24 m from the upstream section of the channel. In addition, a 90° V-notch weir was located under the inlet to collect the intercepted water. The weir was 3.05 m in length, 0.48 m in width and 0.405 m in height. The access water was then drained to the basement sump. A tailgate was used in order to produce subcritical flows. Figure 3.8 shows a sketch of the experimental set up described above and Figure 3.9 is the V-notch weir used in the study.

The ratio of the inlet model to prototype was approximately 1:4. The models and their dimensions are presented in Figure 3.10 to 3.12 while their properties are shown in Table 3.1. Since each inlet has different pattern and configuration, its placement was done with regard to the direction of flows in the prototype. For inlet F-51, the flow was expected to move parallel to the length of the inlet, as the prototype is located in the gutter. However, NF80-Slotted Lid and #6B(F-39) are located in the sump. Therefore, consideration needed to be given for flows from many directions. Since NF80-Slotted Lid was symmetrical, it was efficient to consider only once direction of flow. The unsymmetrical shape of #6B(F-39) leaded to two ways of experiments, namely flows parallel to the flow and flows normal to the flow.

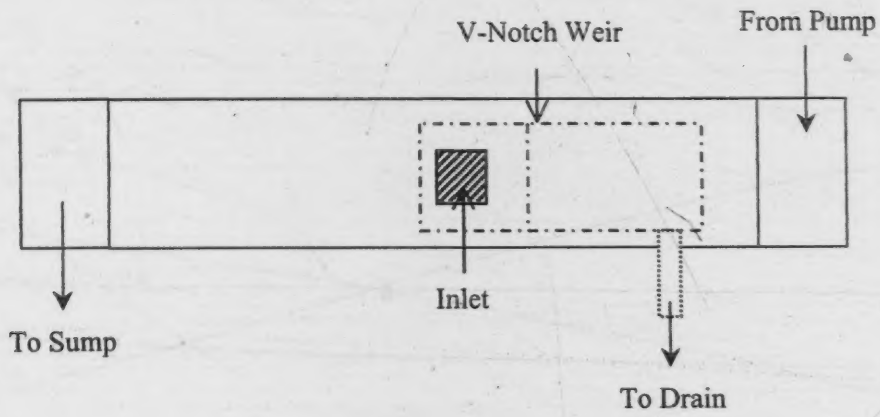

(a)

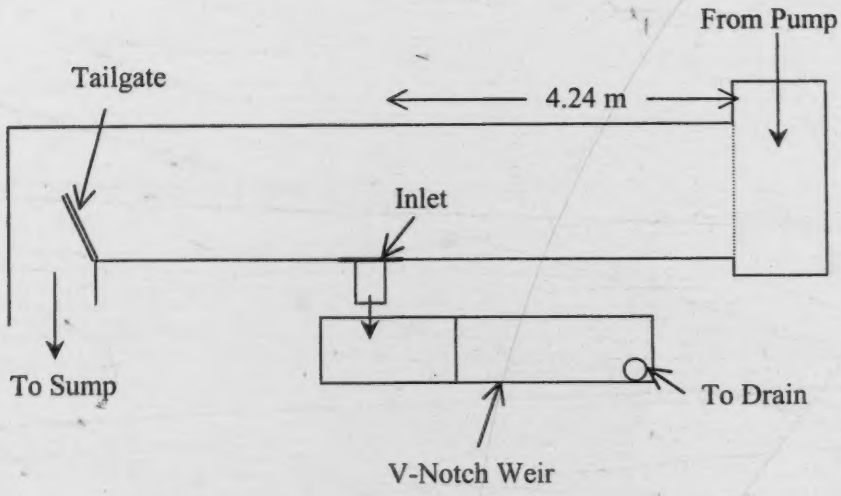

(b)

Figure 3.8: (a) Plan view (b) Side view of street inlet models in the channels (not to scale)

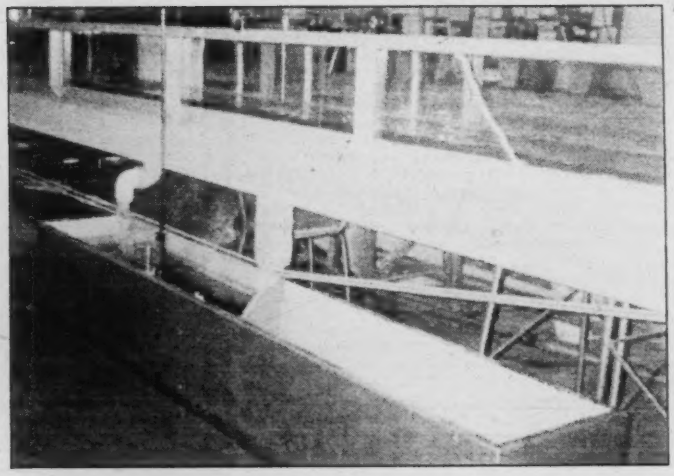

(a)

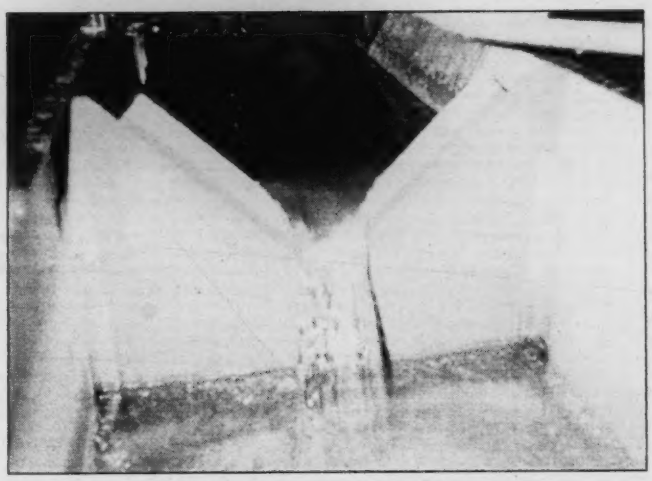

(b)

Figure 3.9 (a) and (b): V-notch weir used in the inlet study

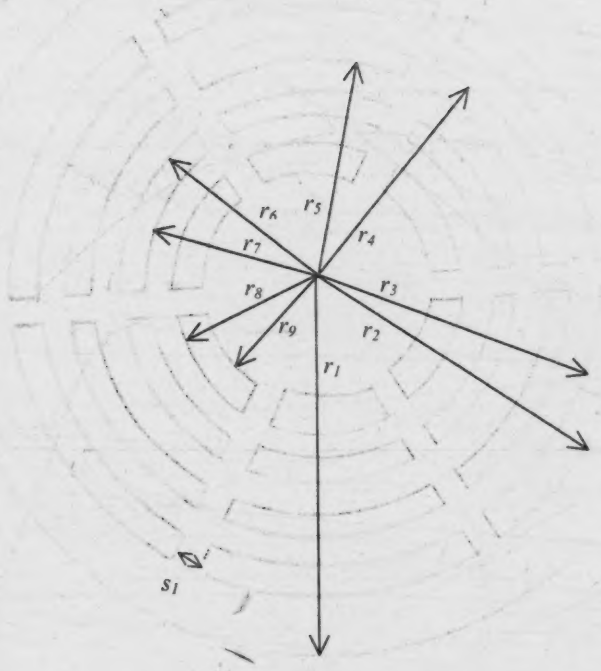

Symbols	Dimensions (cm)
r_1	7.30
r_2	6.03
r_3	5.64
r_4	5.00
r_5	4.60
r_6	3.96
r_7	3.58
r_8	2.95
r_9	2.54
s_1	0.41

Figure 3.10 Street inlet model type NF80-Slotted Lid

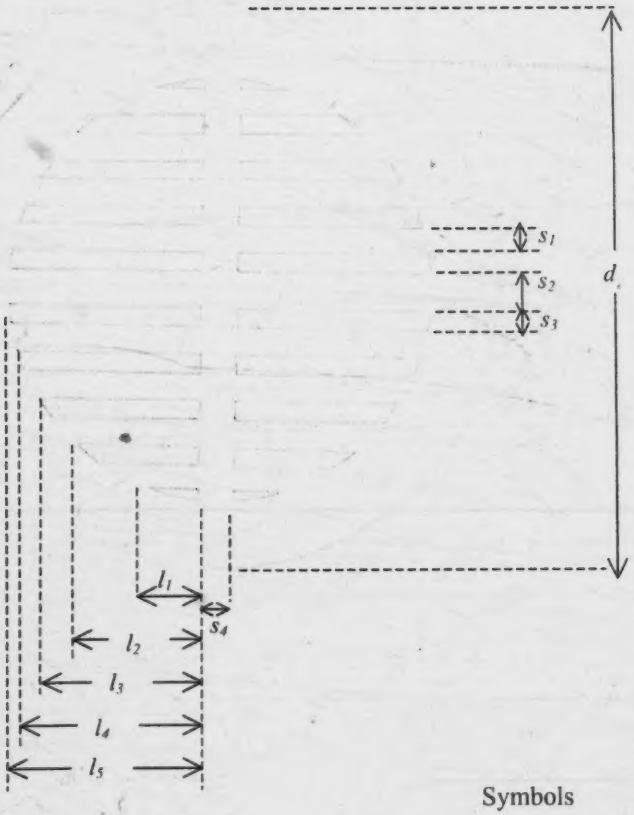

Symbols	Dimensions (cm)
l_1	0.56
l_2	3.10
l_3	4.29
l_4	4.84
l_5	5.16
d	14.6
s_1	0.70
s_2	1.00
s_3	0.48
s_4	1.00

Figure 3.11: Street inlet model type #6B(F-39)

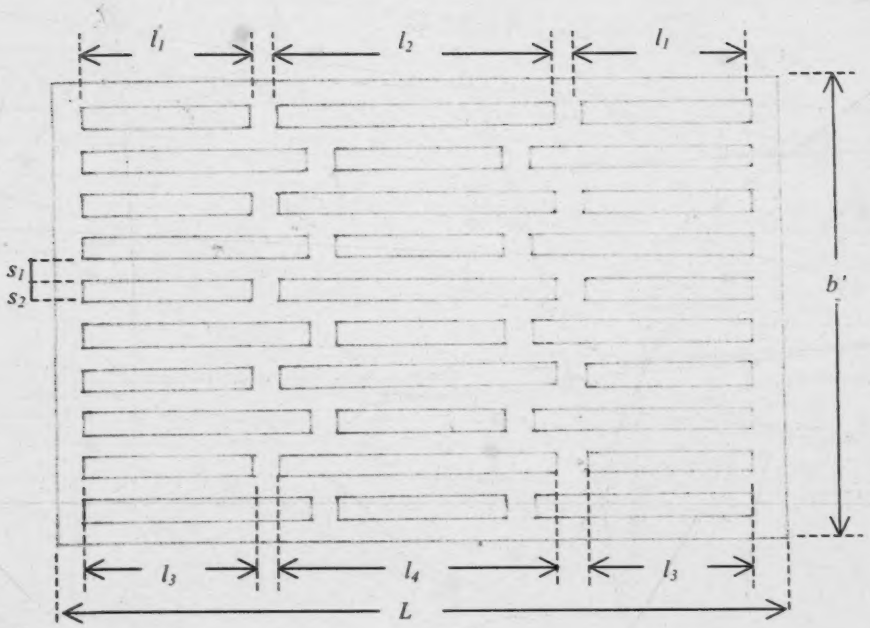

Symbols	Dimensions (cm)
l_1	4.05
l_2	4.60
l_3	4.76
l_4	3.81
L	13.97
b'	9.76
s_1	0.40
s_2	0.25

Figure 3.12: Street inlet model type F-51

Properties / Inlet	*Total Inlet Area* (m^2)	*Total Opening Area* (m^2)	*Porosity* (%)
F-51	0.01363	0.00827	60.6
NF80-Slotted Lid	0.01657	0.00361	21.8
#6B(F-39)	0.01675	0.00342	20.4

Table 3.1: Properties of the street inlet models

3.5 EXPERIMENTS

3.5.1 Orifices in Reservoirs

The main experiment was conducted by using the original set up as described in 3.4.1. Before measurements were made, the reservoir was filled with water by using an external pipe. The water temperature was recorded and a point gage was used to measure the water depth. The depth of water above each orifice was considered to be the head. The depth was computed prior to the opening of the orifice and recorded as the initial depth. Only one orifice was opened at a time. Water was allowed to flow out of the reservoir over a period of approximately one minute and the volume of the collected water measured. The orifice was then closed and a second depth, the final depth, was recorded.

3.5.2 Orifices in Channels

In order to produce a range of Froude numbers in the channel, different discharges, Q (4.2 L/s–32.7 L/s) and slopes, S_o (0%- 1.5%) were applied. The depth of water above each orifice was considered to be the head. However, only the average depth of the channel was used for Froude number computation.

For the single orifice and orifices with roughness on surrounding bed studies, only one orifice was opened at a time. After measuring the water depth, the orifice was opened and the water flowing through the orifice was collected in a bucket for approximately one minute. The orifice was closed and the collected water was then measured.

Unlike the other two studies, all three orifices were opened at the same time for the multiple orifices study. The time duration to collect the water was equal to one minute as well. Three different buckets were used to collect the water and the volume was measured separately.

3.5.3 Street Inlets

Discharges ranged from 1.76 L/s to 37.12 L/s and slopes of 0% to 1% were applied in this study. For each discharge, water depths were recorded along the channel and at least twelve depths were taken above the inlet itself. This was important in order to define the average depth above the inlet as the water depths changed over the inlet. The amount of the intercepted water was obtained from the V-notch measurement. Any observations on the water surface profile above the inlet were also recorded. It was important to observe the behavior of streamlines near the inlet surrounding area and this was done by using a tuft tube.

3.6 ESTIMATE OF UNCERTAINTY

Error analysis is normally conducted in order to determine the inaccuracy and the imprecision of the experimental results. It is believed that all measurements in physics and experiments generally are inaccurate compared to the actual or true values. This term is also referred to as error of observation and

is usually grouped into two categories namely the accidental and systematic errors. Accidental errors are usually due to the observer but systematic errors may arise from the observer or the instrument (Topping, 1962). The accidental errors can be revealed by repeated observations but the systematic errors are sometimes difficult to eliminate. However, systematic errors may be constant or vary in some regular way. If we assume that the systematic errors are constant, we are left with the accidental errors to be distinguished. The relationship between the actual value, observed value and error given by Topping (1962) is written as,

$$\text{Error} = |\text{Actual value} - \text{Observed value}| \tag{3.12}$$

The relative error, ε_i is specified as,

$$\varepsilon_i = \frac{Error}{Actual\ value} \times 100\% \tag{3.13}$$

In this section, only maximum errors were computed in order to determine the worse condition. The depths *(y)* of water in the channel, reservoir and V-notch weir were measured by using a point gage. When the flow was tranquil, the maximum error in depth was expected to be ±2% but when the flow fluctuated, the error was almost ±3%. The magnetic flow meter was used to supply water into channel. Most of the time when the discharge was high, the meter began to be slightly unstable. Due to the flow fluctuations, the maximum error for discharge (Q_o) was estimated to be ±2%.

The intercepted flows (Q_i) were measured by applying two approaches; V-notch weir for street inlets studies and bucket for the orifice-oriented inlet studies. The former was estimated to produce an error of ±2%. As for the latter, the computation was made by considering errors obtained in the water collection and time taken to collect the water. The time was recorded for approximately 1

minute but the maximum estimated error was ±1%. The collected water was measured by using a cylinder and the volume was expected to produce an error of ±2%. Applying the maximum error in the volume and time, the error in theoretical intercepted flows (Q_i) for reservoir studies could reach a maximum of ±1%.

It is necessary to determine the precision of the inlets designed in the laboratory. The diameter *(d)* of the orifice was designed for ½ inch, which is equal to 1.27 cm. However, the observed diameter was 1.3 cm. Error analysis showed that the difference in diameter was ±2% while its area *(a)* produced ±5% error. By applying errors obtained from the inlets area of opening, water depths and intercepted flow, the theoretical discharge coefficient (C_d) for orifice-oriented inlet was expected to have ±5% error.

By using the prototype samples given by the City of Edmonton, models dimensions were designed according to the capability of the channel to deliver and intercept water. Maximum errors in dimensions and area of opening for inlet F-51 was found to be ±9% and ±3%, respectively. NF80-slotted lid, on the other hand, produced the highest error among all inlets with ±15% in its dimension and ±16% in the opening area. The reason for this discrepancy was due to some limitations occurred in the manufacturing process. With the complexity of the inlet pattern itself, it was not easy to manufacture the exact dimensions as proposed. As for inlet #6B(F-39), the estimated error for model dimensions was found to be ±7% with ±6% in its area of opening. By applying all the errors obtained in the inlets area of opening, water depths and intercepted flows, the discharge coefficient (C_d) for all inlets were estimated to have ±2.5% in F-51, ±15.5% in NF80-slotted lid and ±5.5% in #6B(F-39). With regards to the amount of error produced at the design stage, it is expected that results presented in Chapter 4 more or less will be influenced by this discrepancy.

CHAPTER 4
EXPERIMENTAL RESULTS, ANALAYSIS AND DISCUSSION

4.1 INTRODUCTION

Section 3.2 described two significant dimensionless parameters that possibly affect the inlet discharge coefficient, C_d; Reynolds number *(R)* and Froude number *(F)*. The Reynolds number is a ratio between inertial and viscous forces whereas the Froude number corresponds to a ratio between the inertial and gravity forces. These parameters as described in equation 4.1 and 4.2 were calculated by substituting data obtained from the experiments.

$$R = \frac{vd}{\nu} \tag{4.1}$$

$$F = \frac{v_o}{\sqrt{gh}} \tag{4.2}$$

where d is the orifice diameter, h is the average water depth in the channel, v is the velocity of flow through the orifice, v_o is the velocity of approach in the channel and ν is the kinematic viscosity. In this context, v is the velocity through the inlet and is given by the equation,

$$v = \frac{Q_i}{a} \tag{4.3}$$

in which Q_i is the intercepted flow and a could either be the area of the orifice $(\pi d^2/4)$ or inlet. This section presents discussion on the variation of the inlet discharge coefficient, C_d with Reynolds numbers and Froude numbers for four different kinds of inlets. The discharge coefficient, C_d was first computed from equation 2.10. In addition, further explanation on the observations taken during the experiments will also be included at the end of the chapter.

4.2 DISCHARGE COEFFICIENT *(C_d)* WITH REYNOLDS NUMBER *(R)*

Due to some limitations on the experimental set up, the study on the variation of inlet with Reynolds number was only conducted for orifice-oriented inlet, type #6(F-39). Figure 4.2 is a presentation of the discharge coefficient *(C_d)* with the Reynolds number *(R)*. The figure summarizes data taken from orifice in the reservoir (ponding) and channel studies. It indicates that C_d increases from 0.45 to 0.65 as R increases from 3800 to 9000 for channel condition and ranged from 0.608 to 0.656 for R between 9000 and 14500 for ponding condition. The trend however seemed to be constant for R more than 10000.

Comparison was made between the existing results with results obtained from Lea's (1942) plot as shown in Figure 4.1. The author studied the variation of C_d with R for orifices, in which the study involved different types of fluids (water, glycerin and other oils). From Figure 4.2, ponding condition produced constant values with mean value of 0.616, which is comparable to Lea's with value of 0.6. Error computation between Lea's and experimental data showed 0.98% difference, therefore, results obtained from ponding condition were acceptable. Since viscosity is more dominant in ponding studies and Reynolds number is a dimensionless form of viscosity, a final conclusion can be made, in which C_d of an orifice in the ponding condition provides an invariant value of 0.616.

On the other hand, C_d variation for channel condition was not similar to Lea's. Most of these data were obtained from the orifice in the channel study, in which gravity is more dominant. Therefore, R is not the best dimensionless parameter to describe the behavior of orifices in the channel. Further investigations involving Froude number *(F)* as a dimensionless form of gravity was conducted in order to determine the characteristics of flow in this region.

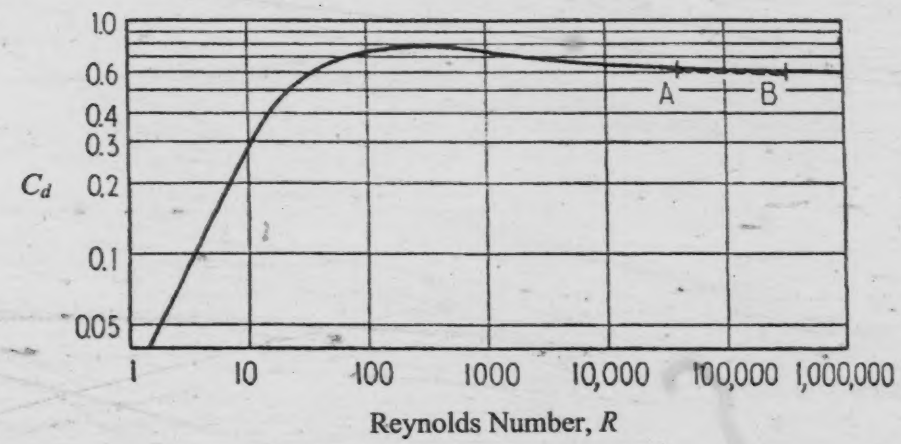

Figure 4.1: C_d versus R [Adapted from Brater *et al.*, 1963]

Figure 4.2: Discharge coefficient, C_d versus Reynolds number, R for orifices studies

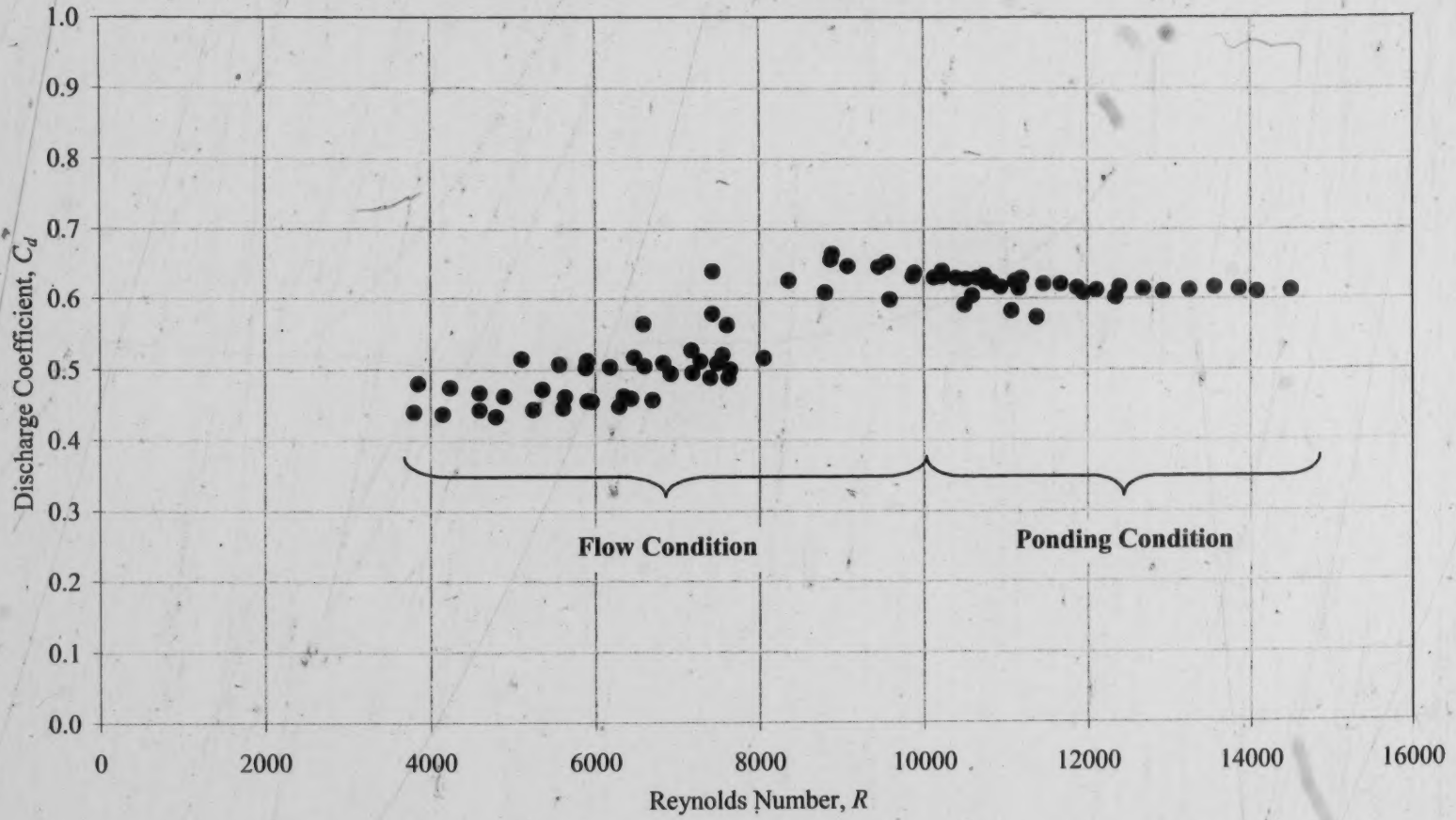

4.3 DISCHARGE COEFFICIENT (C_d) WITH FROUDE NUMBER (F)

This section presents discussion on the orifice-oriented inlet and street inlets that were experimented in the channel. The dominant parameter that describes the flows in the channel is the Froude numbers *(F)*, in which it can be classified into three regions; the subcritical, critical and supercritical. Subcritical occurs when the F is less than 1, critical when F is equal to 1 and supercritical when F is larger than 1. The idea of studying the variation of C_d with F was to produce a plot that summarizes range of C_d for different street flow conditions, which include not only the gutter flow (channel) but also the ponding (reservoir) condition. In the plot, F that is equal to zero will correspond to ponding condition while non-zero values are classified under the gutter flow conditions.

Discussion on the orifice-oriented inlet is made at the beginning of the section followed by the street inlets. It will be revealed later that C_d computation for the street inlets was not as simple as the orifice-oriented inlet. The latter was computed by using depth above the orifice itself (Section 4.3.1) but different methods were applied for the former. This was due to the complicated pattern and configuration of the street inlets compared to the orifice-oriented inlet. The inconsistent water surface profiles formed above the inlets made it difficult to define the exact head acting upon the inlet. Detailed discussions are given to any possible methods that could best used to compute C_d in equation 2.10. Three different methods were proposed to define the head, h in which each method provided different orientation of C_d. The methods include the average depth above the inlet *($\bar{y}$)*, the depth of the flow approaching the inlet *(y_a)* and the specific energy of the flow approaching the inlet *(E_a)*. Section 4.3.2 to 4.3.4 present these methods while 4.3.5 compares the results obtained from these studies.

4.3.1 Depth Above Inlet, y as the Head

As indicated in Chapter 3, studies on orifice-oriented inlets in the channel covered three different cases. Figure 4.3 shows the variations of normalized C_d/C_{do} with Froude numbers for different flow studies. It can be seen from this figure that the value of C_d/C_{do} for a single orifice decreases from 1.0 to 0.72 with an increase in F until it attains a constant C_d for F larger than 2.0. C_{do} was taken as 0.616, in which it corresponds to the average value obtained from the turbulent region of the orifices in the reservoir study. A mean curve was drawn through most of the experimental points, leaving out a few points above and below the curve. An equation for the best-fit line was obtained from the polynomial regression method for a single orifice, written as,

$$C_d = 0.6309 + 0.0715F - 0.1957F^2 + 0.0569F^3 \qquad (4.3)$$

Figure 4.3 also indicates results obtained from the multiple orifices and orifices with roughness on the surrounding bed. The former shows good agreement with the single orifice results while the latter are located somewhat above the rest of the observations.

By placing multiple orifices at a section, C_d variation was found to be similar to the single orifice variation. Comparison was made between the existing results with studies conducted by Rajaratnam (1992) and Hotchkiss (1994), who studied the efficiency of two rectangular shape inlets that were placed in series. Their results showed that two inlets captured more flow compared to a single inlet; in other words, inlets in series were more efficient. However, results obtained from the multiple inlets study did not agree with the authors' hypothesis. This is likely due to the small opening area of the orifices compared to the amount of flow passing over them. Since the opening is small (0.000133 m^2), the difference in performance between these orifices might be even smaller and insignificant.

Therefore, results for common geometrical (rectangular type inlet) obtained by earlier researchers cannot be applied directly for multiple orifice-oriented inlets.

However, if an orifice was surrounded by surface roughness, C_d was larger than orifice that was free from any roughness effect. A mean line was drawn throughout the points and a curve similar to the earlier study was obtained. The roughness thickness produced a hydraulically rough bed condition near the orifice. By assuming the viscous wall layer in the flume is relatively thin, the roughness elements protruded out through this layer and decelerated the flow through the orifice, resulting in a higher amount of water being captured. Therefore, the value of C_d became larger, as C_d is proportional to the amount of water being intercepted. This is one of the reasons why street inlets, especially the manhole covers, are designed with surface roughness surrounding the inlet bed. Not only its existence will intercept more water, but also to avoid slipperiness. In addition, Stephenson (1981) reported that a rough surface would become dry quickly, therefore reducing the amount of water spread on the road.

Figure 4.3: C_d/C_{do} versus Froude number, F for orifices in the channel

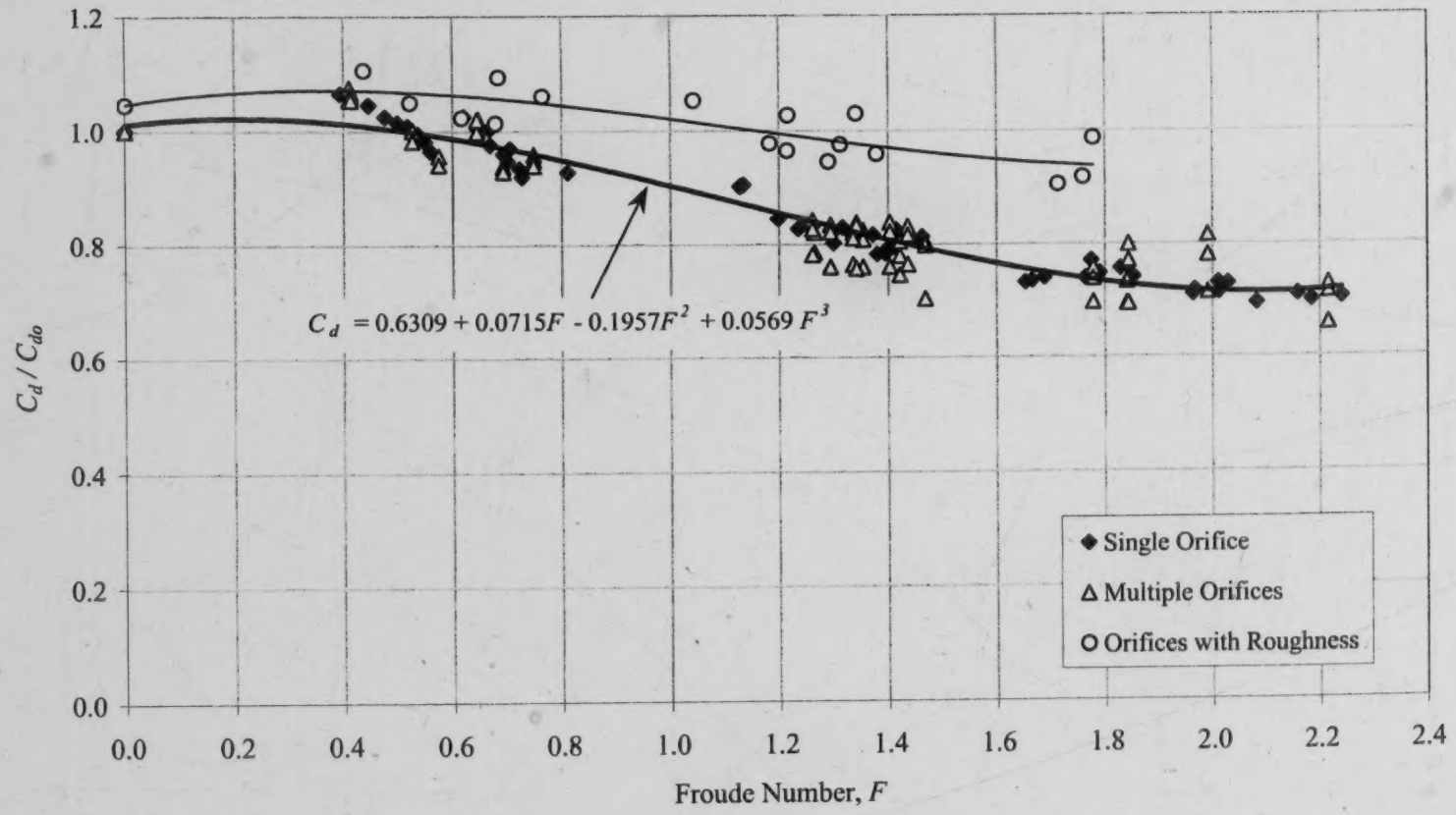

4.3.2 Average Depth Above the Inlet, $\bar{y}$ as the Head

This section presents results obtained from C_d computation by using the average depth above the inlet, $\bar{y}$ as head. The corresponding C_d for this method is referred to as C_d'. The method was selected by directly applying the principle of the orifice equation, in which the equation requires depth of water above the orifice as head. However, only the average depth was applied as head in the inlets computation because the water surface profiles above the inlet at any section changed significantly from one point to another.

It is important to first understand some significant patterns of the water surface profiles observed above the inlets. Generally, the profile decreases from the upstream to the downstream section of the inlet. However, this hypothesis cannot be true for all cases especially in the case of low flows. This is explained in the example given. As all inlets produced similar behavior, only inlet F-51 is included in the discussion. Figure 4.4 is a picture of street inlet F-51 at low discharge (Q = 2.72 L/s and S_o = 0%). From the picture, it is obvious that the water surface profile above the inlet, especially at the downstream section, produced a unique trend. As it was not easy to define the exact pattern by only referring to the picture, the profiles were critically studied and represented in other simpler forms.

Figure 4.5 is a sample of the profile sketch with depths written on it. These depths were found inconsistent everywhere. Another way to understand the profiles was by plotting the water surface cross sections above the inlet, as shown in Figure 4.6. Figure 4.4 to 4.6 reveal that the trend of flow changed drastically once it entered the inlet. It started to decrease from the upstream inlet section to nearly zero in the inlet middle area. However, when the water flowed closer downstream, a ridge formed at the downstream section of the inlet. Further description on ridge is presented in section 4.4.3. Owing to the formation of ridge, water depths near downstream of the inlet increased.

Due to this significant change in depth, it was more convenient to select the average depth above the inlet as head for the orifice equation. Figure 4.7 to 4.10 are C_d' plots for different street inlets. It can be seen from these figures that the data were scattered. Some data were located above and below the other grouped data.

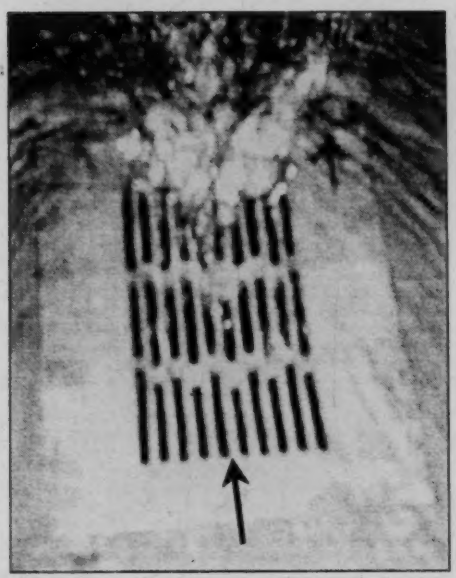

Figure 4.4: Photograph of flow above street inlet type F-51 at low discharge (Q = 2.72 L/s and S_o = 0%)

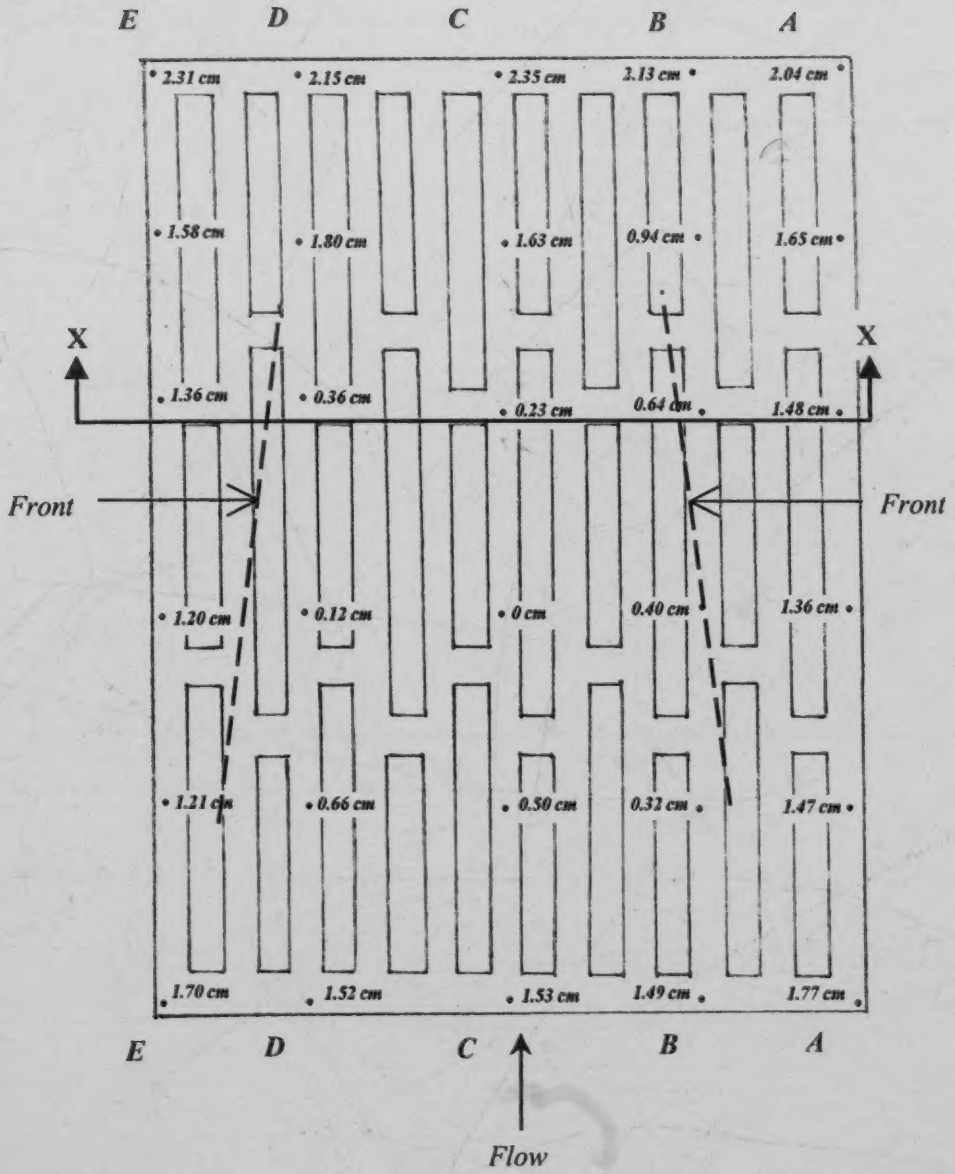

Section X-X

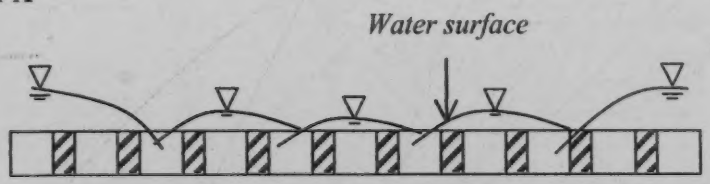

Figure 4.5: Sample profile above street inlet type F-51 at low discharge (Q = 2.72 L/s and S_o = 0%)

Figure 4.6: Cross sections of water surface profile for street inlet type F-51 at low discharge (Q = 2.72 L/s and S_o = 0%)

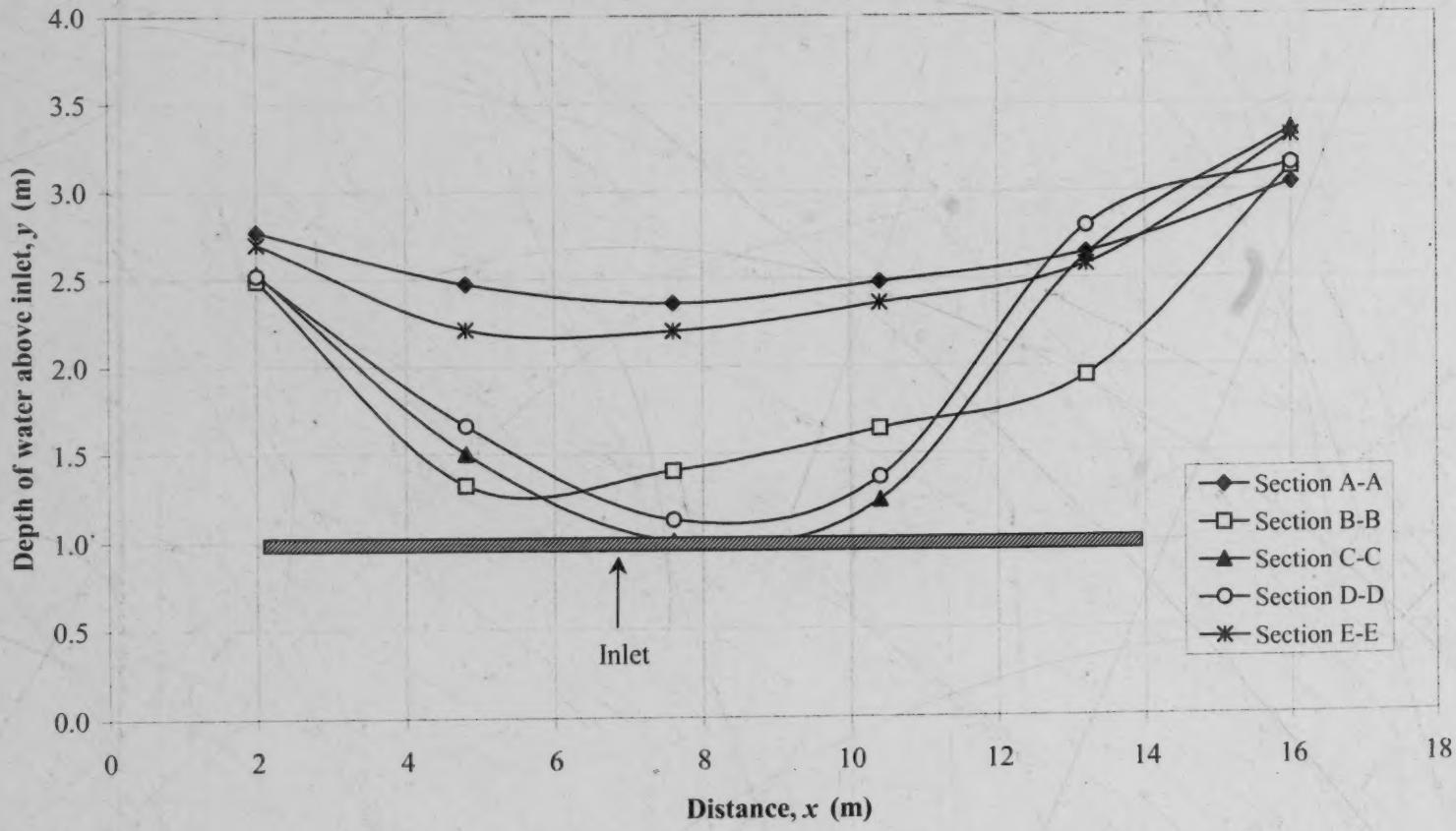

From these figures, inlet type F-51 produced ranged of C_d' between 0.39 to 0.89 and inlet NF80-Slotted Lid from 1.2 to 2.4. As for inlet #6B(F-39), two inlet configurations were tested; inlet located normal and parallel to the approach flow. The former produced C_d' in the range of 0.8 to 1.6 while the latter 1.1 to 1.9. All values obtained from the inlets studies were considered to be large compared to C_d obtained from the orifice-oriented inlet. Due to this large values as well as the scattered pattern formed in the plots, serious discussion were given to any possible factors that could influence the results.

The most significant reason that could possibly describe such results was the existence of area without complete flow-cover during the experiments. This can clearly be seen when the flows were low. Area without complete flow-cover was formed when the flows were mostly intercepted by the openings located closer to the upstream section, leaving the middle and other parts of the inlet uncovered. When the inlet was not completely covered, the average depth computed became smaller. Since C_d in equation 2.10 is inversely proportional to the head in the orifice equation, small heads would give higher C_d values. This is the reason for some data with higher value of C_d' were found to be somewhat above the other grouped data. To illustrate the description of this behavior, a plot showing the discrepancy between flow with and without complete flow-cover is shown in Figure 4.11 for inlet F-51.

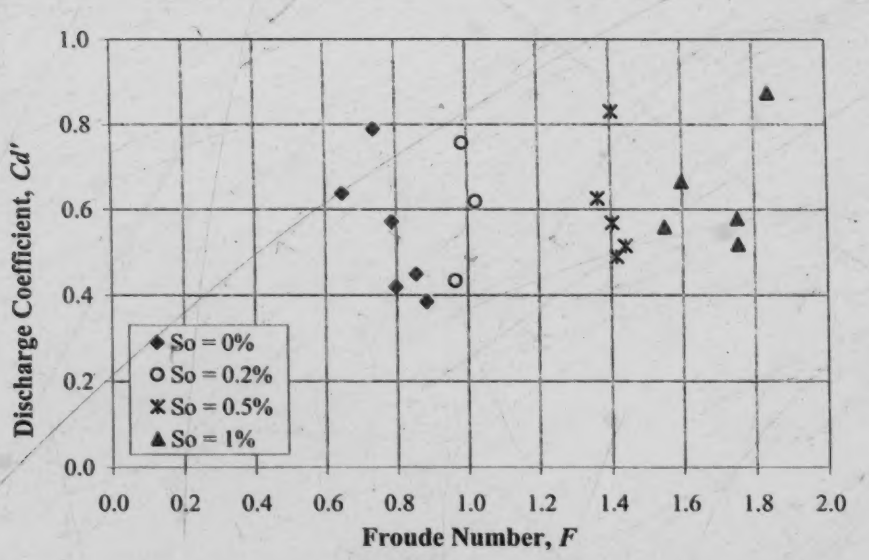

Figure 4.7: Discharge coefficient, C_d' versus the Froude number, F for street inlet F-51

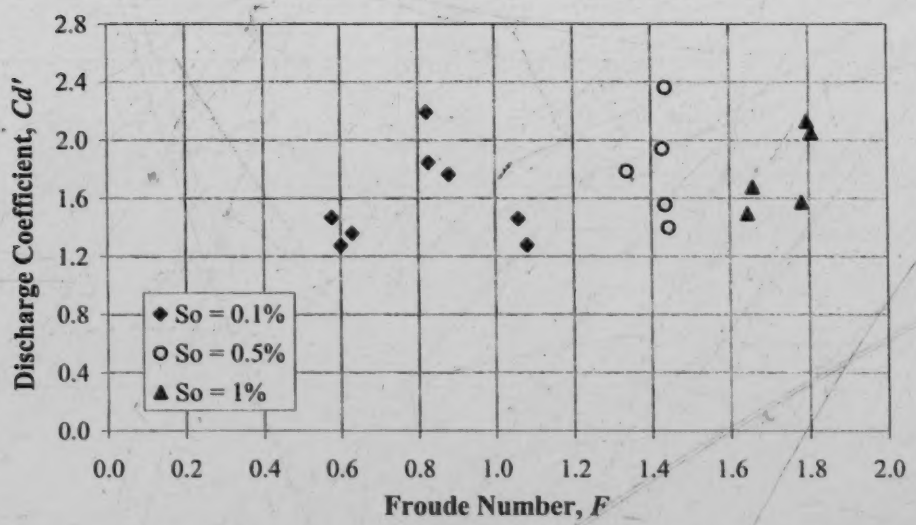

Figure 4.8: Discharge coefficient, C_d' versus the Froude number, F for street inlet NF80-Slotted Lid

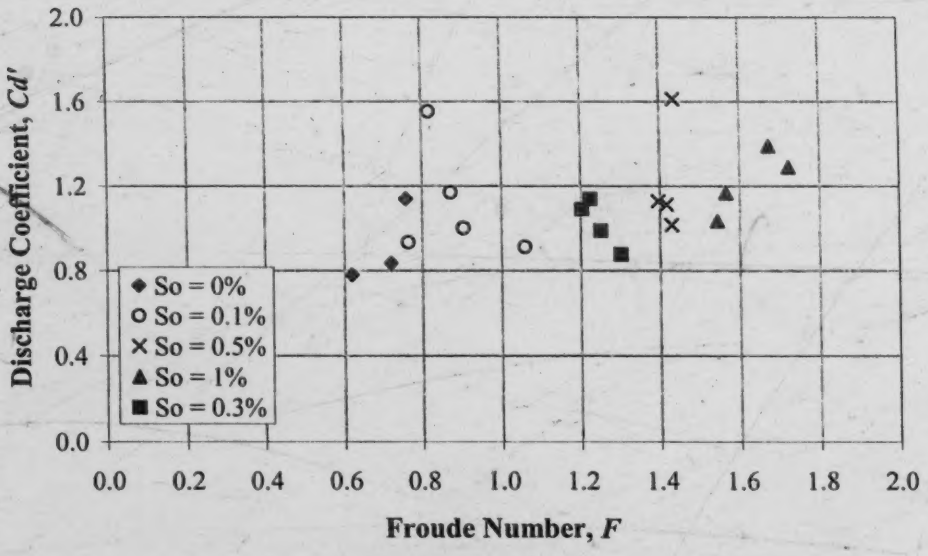

Figure 4.9: Discharge coefficient, C_d' versus the Froude number, F for street inlet #6B(F-39) normal to the flow

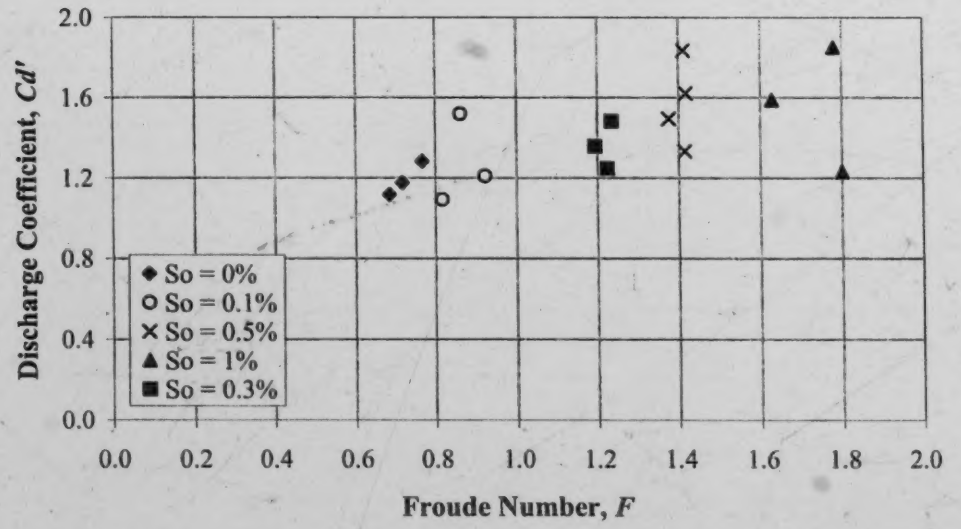

Figure 4.10: Discharge coefficient, C_d' versus the Froude number, F for street inlet #6B(F-39) parallel to the flow

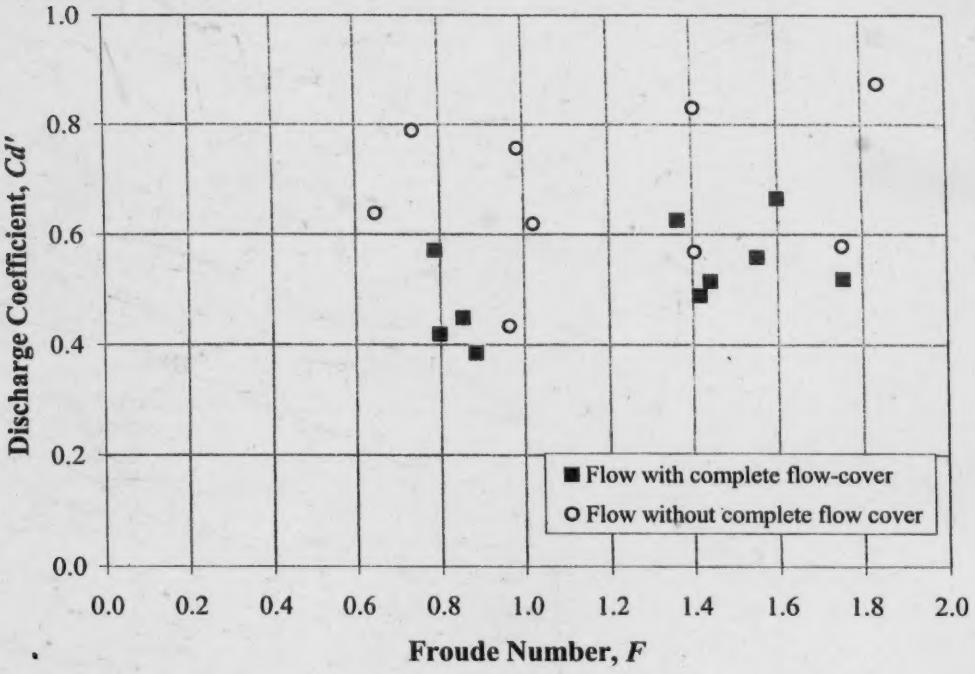

Figure 4.11: Comparison between C_d' for flow with and without complete flow-cover for inlet F-51

Percentage of the uncovered area can be interpreted by defining the ratio of opening area to the total area as written in equation 4.4.

$$a' = \frac{Area\ of\ Opening\ (m^2)}{Total\ Area\ (m^2)} \text{ x } 100\% \qquad (4.4)$$

In order to determine the influence of flow without complete flow-cover to the average water depth $(\bar{y})$, it is necessary to compare $\bar{y}$ with average depth measured in the area of flow with complete flow-cover, $\bar{y}'$. Figure 4.10 is an illustration of $\bar{y}$ and $\bar{y}'$ while Table 4.1 summarizes some data taken in the inlet F-51 study. This table compares water depths measurement between $\bar{y}$ and $\bar{y}'$.

It can be seen from the table that $\bar{y}'$ produced higher depths compared to $\bar{y}$. In order words, $\bar{y}'$ would result in a smaller C_d' than the one obtained from $\bar{y}$. The difference between $\bar{y}$ and $\bar{y}'$ can be computed from equation 4.5 and it was found that $\Delta\bar{y}$ was in the range of 10% to 50% for low flows between 2 L/s to 8 L/s.

$$\Delta\bar{y} = \frac{\bar{y}'-\bar{y}}{\bar{y}} \text{ x } 100\% \qquad (4.5)$$

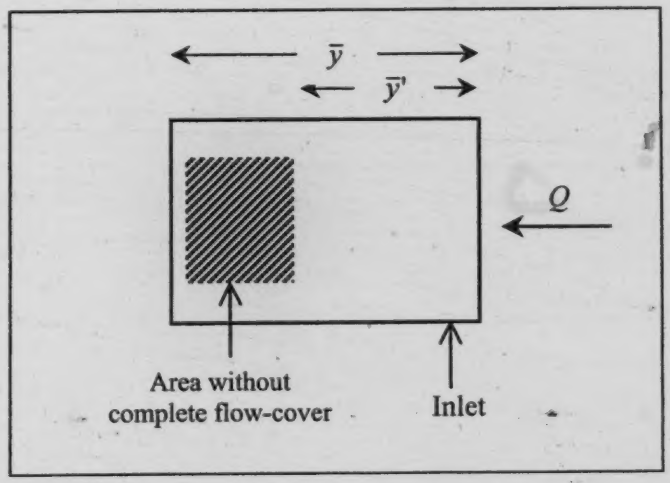

Figure 4.12: $\bar{y}$ and $\bar{y}'$ as the average depth above the inlet

Experiment	*Uncovered Area Ratio, a' (%)*	$\bar{y}$ *(cm)*	$\bar{y}'$ *(cm)*	$\Delta\bar{y}$ (%)
Q_o = 6.72 L/s, S_o = 0%	6.2	1.06	1.18	11.3
Q_o = 2.72 L/s, S_o = 0%	42.2	1.26	1.60	27.0
Q_o = 6.48 L/s, S_o = 0.5%	8.9	1.01	1.29	27.7
Q_o = 7.88 L/s, S_o = 1%	5.8	1.15	1.42	23.5
Q_o = 4.28 L/s, S_o = 0.2%	24.1	1.05	1.34	27.6
Q_o = 5.48 L/s, S_o = 0.2%	18.2	0.79	1.17	48.1

Table 4.1: Comparison between $\bar{y}$ and $\bar{y}'$

4.3.3 Approach Depth, y_a as the Head

A concern arises when dealing with the average depth above the inlet as the head for C_d computation. In the field, it is not always easy to control and predict depth above the inlet as there are many unexpected factors happening along the way. Debris, traffic and pedestrians are examples of disturbances that might contribute to the performance of a street inlet. Not only that, it is more convenient for an engineer to focus on water behavior at the upstream channel before the inlet is placed. In other word, the criteria of the approach flow are the main consideration when designing a desired inlet. By knowing the hydraulics of the approach flow, engineers take into account any circumstances that might take place at the upstream section of the inlet. This method is good as it has the ability to control the allowable depth at the curb and avoid severe ponding from happened. In addition, as mentioned earlier in Chapter 2, Moss and Townsend (1980) reported that it was not practical to measure depths above the inlet because

of the unstable water surface profiles. With regard to the reasons highlighted above, the approach depth located 1ft upstream of the inlet was taken as head for C_d computation. This depth was referred to as y_a and the corresponding C_d was addressed as C_d''. Figure 4.13 to 4.16 are C_d'' plots obtained for different street inlets. Inlet F-51 produced ranged of C_d'' from 0.3 to 0.6, NF80-Slotted Lid from 1.2 to 1.6, #6B(F-39) located normal to the flow from 0.6 to 1.2 and the same type parallel to the approach flow from 0.8 to 1.5.

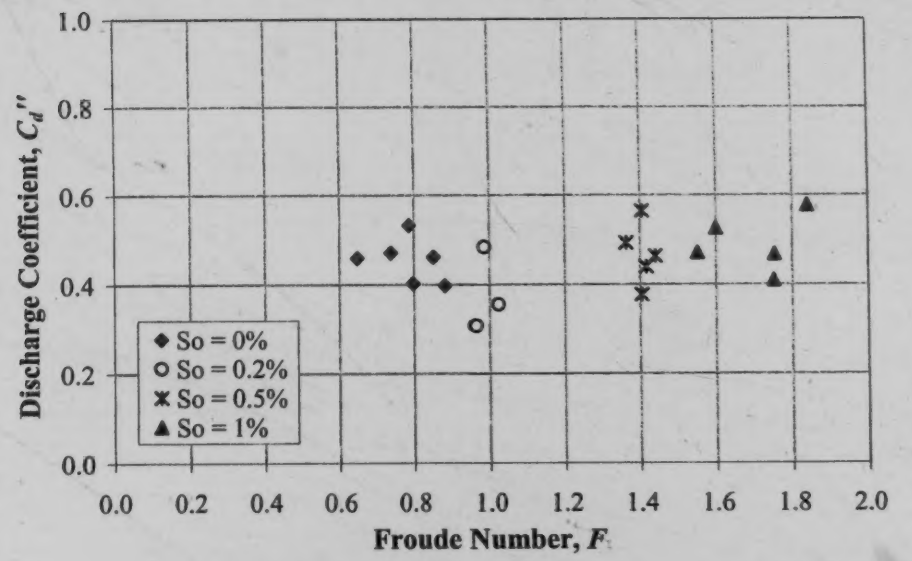

Figure 4.13: Discharge coefficient, C_d'' versus the Froude number, F for street inlet F-51

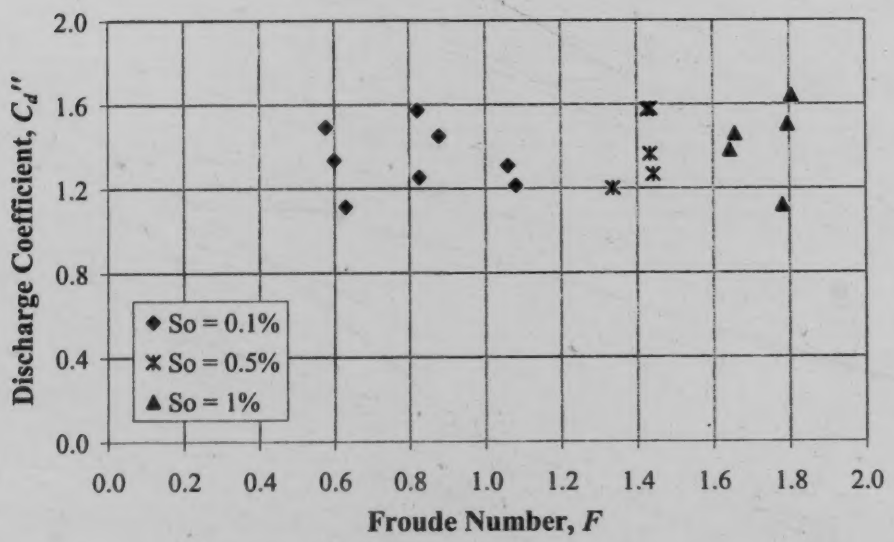

Figure 4.14: Discharge coefficient, C_d'' versus the Froude number, F for street inlet NF80-Slotted Lid

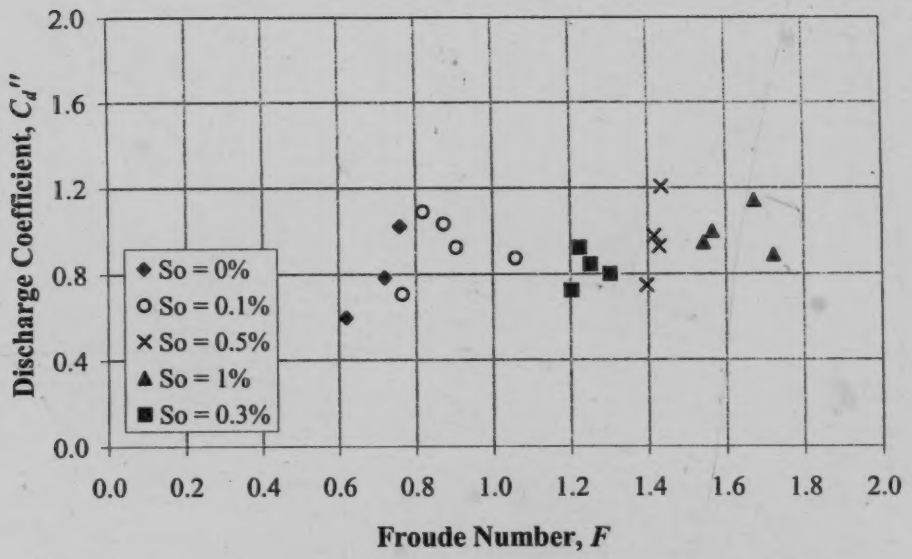

Figure 4.15: Discharge coefficient, C_d'' versus the Froude number, F for street inlet #6B(F-39) normal to the flow

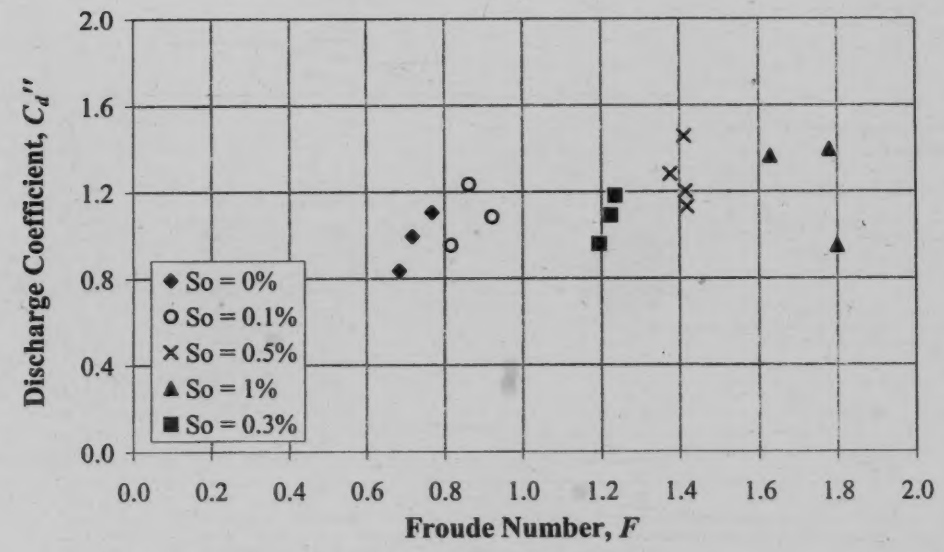

Figure 4.16: Discharge coefficient, C_d'' versus the Froude number, F for street inlet #6B(F-39) parallel to the flow

4.3.4 Approach Specific Energy, E_a as the Head

Specific energy has always being used to describe spatially varied flow with decreasing discharge, which is the case of flows through the street inlets. It is a big advantage for engineers to use the specific energy principles when designing street inlets as they could predict not only the water depth of the approach flow, but also the velocity for that section. Therefore, engineers will be able to design the allowable water depth that corresponds to desired flow velocity. The third method applied the specific energy at the approach flow that was located 1ft upstream of the inlet as the head. The specific energy term which consist of the velocity and depth is given by the equation,

$$E_a = y_a + \frac{v_a^2}{2g} \tag{4.6}$$

where E is the specific energy y is the depth of water, v is the velocity, g is acceleration due to gravity and subscript a refers to the approach flow in the channel.

Figure 4.17 to 4.20 presents discharge coefficients plots obtained for different street inlet. For convenience, the term C_d''' was applied to define the discharge coefficient. From these figures, it was found that inlet F-51 produced C_d''' that ranged from 0.25 to 0.45, NF80-Slotted Lid from 0.7 to 1.4, #6B(F-39) located normal to the flow from 0.6 to 0.9 and the same type parallel to the approach flow from 0.7 to 1.0.

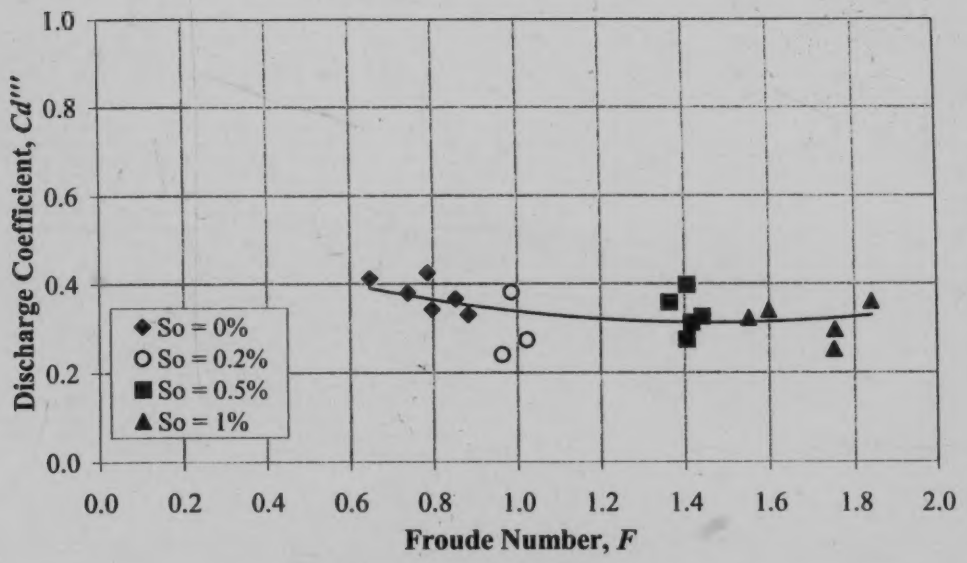

Figure 4.17: Discharge coefficient, C_d''' versus the Froude number, F for street inlet F-51

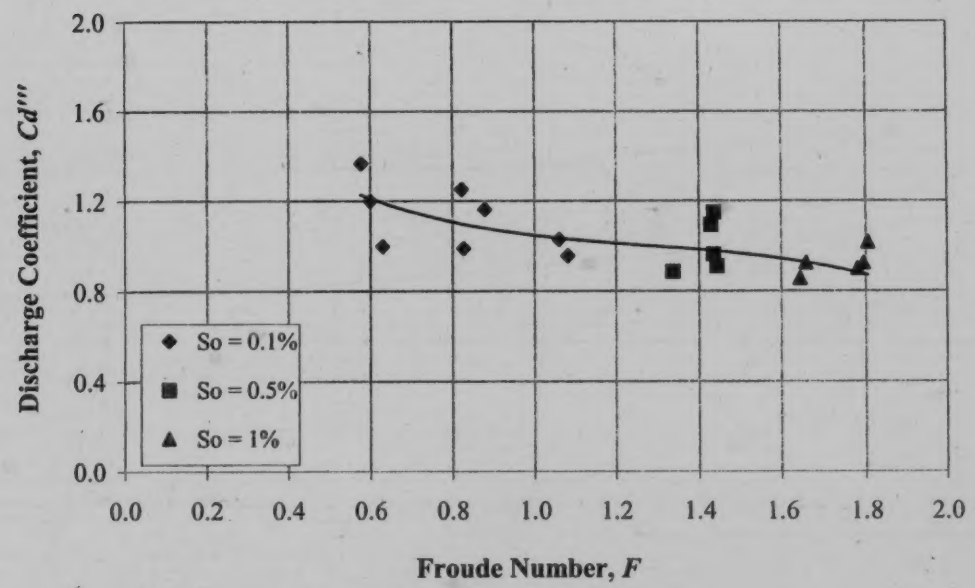

Figure 4.18: Discharge coefficient, C_d''' versus the Froude number, F for street inlet NF80-Slotted Lid

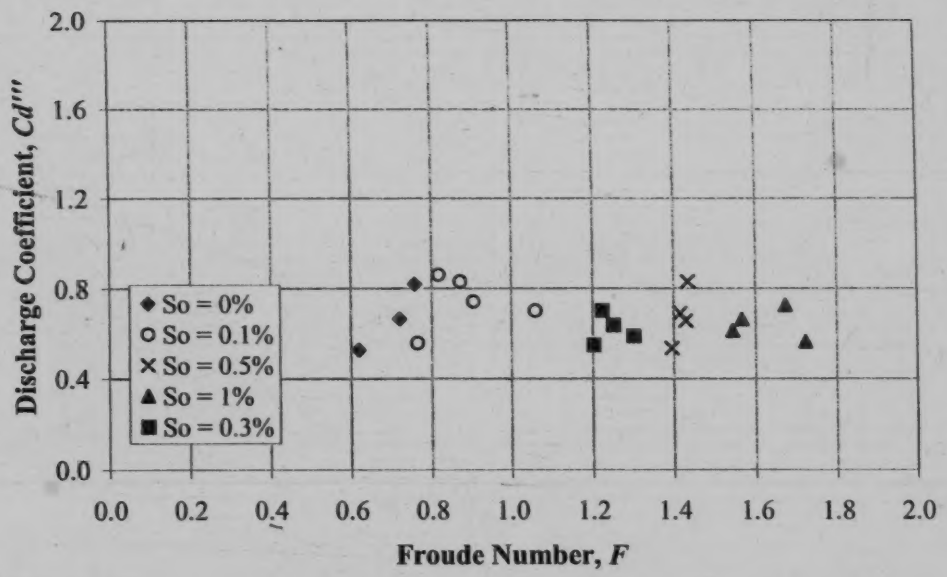

Figure 4.19: Discharge coefficient, C_d''' versus the Froude number, F for street inlet #6B(F-39) normal to the flow

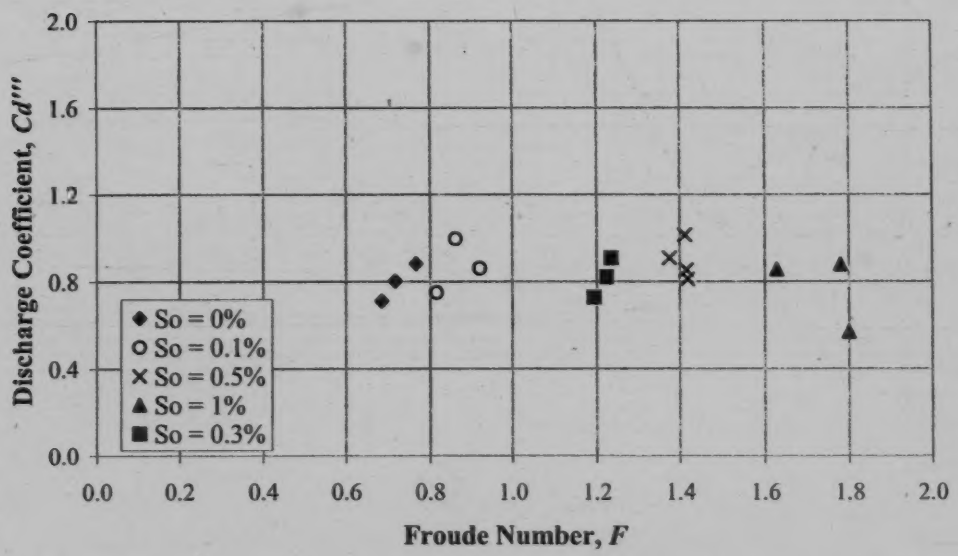

Figure 4.20: Discharge coefficient, C_d''' versus the Froude number, F for street inlet #6B(F-39) parallel to the flow

4.3.5 Comparison Between C_d', C_d'' and C_d'''

Previous sections have presented variations of discharge coefficients obtained from three different methods. The significant difference between these methods were clearly seen when all methods were compared. The head computation was the main reason for this disparity to take place. From the literature we found that earlier studies emphasized more on depths measurements near the ponding area. However, results obtained from this study have proved that flows in the gutter encountered similar problems to that in the sump. Therefore, comparisons should be made between C_d', C_d'' and C_d''' in order to understand the characteristics of heads for street inlets in the gutters.

The first attempt was to make qualitative comparison on these plots by looking at the range of C_d obtained for each method. Data from C_d' plots were found to have the largest values. Not only that, the plots seemed to be widely scattered. C_d'' on the other hand, produced less scattered pattern with smaller C_d range compared to C_d' obtained earlier. Apparently, y_a as the head gave better correlation with the discharge coefficient. Surprisingly, data obtained from studies involving E_a as head produced the least scattered pattern among other methods. C_d''' range were found to be the smallest compared to C_d' and C_d''. As a result, it is believed that the specific energy method provides the best correlation with the inlet discharge coefficients. This result in a way supports the principle of constant specific energy in the bottom inlets as reported by Chow (1959) but disproves the method proposed by Moss and Townsend (1980).

Even though qualitative analyses showed that the specific energy methodology was good, it is important to analyze the results from the statistical point of view. Statistics analyses would best explain the data in a simpler way. In this study, the mean and standard deviation were computed to provide a better understanding on the behavior of the discharge coefficients.

Table 4.2 summarizes the mean and standard deviation for coefficients obtained from these three methods.

Properties / Street Inlet	C_d'		C_d''		C_d'''	
	$\overline{C_d}$'	S_{Cd}'	$\overline{C_d}$''	S_{Cd}''	$\overline{C_d}$'''	S_{Cd}'''
F-51	0.59	0.14	0.46	0.07	0.34	0.05
NF80-Slotted Lid	1.70	0.33	1.38	0.16	1.02	0.16
#6B(F-39): Normal to Flow	1.11	0.22	0.91	0.15	0.67	0.10
#6B(F-39): Parallel to Flow	1.40	0.24	1.14	0.18	0.84	0.11

Table 4.2: Statistical analyses on the discharge coefficients

The table shows that mean discharge coefficients, $\overline{C_d}$ for all inlets decreased from the first to third method. For example, $\overline{C_d}$' for inlet F-51 was 0.59 in the first method, decreased to 0.46 when the second method was applied and even drastically changed to 0.34 when E_a was substituted as the head. Similar trend was found in the standard deviation as well. The standard deviation for C_d' was found to be 0.14, decreased to 0.07 in the C_d'' computation and 0.05 in C_d'''. When the standard deviation becomes small, the data is highly precise. The data became more concentrated in a smaller domain as they were close to each other. Apparently, the third method rearranged and reproduced a more stable variation of C_d.

Discussions on the difference in the discharge coefficients for the four inlets are also included in this section. However, from here beyond, emphasize is only given to the third method, i.e. the C_d''', as the method was found to provide more reliable results. $\overline{C_d}$''' for inlet F-51 was found to be the smallest with value of

0.34 even though it had the largest opening area. It is true that bigger opening area will intercept more water but for this case, its length was larger than width, in which low flows could hardly reach this section. It is noted that inlet with wider width is better than inlet with longer length. Therefore, under certain circumstances, large inlet opening should not be assumed to provide larger C_d. On the other hand, NF80-slotted lid was found to have the biggest mean and standard deviation. Even though the opening area between NF80-slotted lid and #6B(F-39) were almost the same, the difference in the C_d computation was large. This was due to the inlet bar pattern and configuration. The bar orientation in NF80-slotted lid was concentric circular slots while #6B(F-39) was a circular inlet with longitudinal or transverse bars oriented (with respect to the approach flow), depending on the location of the inlet in the channel. The unique pattern of NF80-slotted lid was believed to make it more efficient to intercept more water. Even though the discharge coefficient was considered to be large, it might give a great advantage to engineers, as it is not necessary for them to design a high design (theoretical) flow. The coefficient itself will provide higher value in the actual flow. $\overline{C_d'''}$ obtained for inlet #6B(F-39) that is placed normal to the flow was found to be smaller that the one located parallel to the flow. As reported in the literature, inlets with parallel or longitudinal bars were more efficient than the one with transverse-oriented bars. Therefore, the difference in the results between these two types was reasonably accepted.

It can also be noticed that Froude numbers that are less than 0.6 was not included in the plots. This was due to some limitations in the laboratory set up. Since flows for this region could not be experimented freely by using the initial set up, a tailgate was used for low discharges in order to complete the Froude number range. However, the occurrence of backwater from the downstream channel affected the flow above the inlet. This disturbance formed water circulation above the inlet. Section 4.4.5 illustrates the behavior of circulation profiles in detail. Some discrepancies were observed in the C_d plots obtained from this

method when compared to the original C_d variations that were free from tailgate. The results therefore were not included in the analysis.

It is also interesting to predict the variation of C_d for each inlet regardless of the incomplete range of the Froude numbers. With reference to the C_d variation obtained from the orifice-oriented inlet, C_d was expected to decrease with Froude number in the subcritical region, which extended to the supercritical region, until a constant value was attained. With this hypothesis, similar pattern was observed in C_d''' plots especially for inlet F-51 and NF80-slotted lid, in which this pattern is described by the sketch lines. However, inlet #6B(F-39) showed a very mild decreasing trend that was almost constant for most of the Froude numbers.

4.3.6 Efficiency (η)

Efficiency is another way of describing the performance of an inlet, as it is impossible to measure its effectiveness qualitatively. The efficiency is denoted as the capability of the inlet to intercept water and is written as a ratio described below,

$$\eta = \frac{Q_i}{Q_o} \times 100\% \qquad (4.7)$$

where η is the efficiency, Q_i is the intercepted flow and Q_o is the total flow. Figure 4.22 shows efficiency computed for multiple inlet studies. From the figure it can be seen that efficiency decreased when the total flow increased. This trend agrees with results obtained from Bouchard and Townsend (1984) and Rajaratnam (1992) studies. As discussed earlier in the literature, it is not easy for the inlet to intercept water when the flow is large because of its high velocity. Most flows pass the inlet as carryover flows. Therefore, the ability of the inlet to intercept water diminishes.

In general, the inlets were able to intercept up to 60% of the total flow. This condition is considered to be good regardless of the non-actual roadway model designed in the laboratory. In order to understand the efficiency plot, an example is given for Q_o that is equal to 0.025 m^3/s. From the figure, NF80-slotted lid intercepted the highest with 23% of the total flow, whereas inlet #6B(F-39) (normal to the flow) captured the least with only 13%. On the other hand, F-51 and #6B(F-39) (parallel to the flow) showed better performance than #6B(F-39) (normal to the flow) with 18% interception.

Indirectly, the plot also compares the effectiveness of these inlets. NF80-slotted lid with high efficiency was the most efficient inlet among others. This behavior in a way explains the high C_d values obtained earlier. As for F-51, even though earlier results revealed that its C_d values were the smallest, it was more efficient than inlet #6B(F-39). Comparison is also made between inlet type #6B(F-39) that was located parallel to the flow and the one located normal to the flow. The former showed better performance than the latter. As explained earlier in the previous sections, inlet with parallel bars is more efficient that the one with transverse bars.

Figure 4.23 also explains the efficiency for all inlets by means of comparing the amount of water that can be intercepted for a certain approach flow. The line 100% efficiency corresponds to a condition where the flow in the channel is fully intercepted. From the figure, it can be seen that at the beginning Q_i increased slightly as the total flow increased, until Q_o reached 0.015 m^3/s. However, beyond this value, Q_i appeared to be almost constant by only capturing 0.005 m^3/s of the flow. This behavior indicates that the inlets were not able to intercept more flow as the total flow increases. Therefore, when Q_o was more than 0.015 m^3/s, the approach flows insignificantly affects the performance of the inlets. Other factors were believed to give more influences than the approach flow itself. The experimental set-up might be one of the major factors, followed by the inlet configuration and the inlet opening area.

Since the study did not cover a roadway model, the efficiency plots discussed above could not completely describe the actual inlets performances on the road. A modified efficiency which is referred to as η' is introduced in this study in order to roughly estimate the actual inlets efficiency. However, to apply η', it is necessary to understand the principles of widths between the channel model and the street. By referring to Figure 4.21, the total spread of water on the road, T can be referred to as the laboratory channel width, B. The efficiency in the area of T is defined as η, in which its discussion has been presented earlier. In the roadway model, the approach flow is normally expected to flow within the grating lane with small amount of carryover flow. Grating lane according to Rajaratnam (1992) is defined as an area that covers the whole width of inlet, in which flow is mostly intercepted. Therefore, the efficiency is normally measured within the grating lane. In our case, the grating lane is equal to W and the efficiency is modified to,

$$\eta' = \frac{Q_i}{\frac{Q_o}{B} x W} \tag{4.8}$$

Or,

$$\eta' = \frac{Q_i}{Q_o} \text{ x } \frac{B}{W} \tag{4.9}$$

Which can be simplified as,

$$\eta' = \eta \text{ x } \frac{B}{W} \tag{4.10}$$

where η' is the modified efficiency, η is the efficiency computed in equation 4.7, W is the width of the grate inlet and B is the width of the channel. Figure 4.24 shows the variation of η' to the total flow, Q_o. It can be seen from the figure that η' produced larger values, up to 250% compared to results obtained from η

computation. When the flow was restricted to the whole inlet width, all flows were mostly intercepted, resulting in a more efficient inlet performance. However, when the whole channel width was taken into consideration, there flows were unlikely fully intercepted, allowing carryover flows to occur. As a result, η' was found to be larger than η.

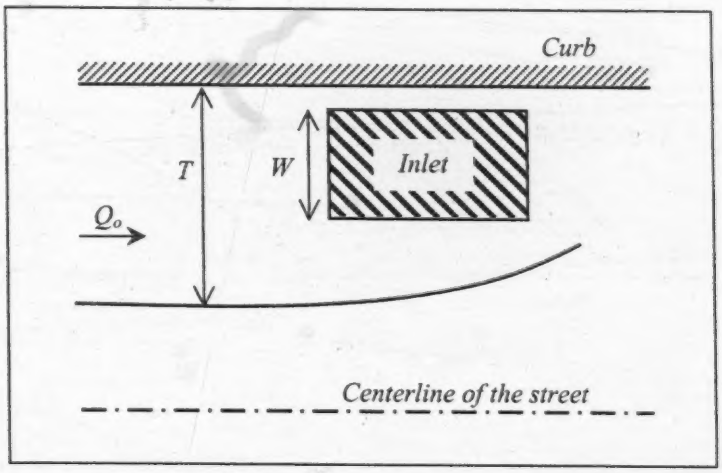

Figure 4.21: Plan view of gutter flow on the street

Figure 4.22: Efficiency, η (%) versus model total flow, Q_o (m^3/s) for multiple inlet studies

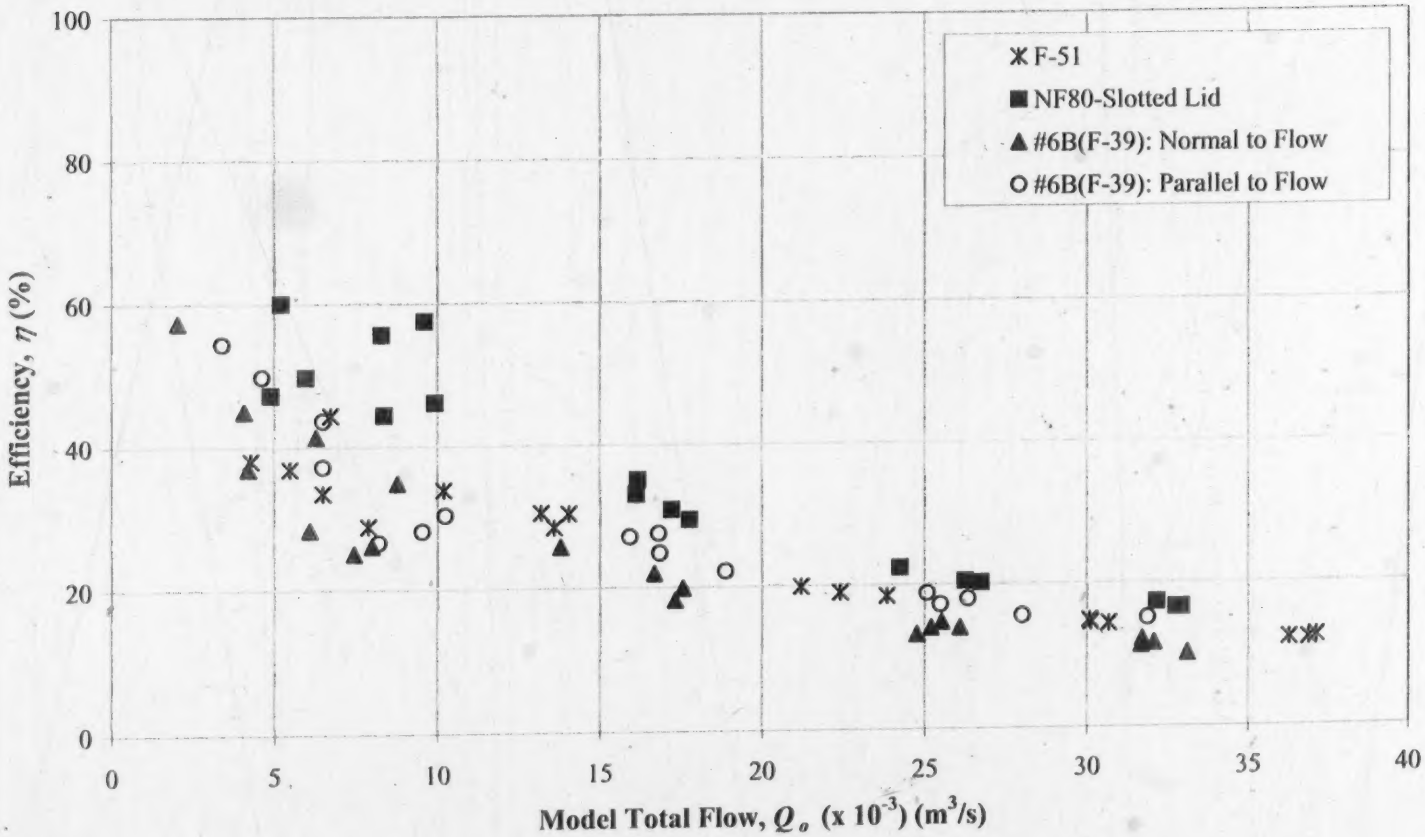

Figure 4.23:Intercepted flows, Q_i (m^3/s) versus model total flows, Q_o (m^3/s) for multiple inlet studies

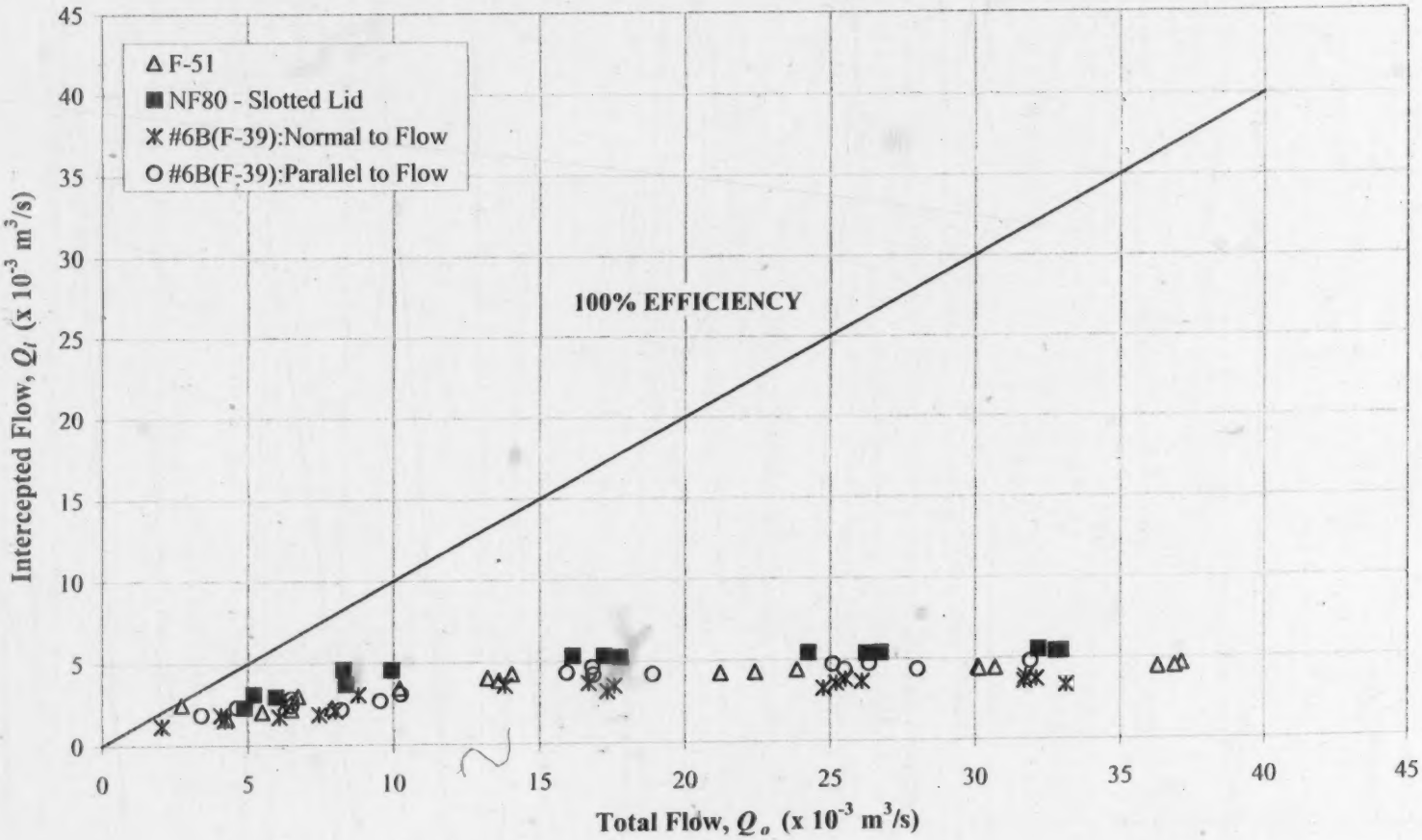

Figure 4.24: Modified efficiency, η' (%) versus model total flow, Q_o (m^3/s) for multiple inlet studies

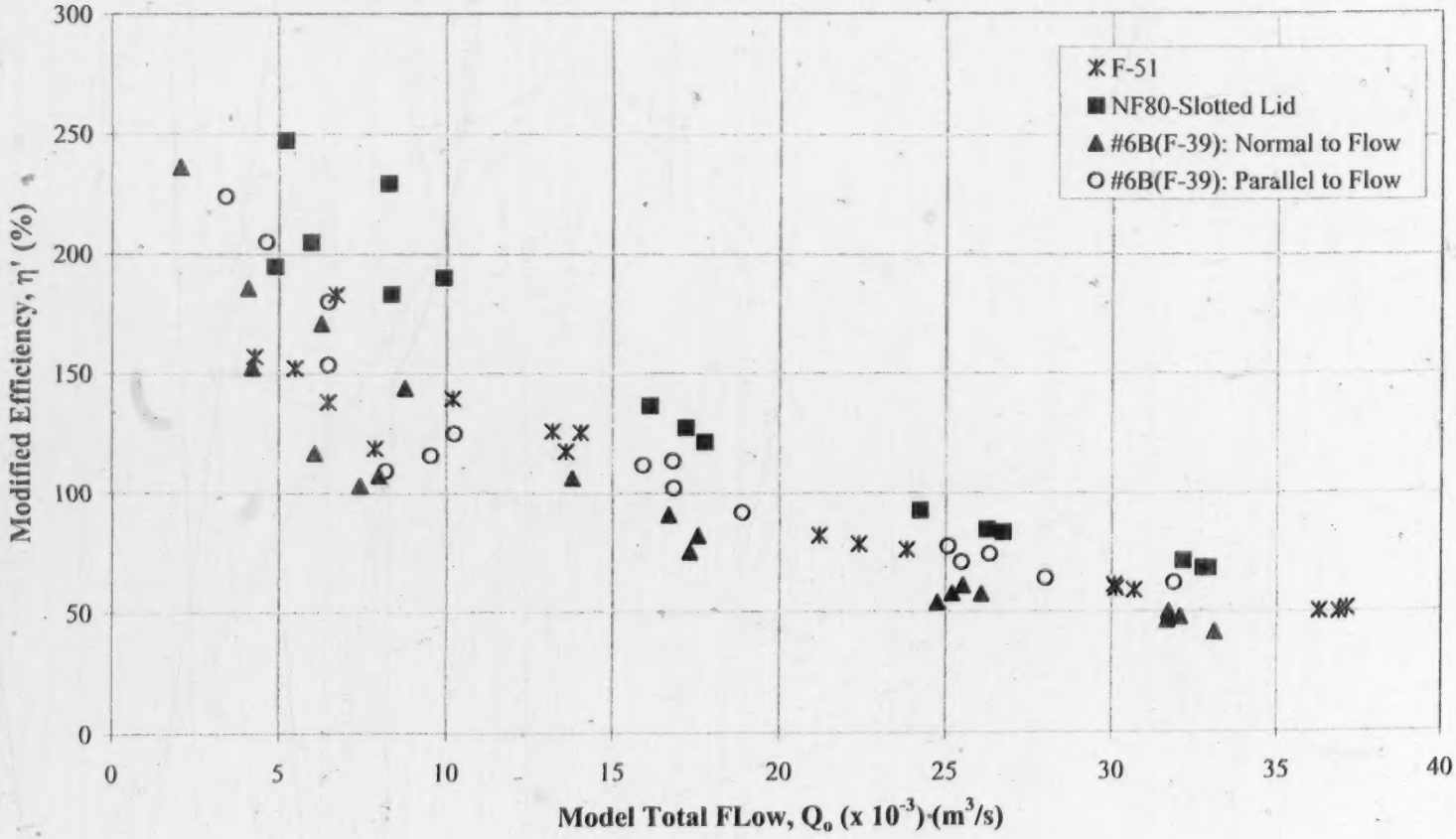

4.4 OBSERVATIONS

This section presents interesting observations made during the experiments, in which the discussions are grouped into two categories; the orifice-oriented inlet and street inlets. The effect of turbulences is explained in the former while the latter emphasized the flow characteristics.

4.4.1 Turbulences

If we recalled a single orifice study in section 3.4.2, orifice 1 *(O1)* and orifice 2 *(O2)* were experimented for orifice-oriented inlet located in the channel. *O1* was located closer to a head tank, producing turbulences at the beginning of the flume. On the other hand, *O2* was placed somewhere in the middle of the channel, which was far from the effect of turbulences. Figure 4.25 shows data obtained from *O1* study. Surprisingly, the variation of C_d with Froude numbers, F was still similar to the one obtained in *O2* regardless of the turbulences.

Turbulent flow is a complex flow with unpredictable characteristics. Its nature is random, nonlinear and it produces a great amount of eddies and air entrainment in the flow. It was thought that the complexity of turbulent flows might contribute to a more complicated analysis on the discharge coefficient of orifices in channels. However, from this observation we can say that the presence of turbulences above an orifice will not effect the original variation of C_d with Froude numbers. The complex nature of turbulent flows seemed to neglect any major impacts on the C_d computations. This observation is important, as most flows in the nature and engineering practice are turbulent.

Figure 4.25: C_d/C_{do} versus Froude number, F for single orifice in the channel study

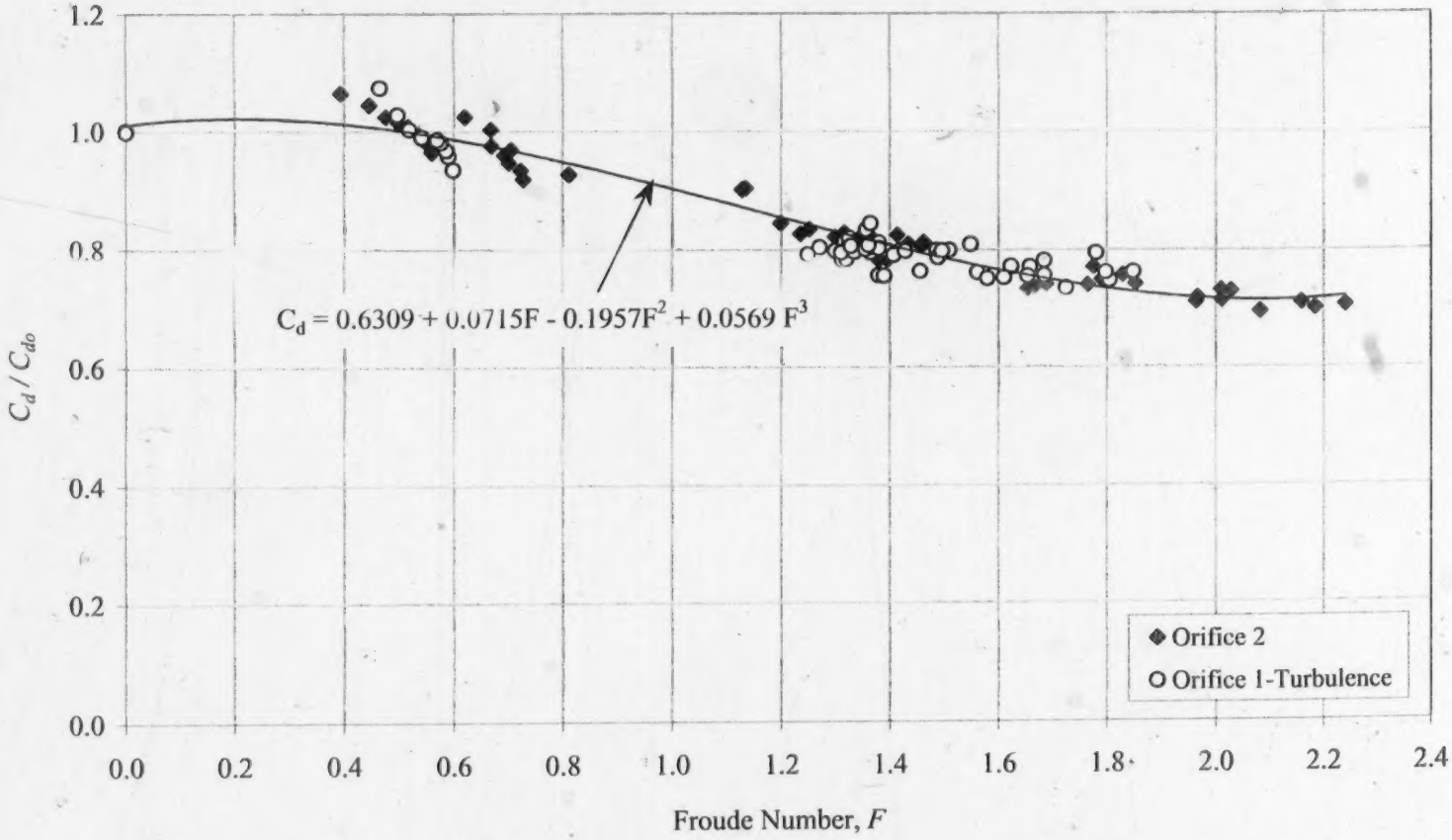

4.4.1 Ridge Characteristics

This section describes two types of ridges that were observed at the downstream section of the inlets. Knowledge of ridge characteristics is useful, especially to engineers, as any disturbances that take place at the downstream section of an inlet will give nuisance to traffic and pedestrians.

One important mechanism that formed ridges was front. Fronts were flows that were not intercepted directly by the inlet but moved from both sides of the inlet towards the middle. Its development was due to the difference in pressures and depths from the upstream towards the downstream section near the inlet area. Curvilinear flow at the inlet resulted in such behavior as the streamlines changed direction from parallel to the middle of the inlet. Not only the fronts, the carryover flows flowing above the inlet also contributed to the ridge formation.

Ridge in the form of undular occurred when the flows were subcritical whereas when the flows were supercritical the ridge became a wedge. Figure 4.26 (a) and 4.26 (b) are examples of undular ridge for subcritical flows observed in inlet F-51 while Figure 4.28 (a) and 4.28 (b) are pictures taken for wedge ridge in the supercritical flows. Their cross sections are attached in Figure 4.27 (a) and 4.29 (a). From these plots, it was found that the flow decreased from both sides to the middle when suddenly a peak formed at the center of the downstream inlet. Wedge ridge produced a higher peak than the undular ridge. Also, flows from both sides of wedge ridge formed a steeper slope compared to slope observed in the undular ridge. The fronts moved towards the center of the inlet with an angle developed near the sides of the inlet. This can be seen in Figure 4.26 (c) and 4.28 (c). The angles varied with flows and the types of inlet. In the studies, the angle was found to be in the range of 60° to 85°.

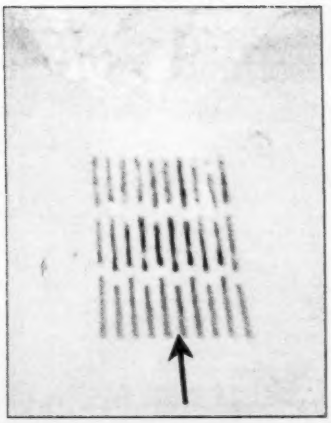

(a)

(b)

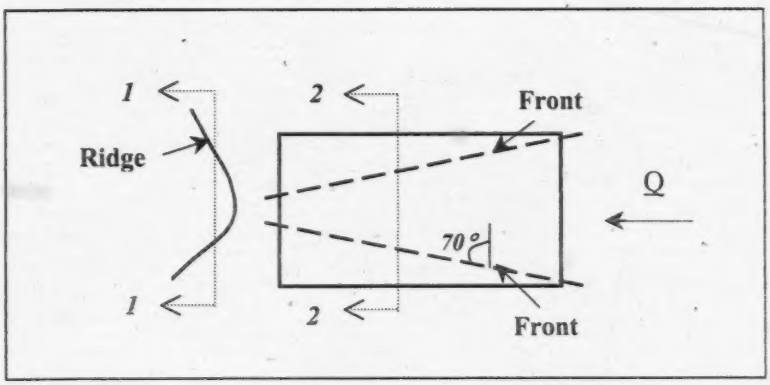

(c)

Figure 4.26: (a) Plan view (b) Side view (c) Sketch of subcritical flow for street inlet type F-51 at Q =5.32 L/s and S_o = 0.2%

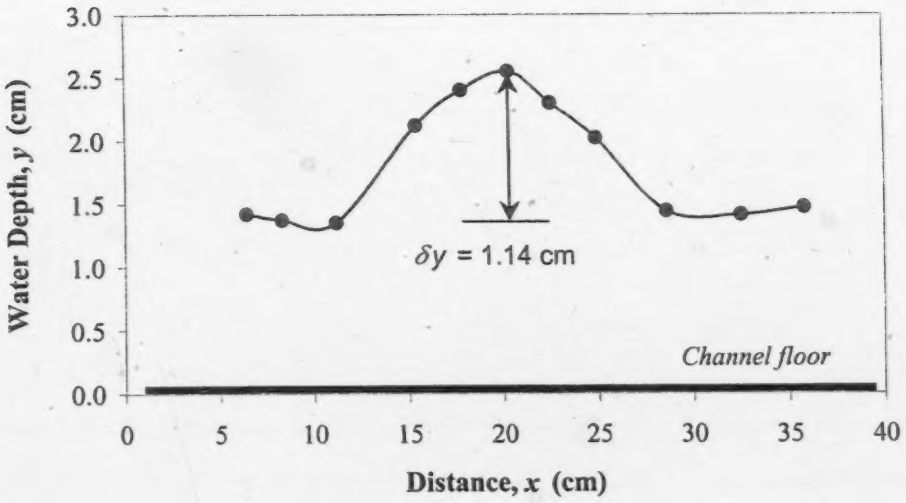

(a)

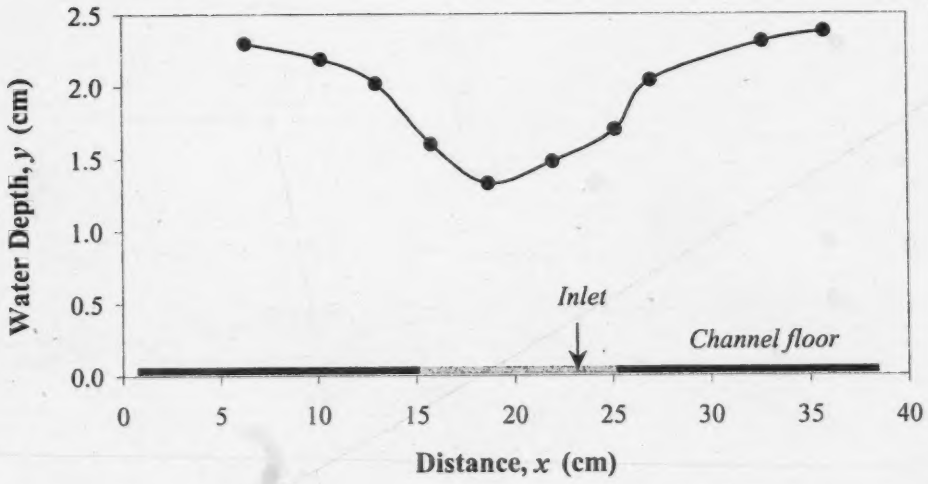

(b)

Figure 4.27: (a) Cross section 1-1 (b) Cross section 2-2 of subcritical flow for street inlet type F-51 at Q =5.32 L/s and S_o = 0.2%

(a)

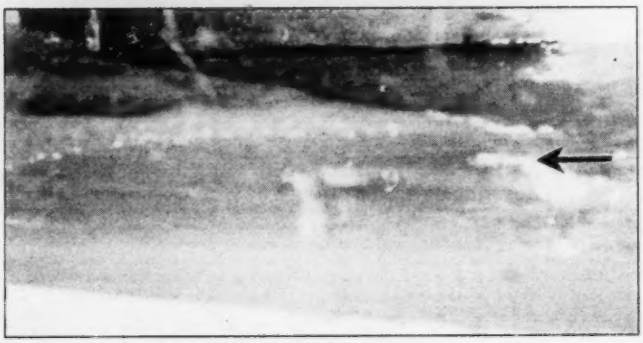

(b)

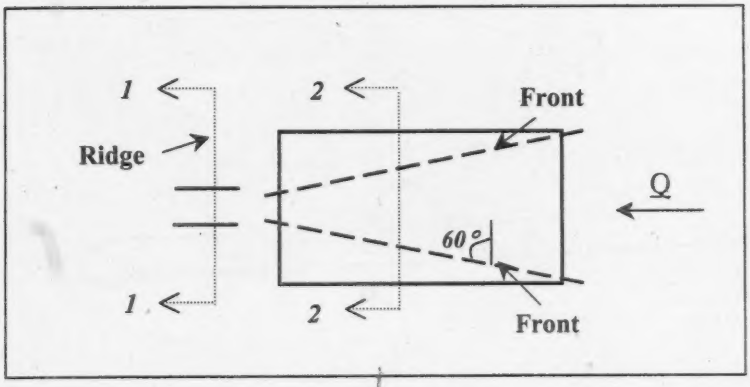

(c)

Figure 4.28: (a) Plan view (b) Side view (c) Sketch of supercritical flow for street inlet type F-51 at Q =21.08 L/s and S_o = 0.5%

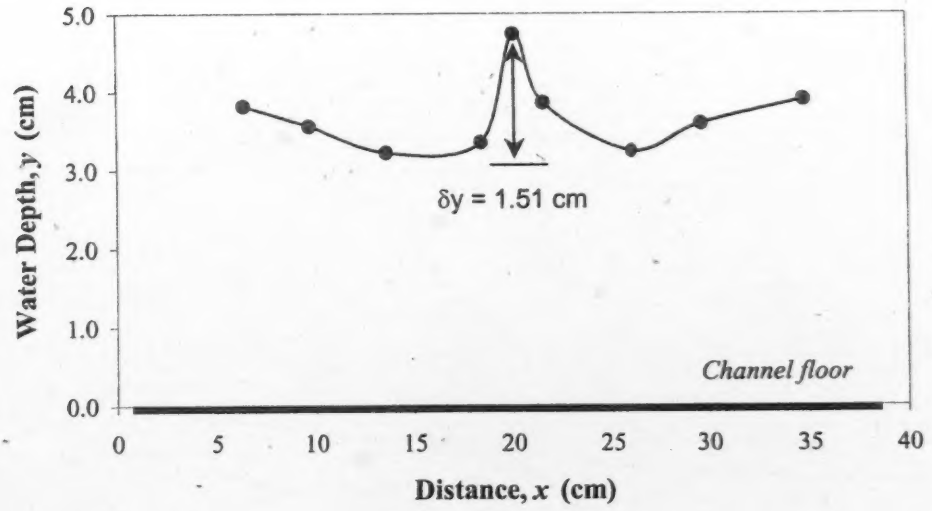

(a)

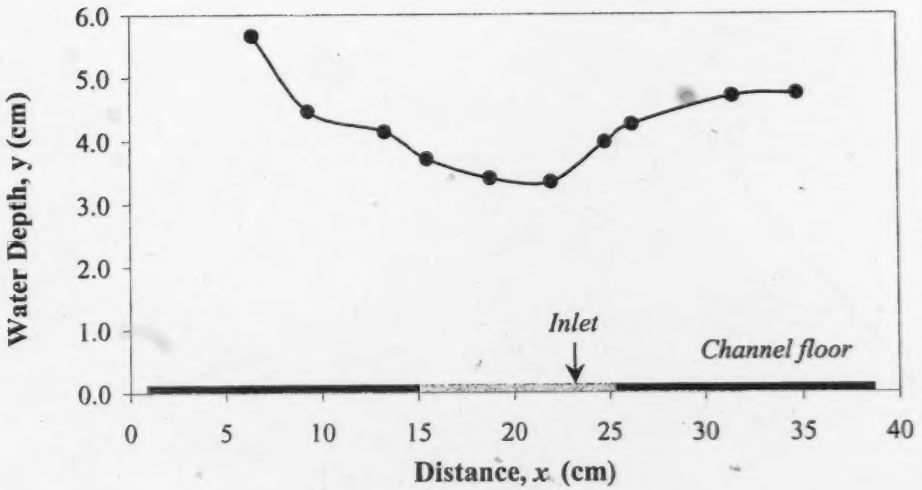

(b)

Figure 4.29: (a) Cross section 1-1 (b) Cross section 2-2 of supercritical flow for street inlet type F-51 at Q =21.08 L/s and S_o = 0.5%

Similar ridges formed by inlet F-51 as described earlier were also found in other inlets, in which the examples are given in Figure 4.30 and Figure 4.31. The pictures were detailed with their flow conditions, i.e. the approach flow (Q_o) and channel slope (S_o). In this study, the slopes were varied from 0% to 1% in order to obtain ranges of Froude numbers. The slopes, however, indirectly influenced the characteristics of ridges formed near the inlet. It is noticed that undular ridges in Figure 4.30 were formed by smaller slopes compared to wedge ridges. From observations, slopes that were less than 0.2% produced undular ridges whereas wedge ridges were formed when the slopes were set to be more than 0.2%.

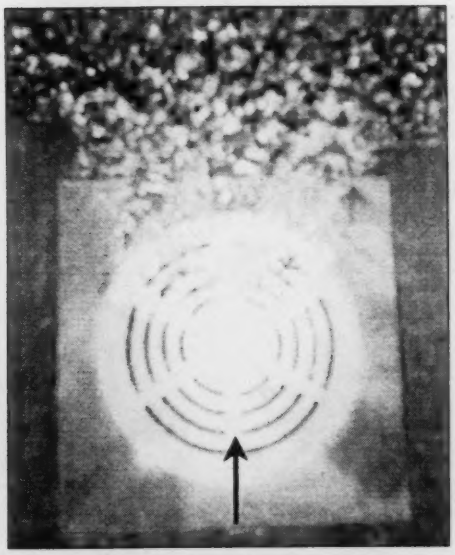

(a) Inlet NF80-Slotted Lid

(Q_o = 8.28 L/s and S_o = 0.1%)

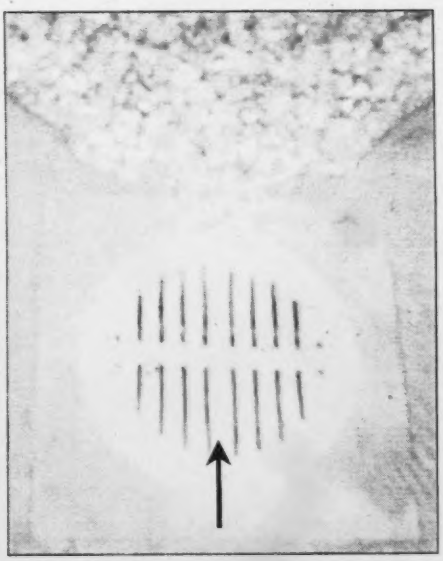

(b) Inlet #6B(F-39): Parallel to flow

(Q_o = 6.1 L/s and S_o = 0.2%)

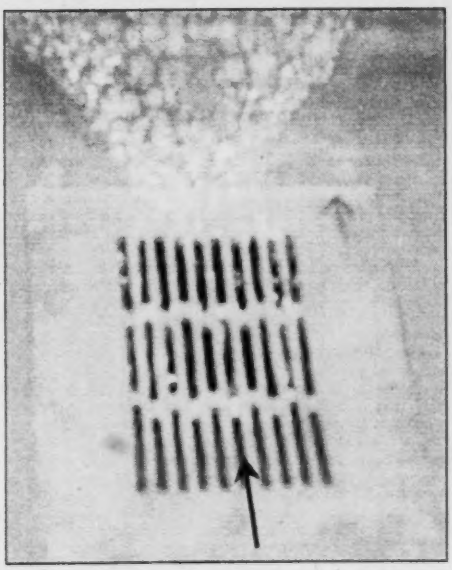

(c) Inlet F-51

(Q_o = 4.28 L/s and S_o = 0.2%)

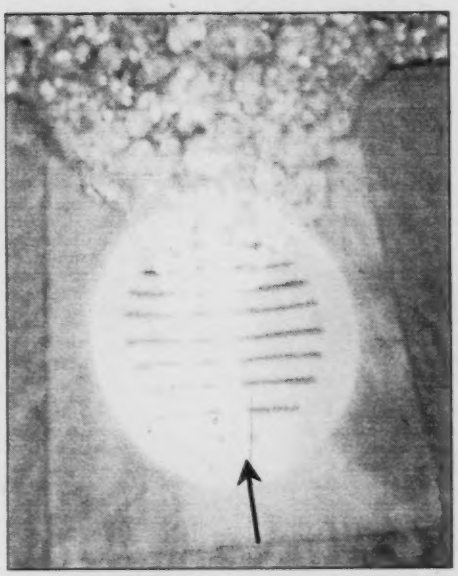

(b) Inlet #6B(F-39): Normal to flow

(Q_o = 8.78 L/s and S_o = 0.1%)

Figure 4.30: Undular ridge

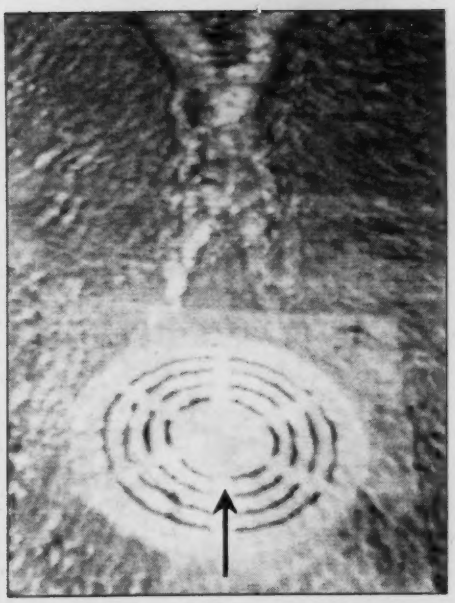

(a) Inlet NF80-Slotted Lid

(Q_o = 17.76 L/s and S_o = 1%)

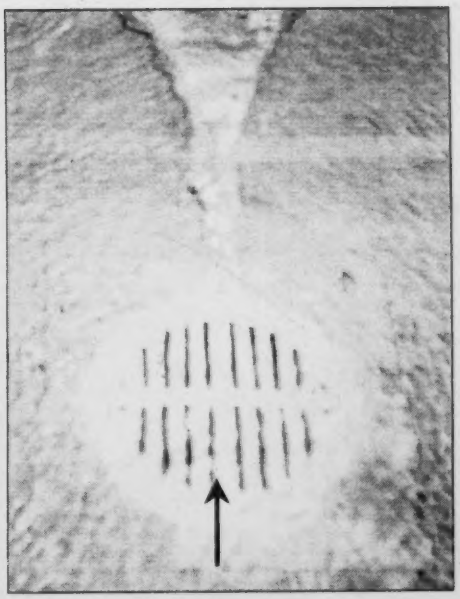

(b) Inlet #6B(F-39): Parallel to flow

(Q_o = 16.16 L/s and S_o =0.5%)

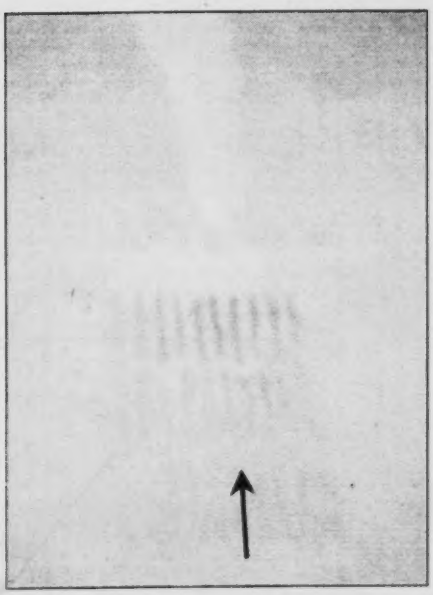

(c) Inlet F-51

(Q_o = 21.2 L/s and S_o = 0.5%)

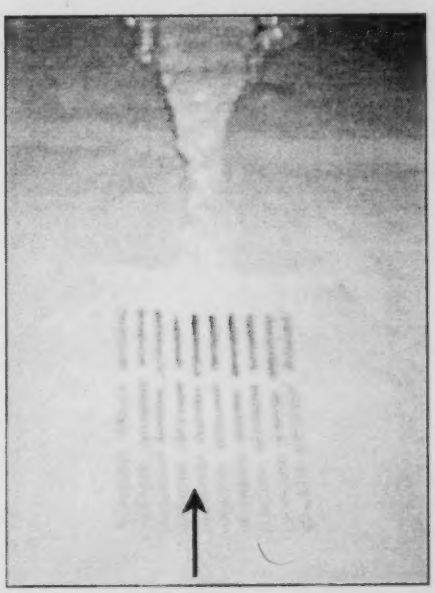

(d) Inlet F-51

(Q_o = 13.2 L/s and S_o = 0.5%)

Figure 4.31: Wedge ridge

4.4.2 Flow Transformation

The most interesting observation found in the street inlet studies was the transformation of flows from the subcritical to supercritical state. The approach flows were increased in order to see the transformation. It was noticed that all inlets produced similar transformation pattern for a particular flow region. The region was defined by observing the water surface profiles above the inlet. They were classified into five main regions; Region I, II, III, IV and V. All regions are based on the Froude number *(F)* computation, which are later addressed as the subcritical, critical and supercritical. For each region, the inlet openings could either be fully covered or not fully covered. A ridge was formed in each region but it could vary in location and type. As explained earlier, two types of ridges were observed; undular and wedge. Figure 4.32 (a) to (e) are presentation of regions observed in the studies, which consist of sketches of flow regions accompanied by its description.

Region I:

Subcritical: Openings Not Fully Covered

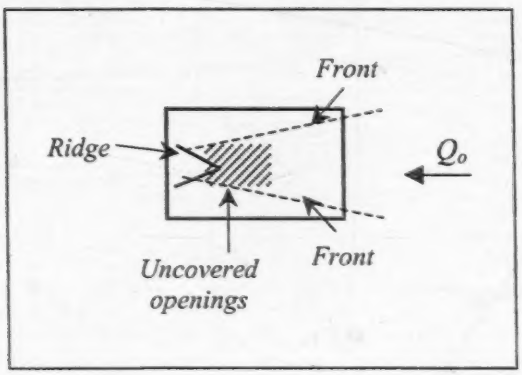

(a)

Not all openings are covered. The inlet mainly intercepts flows immediately upstream of the inlet. Fronts form a small ridge above the inlet. As the discharge gets higher, more openings will be submerged and the ridge becomes bigger.

Region II:

Subcritical: Openings Fully Covered

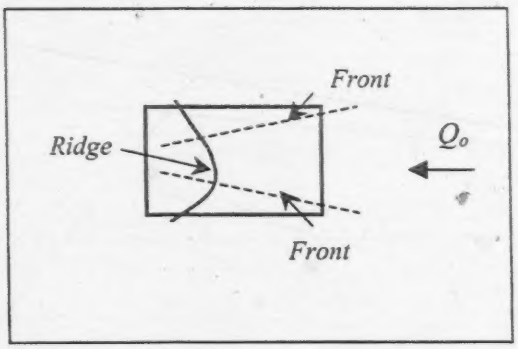

Openings are fully covered. Fronts produce undular ridge. Ridge occurs above the inlet itself. As the discharge gets higher, the ridge moves closer to the downstream inlet section.

(b)

Region III:

Critical

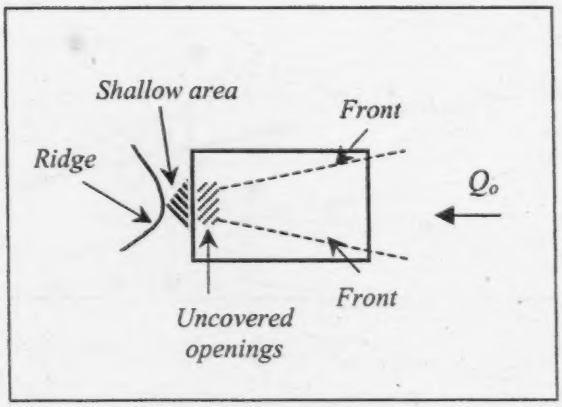

In some cases, not all openings are covered. Undular ridge is formed after the inlet. Fronts and carry over flows produce area with shallow depths immediately after the inlet.

(c)

Region IV:

Supercritical: Openings Fully Covered

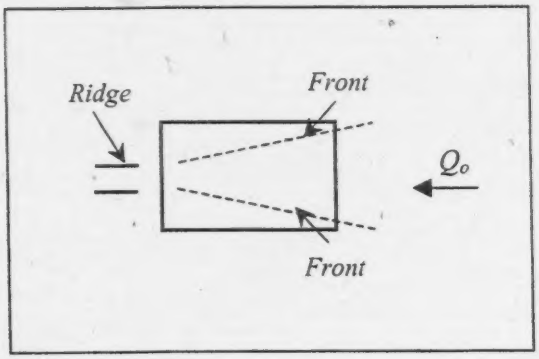

Openings are fully covered. Fronts produce wedge ridge and is located further downstream of the inlet section. The depth of ridge increases, as the discharge gets higher.

(d)

Region V:

Supercritical: Openings Not Fully Covered

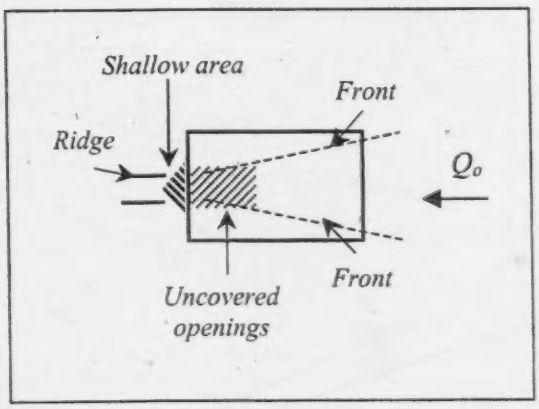

Not all openings are covered. Fronts and carry over flows produce shallow area immediately after the inlet, followed by a wedge ridge at the inlet downstream section.

(e)

Figure 4.32 (a) – (e): Flow transformation in the inlet studies

Not only the difference in patterns were observed in the flow transformation, but also the transitions of inlet opening flow-cover. For each channel slope (S_o), as the approach flow increased, flows above the inlet were expected to transform from non-complete to complete flow-cover, regardless of the water surface patterns. As discussed earlier in section 4.3.2, flows without complete flow-cover produced inconsistent depths above the inlet, resulting in a significant change in the C_d computation. Therefore, as the flow transformed from non-complete to complete flow-cover, the inlet experienced a condition that is referred to as the *full catch capacity*. This condition took place when the inlet started to have sufficient amount of water to completely cover the inlet surface. In other words, the inlet reached its capability to fully intercept water flowing passing it. The full catch capacity, however, varied between inlets at a certain channel slope. Table 4.3 summarizes values of full catch capacity for different types of inlets.

S_o / Inlets	0%	0.1%	0.2%	0.3%	0.5%	1%
F-51	6.72 L/s	-	5.48 L/s	-	13.2 L/s	13.6 L/s
NF80-Slotted Lid	-	5.2 L/s	-	-	5.96 L/s	4.88 L/s
#6B(F-39): Normal to Flow	2.04 L/s	4.20 L/s	-	7.44 L/s	6.08 L/s	8.00 L/s
#6B(F-39): Parallel to Flow	3.40 L/s	6.48 L/s	-	9.54 L/s	10.24L/s	16.84L/s

Table 4.3: Full catch capacity for street inlets

These discharges were categorized as a transition point from flows without complete to complete flow-covers. Beyond these discharges, flows above the inlet were completely covered.

The table shows that discharges for full catch capacity differed between inlets. Some inlets were not tested under certain range of slopes. This is because the existing data were sufficient enough to complete the Froude number ranges. Therefore, it was unnecessary to conduct experiments for other slopes.

In order to understand the table, an example is given for discharges under 0.5% slope. Among these four street inlets, inlet F-51 was found to have the highest discharge of 13.2 L/s for its full catch capacity. Even though the value was large, it was reasonably accepted due to its large opening area. As a result, it needed more flow to completely cover the inlet surface. Apparently, the unique bar orientation of inlet NF80-Slotted Lid only required low discharge (5.96 L/s) for full inlet surface coverage. This type of bar configuration is believed to provide advantages to the street drainage system, especially in reducing waves or splashes that normally occur above the inlet. As for inlet #6B(F-39), the one located parallel to the flow required higher discharge than the one located normal to the flow. Since inlet with longitudinal bars is known to intercept more water compared to transverse bars, the same reason also applied when determining its full catch capacity. More flows were needed to cover inlets with longitudinal bars. Transverse bars which tended to splash more water above the inlet, in a way reduced the actual amount of approach flow that was required to cover the inlet surface.

4.4.3 Flow Circulation

A tailgate was used in the channel study to produce subcritical flows due to some limitations on the initial experimental set up. Subcritical flows correspond to flows with low discharge. In the experiments, low discharged tended to produce very shallow water depth. Measurements for shallow depths should be avoided in order to avoid the effect of surface tension. The tailgate in a way helped to increase depth of water for low flows. The depth continuously

decreased from downstream to upstream sections of the channel. This behavior that is also described as backwater significantly influenced the water surface profiles above the inlets. In the studies, all inlets produced similar water surface profile pattern, in which it resembled a pattern of water circulation. This pattern is illustrated in Figure 4.33 while Figure 4.34 presents some examples of flow observed in other inlets. Two factors forming the circulation were the backwater that moved towards the inlet and discharge released by pump. In some cases, the openings can either be fully covered or not fully covered.

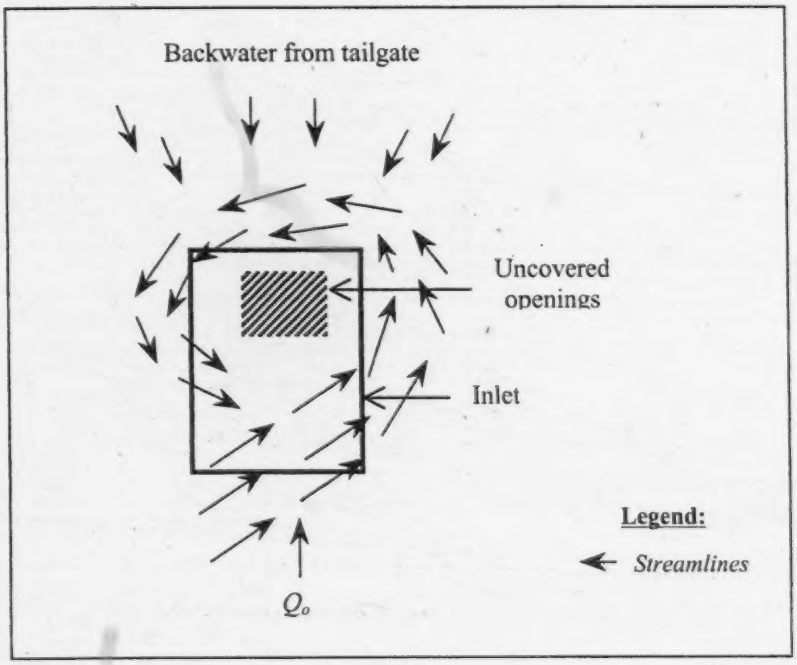

Figure 4.33: Sketch of water circulation above the inlet

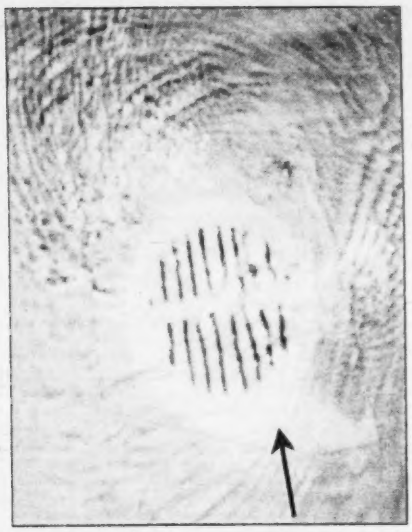

(a) Inlet #6B(F-39): Parallel to flow

(Q_o = 2 L/s and S_o =0%)

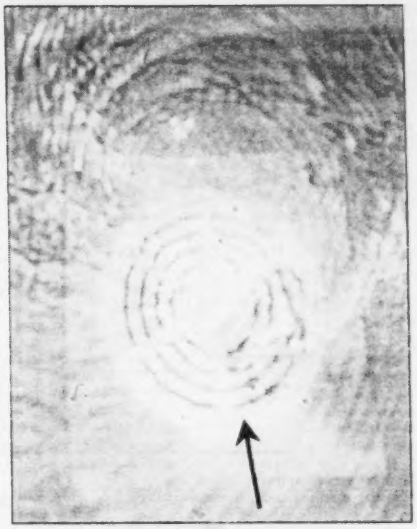

(b) Inlet NF80-Slotted Lid

(Q_o = 2.08 L/s and S_o =0.1%)

(c) Inlet #6B(F-39): Normal to flow

(Q_o = 1.76 L/s and S_o =0%)

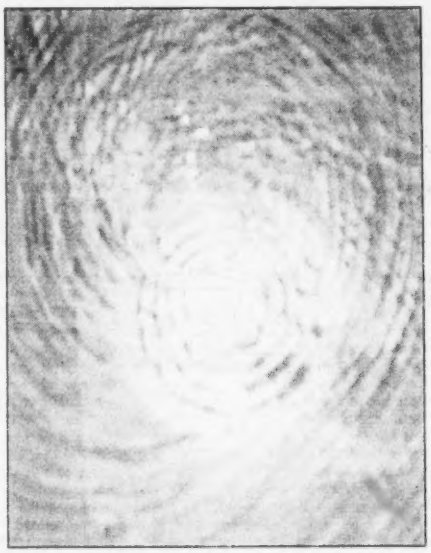

(d) Inlet NF80-Slotted Lid

(Q_o = 2.32 L/s and S_o =0.05%)

Figure 4.34: Flow circulation

CHAPTER 5
CONCLUSIONS

The present work on the characteristics of the discharge coefficient, C_d of the street inlets involved experimental work that covered aspects of ponding (reservoir) and gutter flow (channel) studies. The experimental results provided quantitative information about the variation of C_d with two dimensionless parameters, the Froude number *(F)* and Reynolds number *(R)*. These results are applicable to the computations of the actual flows entering the inlet for different flow conditions. The experiments did not, however, provide a validation for the actual street model, as its aim was to determine a general C_d variation that would be applicable for other similar inlet structures as well.

C_d for orifice-oriented inlet in the ponding condition was found to be invariant with R. On the other hand, for the case of the gutter flows, the Froude number was more dominant and C_d appeared to have a decreasing trend from the subcritical to the supercritical region as F increases, until it attained a constant value beyond this range. The plot C_d versus F in a way summarizes a complete variation of C_d for different types of flows, which include not only flows in the gutters, but also ponding condition.

Similar to ponding studies developed earlier by other researchers, depth computations near the inlets for flows in the channel (gutter) were also a major concern. Three approaches were proposed in determining the head for the C_d computations, which include the average depth above the inlet *($\bar{y}$)*, the depth of the flow approaching the inlet *(y_a)* and the specific energy of the flow approaching the inlet *(E_a)*. Results showed that E_a gave the best correlation in describing the inlet behavior between the discharge coefficient and the Froude number. This method offers a big advantage to engineers, as it provides information on the depth and velocity at the approach section.

By placing multiple openings close to each other, C_d variation showed no significant change. The disparity between the existing results and earlier studies was likely due to the size of opening area. Roughening the surrounding inlet surface, however, resulted in a higher C_d values.

Inlet pattern and the area of opening were found to significantly affect the variations of C_d. An inlet with circular concentric bar orientation could not be described as less efficient owing to the occurrence of transverse bars. Inlets with longitudinal bars, however, are more efficient compared to the transverse oriented-inlet. Under certain circumstances, bigger opening does not imply the effectiveness of an inlet because its dimensions influence the way the flow being captured.

Observations showed that water surface profiles at the downstream section of the inlets were in the form of a ridge, the existence of which might cause interference to the traffic and pedestrians. The ridge was categorized as undular or wedge, depending on the flow conditions.

With the knowledge obtained from this study, a proper C_d value for the street inlet can be easily predicted for a certain flow condition. The assumption of C_d that is equal to 0.6 in the orifice equation was proven to be wrong, especially during ponding condition. It is hoped that the selection of proper C_d will result in a good, adequate, safe and economical street inlet design.

Suggestions for future study would include the development of experimental work that considers the actual roadway hydraulics as well as the field study, to provide a justification on the existing results. The study should cover a range of Froude numbers as wide as possible, especially in the subcritical region. It might also be interesting to apply other inlets with unique and complicated designs so that advanced investigation can be made on the inlet characteristics. Further investigation and analysis can also be conducted for other inlet types such as the

curb inlet and combination inlet. Comparisons should be made between the future results and results obtained from grate inlets studies.

REFERENCES

Adam, K.M and Brandson, N.B (1974). *"Hydraulic Analysis of Winnipeg Sump Inlets"*. Journal of Water Pollution Control Federation, V46, n12, pp 2755-2763.

American Society of Civil Engineers, ASCE (1992). *"Design and Construction of Urban Stormwater Management Systems"*. ASCE Manuals and Reports of Engineering Practice No. 77, Water Environment Federation (WEF) Manual of Practice FD-20, 714p.

Bohac, D.E (1991). *"Assessing the Utility of Previously Derived Equations Measuring the Efficiency of Inlets: Comparison of Data Results from a Laboratory Analysis of Gutter Inlets with Equations Derived by Previous Research"*. M.S thesis. University of Nebraska-Lincoln, 106p.

Bouchard, M.G and Townsend, R.D (1984). *"Laboratory Tests on the Influence of Grating Pattern on Street Inlet Hydraulics"*. Proceedings, Annual Conference Canadian Society for Civil Engineering, Montreal, v2, pp 685-698.

Brater, E.F., King, H.W., Lindell, J.E. and Wei, C.Y. (1963). *"Handbook of Hydraulics"*. McGraw-Hill Book Co. Inc., New York, N.Y., 14.76p.

Brune, A.W., Graf, W.H., Appel, E. and Yee, P.P. (1975). *"Performance of Pennsylvania Highway Drainage Inlets"*. Journal of the Hydraulics Division, Dec '75, v101, pp 1519-1536.

Chapra, S.C. and Canale, R.P. (2002). *"Numerical Methods for Engineers"*. McGraw-Hill Book Co. Inc., New York, N.Y., 900p.

Chow, V.T. (1959) *"Open-Channel Hydraulics"*. McGraw-Hill Book Co. Inc., New York, N.Y., 621p.

Daugherty, R.L., Franzini, J.B., Finnemore, E.J. (1985). *"Fluid Mechanics with Engineering Applications"*. McGraw Hill Book Co. Inc., 564p.

Guo, J.C.Y. (1997). *"Street Hydraulics and Inlet Sizing"*. Water Resources Publication, LLC, Colorado, 60p.

Hotchkiss, R.H. (1994). *"Improvements in Curb-Opening and Grate Inlet Efficiency"*. Transportation Research Board, n1471, Dec '94, pp 24-30.

John Hopkins University (1956). *"The Design of Storm-Water Inlets"*. Report of the Storm Drainage Research Committee, Department of Sanitary Engineering and Water Resources, Baltimore, Md. 128p.

McNown, J.S. and Tai, C.H. (1972). *"Balanced Storm Drainage (Storm Drains for Roadways)"*. Kansas Water Resources Research Institute, Project Completion Report for Period July 1970 to September 1971, 37p.

Mays, L.R. (2001). *"Water Resources Engineering"*. John Wiley & Sons, Inc., New York, N.Y., 747p.

Montes, S. (1998). *"Hydraulics of Open Channel Flow"*. American Society of Civil Engineers (ASCE), 697p.

Rajaratnam, N. (1992). *"Hydraulics of K-7 Gratings"*. A report of Hydraulic Tests Prepared for the City of Edmonton, Sept '92, 12p.

Ranga Raju, K.G. (1981). *"Flow Through Open Channels"*. Tata McGraw-Hill Publishing Company Limited, New Delhi, 303p.

Sharp, J.J. (1981). *"Hydraulic Modelling"*. Butterworth & Co (Publishers) Ltd., 237p.

Schuster, C.K. (1984). *"Creative Solution Ends Flooding Problem"*. Public Works, Sept '84, v115, p2, pp 94-95.

Stephenson, D. (1981). *"Stormwater Hydrology and Drainage"*. Elsevier Scientific Publishing Company, Amsterdam, The Netherlands, 270p.

Townsend, R.D. (1985). *"A Study of Inlet Control Alternatives for SWM"*. Advances in Underground Pipeline Engineering: Proceedings of the International Conference, Aug '85, pp 417-427.

Topping, J. (1962). *"Errors of Observation and Their Treatment"*. The Institute of Physics and the Physical Society: Monographs for Students, 115p.

Wilson, D. (1983). *"Capacities of Catch Basin Inlets Based on Use in Alberta"*. TECHNA-WES, September 1983, 32p.

APPENDIX I

OTHER TYPES OF STREET INLETS OR SIMILAR STRUCTURES

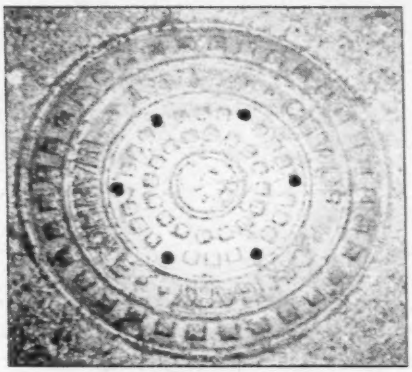

(a) Manhole cover in the city of Calgary

(b) Grate inlet in the city of Vancouver

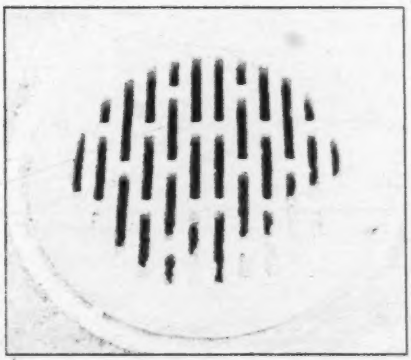

(c) Grate inlet in the city of Vancouver

Figure I.1: Other types of street inlets

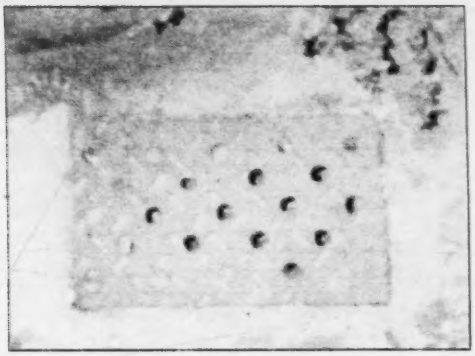

(a)

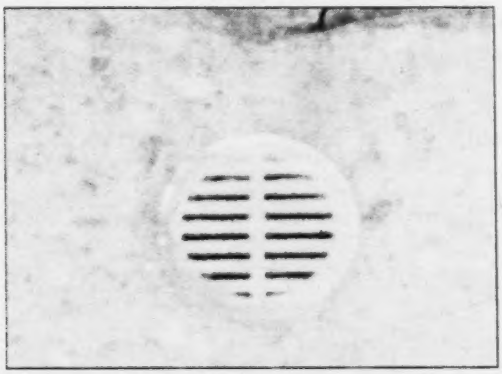

(b)

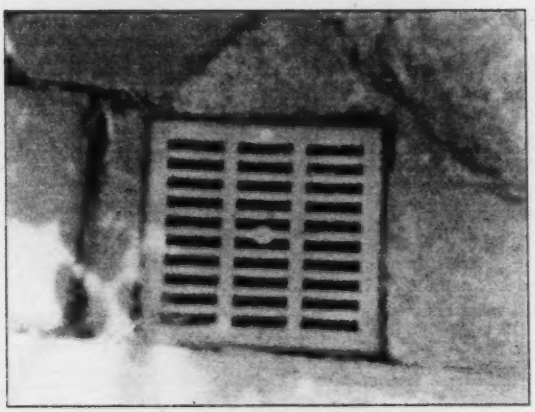

(c)

Figure I.2: Inlets in the Butchard Garden, Victoria

APPENDIX II

MODEL EXPERIMENTAL DATA FOR ORIFICES IN RESERVOIR

Q_i (m^3/s)	y (m)	R
0.000154	0.1835	14497
0.000149	0.1740	14077
0.000147	0.1662	13854
0.000144	0.1580	13555
0.000141	0.1528	13244
0.000137	0.1465	12923
0.000135	0.1395	12679
0.000132	0.1320	12391
0.000127	0.1258	11947
0.000124	0.1154	11672
0.000118	0.1077	11155
0.000118	0.1032	11111
0.000116	0.1027	10936
0.000115	0.0982	10825
0.000114	0.0972	10753
0.000113	0.0933	10644
0.000112	0.0914	10512
0.000110	0.0889	10388
0.000109	0.0855	10218
0.000107	0.0843	10121
0.000105	0.0786	9882

Table II.1: Model experimental data for orifice 1 *(O1)*

(continued)

0.000105	0.0796	9865
0.000100	0.0700	9450
0.000096	0.0643	9076
0.000094	0.0596	8868
0.000142	0.1523	13382
0.000135	0.1376	12723
0.000129	0.1234	12121
0.000117	0.1089	11027
0.000110	0.0862	10323

Table II.1: Model experimental data for orifice 1 *(O1)*

Q_i (m^3/s)	y (m)	R
0.000159	0.1885	14961
0.000156	0.1788	14695
0.000151	0.1695	14228
0.000148	0.1610	13947
0.000146	0.1523	13730
0.000141	0.1435	13311
0.000137	0.1351	12910
0.000134	0.1267	12636
0.000130	0.1185	12243

Table II.2: Model experimental data for orifice 2 *(O2)*

(continued)

0.000126	0.1108	11897
0.000124	0.1047	11649
0.000121	0.0991	11369
0.000117	0.0920	11020
0.000113	0.0853	10660
0.000110	0.0794	10374
0.000107	0.0748	10080
0.000105	0.0695	9919
0.000101	0.0637	9553
0.000098	0.0582	9267
0.000098	0.0549	9226
0.000154	0.1715	14503
0.000149	0.1606	14072
0.000144	0.1489	13591
0.000138	0.1331	13014
0.000131	0.1197	12378
0.000125	0.1058	11726
0.000119	0.0943	11239
0.000113	0.0817	10614

Table II.2: Model experimental data for orifice 2 *(O2)*

Q_i (m^3/s)	y (m)	R
0.000155	0.1676	15812
0.000151	0.1559	15390
0.000141	0.1452	14354
0.000140	0.1336	14320
0.000135	0.1234	13798
0.000130	0.1143	13306
0.000126	0.1050	12807
0.000121	0.0959	12337
0.000114	0.0826	11640
0.000109	0.0724	11100

Table II.3: Model experimental data for orifice 2 *(O2)* in the wall study

Q_i (m^3/s)	y (m)	R
0.000156	0.1730	13254
0.000152	0.1600	12939
0.000149	0.1520	12683
0.000146	0.1457	12451
0.000140	0.1328	11944
0.000137	0.1261	11676
0.000134	0.1188	11428

Table II.4: Model experimental data for orifice 2 *(O2)* with roughness on surrounding bed

APPENDIX III

MODEL EXPERIMENTAL DATA FOR ORIFICES IN CHANNEL

S_o (%)	Q_o (m^3/s)	Q_i (m^3/s)	y_o or y (m)	R
0	0.02754	0.000114	0.1105	11630
	0.02448	0.000113	0.1032	11518
	0.02229	0.000111	0.0974	11304
	0.01908	0.000107	0.0888	10936
	0.01659	0.000103	0.0815	10528
	0.01392	0.000099	0.0750	10144
	0.01101	0.000095	0.0660	9642
	0.00786	0.000088	0.0542	8958
	0.00519	0.000082	0.0430	8337
0.2	0.02760	0.000076	0.0670	7910
	0.02436	0.000073	0.0602	7594
	0.02133	0.000069	0.0556	7155
	0.01929	0.000067	0.0513	6949
	0.01434	0.000060	0.0410	6254
	0.01017	0.000055	0.0335	5709
	0.00813	0.000052	0.0284	5345
	0.00491	0.000044	0.0202	4565
0.3	0.02946	0.000077	0.0708	7652
	0.02451	0.000072	0.0601	7180
	0.01926	0.000066	0.0505	6541

Table III.1: Model experimental data for orifice 1 *(O1)* in the single orifice study (continued)

	0.01455	0.000060	0.0414	5930
	0.01092	0.000055	0.0346	5413
	0.00837	0.000050	0.0289	4989
0.4	0.02751	0.000075	0.0655	7610
	0.02490	0.000072	0.0596	7342
	0.02250	0.000069	0.0566	7082
	0.01980	0.000066	0.0504	6695
	0.01533	0.000060	0.0423	6086
	0.01146	0.000054	0.0345	5538
0.5	0.03030	0.000076	0.0698	7729
	0.02802	0.000074	0.0660	7534
	0.02550	0.000072	0.0606	7319
	0.02232	0.000068	0.0540	6943
	0.01836	0.000063	0.0460	6406
	0.01587	0.000059	0.0417	6009
	0.01389	0.000057	0.0378	5808
	0.01113	0.000053	0.0328	5404
	0.00813	0.000048	0.0260	4879
1.0	0.03030	0.000072	0.0675	7346
	0.02778	0.000070	0.0634	7110
	0.02646	0.000068	0.0595	6961
	0.01911	0.000059	0.0455	6057
	0.01596	0.000056	0.0395	5724

Table III.1: Model experimental data for orifice 1 *(O1)* in the single orifice study (continued)

	0.01296	0.000052	0.0339	5304
	0.01014	0.000048	0.0292	4929
	0.00750	0.000044	0.0233	4458
	0.00516	0.000039	0.0175	3928
1.5	0.03270	0.000071	0.0654	7277
	0.02727	0.000066	0.0575	6729
	0.02664	0.000065	0.0559	6648
	0.02322	0.000062	0.0501	6317
	0.01887	0.000057	0.0431	5865
	0.01644	0.000053	0.0387	5400
	0.01398	0.000050	0.0337	5131
	0.01083	0.000047	0.0285	4804
	0.00834	0.000043	0.0235	4366

Table III.1: Model experimental data for orifice 1 *(O1)* in the single orifice study

S_o (%)	Q_o (m^3/s)	Q_i (m^3/s)	y_o (m)	y (m)	R
0	0.02754	0.000121	0.1156	0.1169	12340
	0.02448	0.000119	0.1081	0.1089	12108
	0.02229	0.000116	0.1022	0.1035	11873
	0.01908	0.000112	0.0932	0.0947	11458
	0.01659	0.000110	0.0869	0.0880	11193

Table III.2: Model experimental data for orifice 2 *(O2)* in the single orifice study (continued)

	0.01392	0.000105	0.0792	0.0800	10738
	0.01101	0.000100	0.0699	0.0710	10219
	0.00786	0.000094	0.0584	0.0597	9554
	0.00519	0.000087	0.0481	0.0497	8885
0.2	0.02760	0.000110	0.0972	0.1058	11378
	0.02436	0.000107	0.0898	0.0970	11068
	0.02133	0.000102	0.0836	0.0825	10587
	0.01929	0.000101	0.0784	0.0848	10491
	0.01434	0.000092	0.0649	0.0689	9584
	0.01017	0.000085	0.0528	0.0562	8802
	0.00813	0.000081	0.0456	0.0479	8355
	0.00491	0.000072	0.0342	0.0363	7429
0.3	0.02946	0.000081	0.0713	0.0718	8054
	0.02451	0.000076	0.0626	0.0620	7551
	0.01926	0.000072	0.0548	0.0545	7169
	0.01455	0.000077	0.0473	0.0538	7603
	0.01092	0.000066	0.0390	0.0401	6584
	0.00837	0.000075	0.0408	0.0485	7426
0.4	0.02751	0.000075	0.0659	0.0650	7645
	0.02490	0.000073	0.0606	0.0602	7481
	0.02250	0.000071	0.0563	0.0563	7281
	0.01980	0.000067	0.0510	0.0500	6827

Table III.2: Model experimental data for orifice 2 *(O2)* in the single orifice study (continued)

	0.01533	0.000063	0.0442	0.0436	6474
	0.01146	0.000058	0.0368	0.0369	5901
0.5	0.03030	0.000075	0.0675	0.0679	7620
	0.02802	0.000073	0.0636	0.0639	7399
	0.02550	0.000070	0.0593	0.0585	7180
	0.02232	0.000068	0.0546	0.0545	6916
	0.01836	0.000065	0.0471	0.0475	6601
	0.01587	0.000061	0.0423	0.0419	6179
	0.01389	0.000058	0.0387	0.0381	5884
	0.01113	0.000055	0.0333	0.0335	5566
	0.00813	0.000050	0.0276	0.0274	5108
1.0	0.03030	0.000066	0.0598	0.0597	6694
	0.02778	0.000063	0.0562	0.0547	6434
	0.02646	0.000062	0.0539	0.0525	6345
	0.01911	0.000055	0.0421	0.0415	5633
	0.01596	0.000053	0.0365	0.0359	5360
	0.01296	0.000048	0.0315	0.0312	4895
	0.01014	0.000045	0.0274	0.0270	4597
	0.00750	0.000042	0.0220	0.0222	4237
	0.00516	0.000038	0.0175	0.0179	3851
1.5	0.03270	0.000062	0.0561	0.0550	6290
	0.02727	0.000058	0.0487	0.0477	5953
	0.02664	0.000058	0.0482	0.0468	5907

Table III.2: Model experimental data for orifice 2 *(O2)* in the single orifice study (continued)

	0.02322	0.000055	0.0440	0.0442	5610
	0.01887	0.000051	0.0389	0.0390	5246
	0.01644	0.000047	0.0341	0.0341	4795
	0.01398	0.000045	0.0299	0.0300	4597
	0.01083	0.000041	0.0250	0.0251	4148
	0.00834	0.000037	0.0207	0.0208	3800

Table III.2: Model experimental data for orifice 2 *(O2)* in the single orifice study

S_o (%)	Q_o (m^3/s)	Q_i (m^3/s)	y_o (m)	y (m)	R
0	0.02970	0.000120	0.1194	0.1205	11978
	0.01572	0.000106	0.0829	0.0839	10639
	0.00509	0.000085	0.0461	0.0469	8710
	0.00518	0.000085	0.0464	0.0471	8478
0.2	0.02970	0.000113	0.1001	0.1036	11309
	0.01572	0.000091	0.0690	0.0694	9054
	0.00504	0.000070	0.0339	0.0353	7139
	0.00492	0.000068	0.0334	0.0348	6788
0.3	0.02970	0.000080	0.0706	0.0713	8035
	0.01578	0.000066	0.0464	0.0461	6624
0.4	0.02970	0.000078	0.0675	0.0662	7772
	0.01578	0.000064	0.0447	0.0449	6363

Table III.3: Model experimental data for orifice 2 *(O2)* in the multiple orifices study (continued)

	0.00638	0.000048	0.0249	0.0246	4893
	0.01149	0.000058	0.0360	0.0358	5806
0.5	0.02970	0.000075	0.0653	0.0655	7542
	0.01590	0.000060	0.0421	0.0417	6011
	0.00627	0.000047	0.0234	0.0236	4816
	0.00810	0.000050	0.0273	0.0273	5028
1.0	0.02970	0.000065	0.0562	0.0556	6542
	0.01590	0.000051	0.0362	0.0358	5106
	0.00621	0.000040	0.0184	0.0177	4058
	0.00518	0.000038	0.0171	0.0168	3793
1.5	0.008340	0.00004	0.0208	0.0209	3787

Table III.3: Model experimental data for orifice 2 *(O2)* in the multiple orifices study

S_o (%)	Q_o (m^3/s)	Q_i (m^3/s)	y_o (m)	y (m)	R
0	0.02970	0.000122	0.1194	0.1205	12172
	0.01572	0.000106	0.0829	0.0839	10622
	0.00509	0.000084	0.0461	0.0469	8563
	0.00518	0.000084	0.0464	0.0471	8435
0.2	0.02970	0.000112	0.1001	0.1036	11194
	0.01572	0.000091	0.0690	0.0694	9057
	0.00504	0.000069	0.0339	0.0353	7036

Table III.4: Model experimental data for orifice 3 *(O3)* in the multiple orifices study (continued)

	0.00492	0.000068	0.0334	0.0348	6822
0.3	0.02970	0.000080	0.0706	0.0713	8025
	0.01578	0.000065	0.0464	0.0461	6505
0.4	0.02970	0.000076	0.0675	0.0662	7617
	0.01578	0.000063	0.0447	0.0449	6289
	0.00638	0.000047	0.0249	0.0246	4816
	0.01149	0.000058	0.0360	0.0358	5770
0.5	0.02970	0.000073	0.0653	0.0655	7303
	0.01590	0.000060	0.0421	0.0417	5964
	0.00627	0.000046	0.0234	0.0236	4720
	0.00810	0.000049	0.0273	0.0273	4940
1.0	0.02970	0.000064	0.0562	0.0556	6383
	0.01590	0.000051	0.0362	0.0358	5088
	0.00621	0.000038	0.0184	0.0177	3881
	0.00518	0.000037	0.0171	0.0168	3659
1.5	0.00834	0.000039	0.0208	0.0209	3857

Table III.4: Model experimental data for orifice 3 *(O3)* in the multiple orifices study

S_o (%)	Q_o (m^3/s)	Q_i (m^3/s)	y_o (m)	y (m)	R
0	0.02970	0.000121	0.1194	0.1222	12055
	0.01572	0.000105	0.0829	0.0842	10449

Table III.5: Model experimental data for orifice 4 *(O4)* in the multiple orifices study (continued)

	0.00509	0.000084	0.0461	0.0469	8540
	0.00518	0.000084	0.0464	0.0472	8390
0.2	0.02970	0.000109	0.1001	0.1006	10915
	0.01572	0.000091	0.0690	0.0712	9082
	0.00504	0.000071	0.0339	0.0358	7223
	0.00492	0.000070	0.0334	0.0355	7039
0.3	0.02970	0.000076	0.0706	0.0701	7616
	0.01578	0.000061	0.0464	0.0452	6083
	0.00489	0.000067	0.0272	0.0341	6869
0.4	0.02970	0.000072	0.0675	0.0674	7223
	0.01578	0.000059	0.0447	0.0445	5903
	0.006375	0.000044	0.0249	0.0245	4449
	0.01149	0.000053	0.0360	0.0362	5276
0.5	0.02970	0.000070	0.0653	0.0648	6953
	0.01590	0.000052	0.0421	0.0410	5220
	0.00627	0.000042	0.0234	0.0232	4328
	0.00810	0.000047	0.0273	0.0276	4647
1.0	0.02970	0.000060	0.0562	0.0553	6006
	0.01590	0.000048	0.0362	0.0358	4818
	0.00621	0.000035	0.0184	0.0178	3563
	0.00518	0.000033	0.0171	0.0172	3337
1.5	0.00834	0.000035	0.020825	0.0206	3465

Table III.5: Model experimental data for orifice 4 *(O4)* in the multiple orifices study

S_o (%)	Q_o (m^3/s)	Q_i (m^3/s)	y_o (m)	y (m)	R
0	0.02936	0.000127	0.1131	0.1141	12411
	0.01629	0.000113	0.0854	0.0860	11059
	0.00657	0.000094	0.0525	0.0534	9178
0.2	0.02727	0.000118	0.0932	0.0915	11520
	0.01638	0.000101	0.0719	0.0737	9885
	0.00657	0.000081	0.0389	0.0409	7944
0.3	0.02727	0.000094	0.0685	0.0712	9242
	0.01638	0.000082	0.0496	0.0518	7990
	0.00657	0.000070	0.0294	0.0326	6825
0.4	0.02727	0.000089	0.0658	0.0666	8762
	0.01644	0.000078	0.0464	0.0481	7680
	0.00657	0.000063	0.0265	0.0278	6148
0.5	0.0165	0.000076	0.0462	0.0462	7402
	0.00657	0.000062	0.0266	0.0266	6030
1.0	0.02721	0.000077	0.0544	0.0543	7570
	0.01650	0.000067	0.0383	0.0395	6549
	0.00657	0.000054	0.0206	0.0227	5337

Table III.6: Model experimental data for orifices with roughness on surrounding bed study

APPENDIX IV

MODEL EXPERIMENTAL DATA FOR STREET INLETS

S_o (%)	Q_o (m^3/s)	Q_i (m^3/s)	y_o (m)	$\bar{y}$ (m)	y_a (m)	E_a (m)
0	0.03712	0.00459	0.1040	0.1062	0.0995	0.1439
	0.03008	0.00444	0.0968	0.0838	0.0911	0.1258
	0.02384	0.00439	0.0793	0.0713	0.0676	0.1072
	0.01404	0.00427	0.0588	0.0416	0.0479	0.0753
	0.00672	0.00298	0.0375	0.0106	0.0299	0.0460
	0.00272	0.00246	0.0224	0.0111	0.0215	0.0266
0.2	0.00428	0.00163	0.0233	0.0105	0.0209	0.0343
	0.00548	0.00202	0.0264	0.0079	0.0241	0.0406
	0.01020	0.00345	0.0409	0.0155	0.0379	0.0610
0.5	0.00648	0.00217	0.0239	0.0108	0.0247	0.0466
	0.01320	0.00402	0.0383	0.0175	0.0379	0.0766
	0.02120	0.00420	0.0536	0.0336	0.0543	0.1029
	0.03068	0.00438	0.0661	0.0538	0.0666	0.1342
	0.03688	0.00444	0.0756	0.0615	0.0764	0.1507
1.0	0.00788	0.00227	0.0235	0.0115	0.0230	0.0604
	0.01360	0.00387	0.0327	0.0146	0.0335	0.0860
	0.02240	0.00425	0.0500	0.0304	0.0486	0.1163
	0.03012	0.00434	0.0622	0.0450	0.0635	0.1352
	0.03628	0.00439	0.0649	0.0533	0.0658	0.1627

Table IV.1: Model experimental data for street inlet type F-51

S_o (%)	Q_o (m^3/s)	Q_i (m^3/s)	y_o (m)	$\bar{y}$ (m)	y_a (m)	E_a (m)
0.05	0.00232	0.00183	0.0424	0.0326	0.0445	0.0454
	0.00416	0.00300	0.0303	0.0190	0.0284	0.0352
	0.00320	0.00229	0.0456	0.0360	0.0465	0.0480
	0.00360	0.00268	0.0457	0.0372	0.0465	0.0484
0.1	0.00828	0.00461	0.0401	0.0173	0.0336	0.0530
	0.01612	0.00534	0.0598	0.0359	0.0531	0.0825
	0.02424	0.00542	0.0694	0.0540	0.0673	0.1086
	0.03216	0.00554	0.0826	0.0733	0.0813	0.1312
	0.00520	0.00312	0.0293	0.0112	0.0243	0.0389
0.5	0.00596	0.00296	0.0233	0.0108	0.0238	0.0438
	0.00992	0.00457	0.0312	0.0147	0.0328	0.0619
	0.01720	0.00531	0.0452	0.0293	0.0445	0.0921
	0.02672	0.00539	0.0605	0.0469	0.0610	0.1221
	0.03292	0.00542	0.0692	0.0588	0.0717	0.1389
1.0	0.00488	0.00231	0.0169	0.0084	0.0166	0.0441
	0.00836	0.00371	0.0240	0.0119	0.0238	0.0631
	0.01776	0.00523	0.0395	0.0255	0.0397	0.1035
	0.02624	0.00536	0.0543	0.0401	0.0528	0.1315
	0.03276	0.00540	0.0633	0.0511	0.0598	0.1554

Table IV.2: Model experimental data for street inlet type NF80-Slotted Lid

S_o (%)	Q_o (m^3/s)	Q_i (m^3/s)	y_o (m)	$\overline{y}$ (m)	y_a (m)	E_a (m)
0	0.00408	0.00183	0.0274	0.0211	0.0239	0.0332
	0.00628	0.00260	0.0352	0.0227	0.0283	0.0440
	0.00204	0.00117	0.0191	0.0098	0.0167	0.0215
0.1	0.00420	0.00155	0.0268	0.0121	0.0210	0.0337
	0.00878	0.00306	0.0419	0.0169	0.0344	0.0552
	0.01668	0.00365	0.0615	0.0426	0.0546	0.0843
	0.02552	0.00376	0.0797	0.0618	0.0724	0.1120
	0.03172	0.00382	0.0830	0.0767	0.0836	0.1295
0.3	0.00744	0.00186	0.0290	0.0127	0.0286	0.0502
	0.01732	0.00315	0.0504	0.0333	0.0509	0.0878
	0.02476	0.00323	0.0630	0.0467	0.0638	0.1118
	0.03312	0.00331	0.0745	0.0622	0.0747	0.1373
0.5	0.00608	0.00172	0.0230	0.0102	0.0231	0.0452
	0.0138	0.00356	0.0389	0.0213	0.0380	0.0800
	0.02608	0.00362	0.0600	0.0464	0.0600	0.1202
	0.03208	0.00369	0.0685	0.0577	0.0692	0.1377
1.0	0.03168	0.00355	0.0645	0.0514	0.0614	0.1462
	0.0252	0.00352	0.0549	0.0396	0.0544	0.1228
	0.01756	0.00348	0.0413	0.0274	0.0406	0.1002
	0.00800	0.00208	0.0240	0.0114	0.0240	0.0594

Table IV.3: Model experimental data for street inlet type #6B(F-39) normal to the flow

S_o (%)	Q_o (m^3/s)	Q_i (m^3/s)	y_o (m)	$\overline{y}$ (m)	y_a (m)	E_a (m)
0	0.00340	0.00185	0.0251	0.0120	0.0214	0.0294
	0.00462	0.00230	0.0298	0.0167	0.0234	0.0358
	0.00648	0.00283	0.0357	0.0213	0.0286	0.0450
0.1	0.00648	0.00241	0.0343	0.0129	0.0280	0.0451
	0.01592	0.00431	0.0601	0.0352	0.0532	0.0817
	0.02548	0.00436	0.0787	0.0568	0.0707	0.1121
0.3	0.00592	0.00166	0.0271	0.0111	0.0248	0.0430
	0.00954	0.00268	0.0344	0.0170	0.0341	0.0590
	0.01888	0.00418	0.0530	0.0347	0.0546	0.0927
	0.02800	0.00433	0.0694	0.0527	0.0688	0.1216
0.5	0.03188	0.00478	0.0687	0.0562	0.0691	0.1369
	0.02508	0.00470	0.0596	0.0432	0.0588	0.1168
	0.0168	0.00462	0.0449	0.0277	0.0439	0.0906
	0.01024	0.00310	0.0322	0.0160	0.0329	0.0638
1.0	0.00820	0.00217	0.0237	0.0137	0.0229	0.0638
	0.01684	0.00417	0.0385	0.0222	0.0390	0.0984
	0.02632	0.00472	0.0550	0.0386	0.0523	0.1330

Table IV.4: Model experimental data for street inlet type #6B(F-39) parallel to the flow